eman ta zabal zazu

Universidad del País Vasco
Euskal Herriko Unibertsitatea

Quantum Biomimetics

Unai Alvarez Rodriguez

Supervisor:
Prof. Enrique Solano

Departamento de Química Física
Facultad de Ciencia y Tecnología
Universidad del País Vasco UPV/EHU

Leioa, November 2016

A smooth sea never made a
skilled sailor.

English Proverb

Resumen

En esta tesis introducimos el concepto de "Biomimética Cuántica", con el objetivo de diseñar protocolos de información cuántica que imiten rasgos significativos de propiedades exclusivas de los seres vivos mediante su codificación en registros cuánticos. Nuestro estudio indaga en las diferencias de cada protocolo con respecto a su equivalente clásico así como en la posible explotación de las mismas para la mejora de algoritmos cuánticos.

La idea subyacente en la biomimética es la robustez y eficiencia de las creaciones biológicas, impulsadas por el mecanismo de selección natural, en comparación a los ingenios humanos. Más allá de la elegancia de la idea, obtener inspiración de situaciones similares dadas en la naturaleza ha permitido el desarrollo de múltiples aplicaciones en diferentes ramas científicas y tecnológicas, por no hablar del instinto que ha llevado al ser humano a mejorar sus creaciones mediante analogías establecidas con su entorno. En otras palabras, la metodología biomimética lleva siendo aplicada mucho antes de que el término que la describe fuese acuñado. Así mismo, la imitación a la naturaleza incorpora una herramienta adicional al conjunto de técnicas para la optimización de problemas, y supone por tanto, un avance sustancial.

Existe una aparente contradicción en el planteamiento del estudio, por el hecho de buscar la reproducción de propiedades que emergen de la interacción entre sistemas macroscópicos complejos en un sistema físico microscópico de menos grados de libertad. Sin embargo, proveemos un argumento que permite eludir esta contradicción. En primer lugar, cabe destacar que nuestros algoritmos no buscan una copia exacta de las propiedades a imitar, más bien, su codificación en un sistema simplificado cuya dinámica efectiva permita la analogía. Nótese que este planteamiento es diferente al de buscar un sistema físico regido por un modelo matemático similar al original. Precisamente esta distinción es la que se hace entre simulación y emulación de un sistema, la primera aspira a imitar los engranajes del sistema mientras que la otra solo

los resultados de su dinámica. Por tanto, al restringirse a la emulación de ciertas características del sistema no se requiere un sistema del mismo grado de complejidad que el original. Concretamente, la selección de un formalismo matemático que codifique el sistema depende tanto del grado de exactitud que se quiera obtener en la emulación como de la diferencia entre la dinámica que describe al sistema original y la del sistema físico que sirve como soporte.

La tesis consta de introducción y tres partes, una por cada concepto clásico que inspira los protocolos cuánticos: selección natural, memoria e inteligencia. Cabe destacar que mientras la selección natural y la inteligencia se dan únicamente en organismos de cierta complejidad, la memoria, definida como dependencia explicita de la evolución temporal de un sistema de tiempos previos, abarca también el reino inanimado. Por tanto, el lugar que ocupa parece inapropiado porque no sigue el espíritu biomimético tal y como lo hemos definido previamente. Aún así, se le ha otorgado una parte independiente porque las técnicas explicadas sirven como herramienta para el posterior desarrollo de protocolos cuánticos "vivos" e "inteligentes".

En la introducción se describe la motivación de la tesis y se mencionan trabajos relacionados con la misma. También se incluye una breve descripción del campo de información cuántica así como un resumen con la estructura del documento.

La primera parte consta de protocolos cuánticos que imitan rasgos básicos del modelo de selección natural darwiniano. En primer lugar, concretamente en el Capítulo 2, se explica un protocolo de clonación cuántica parcial. La clonación cuántica es una operación para obtener un estado idéntico a un estado arbitrario y desconocido mediante la acción de medidas y de operaciones unitarias. El estado original debe preservarse, y la copia ha de obtenerse en un registro físico diferente. Si bien la mecánica cuántica prohíbe la clonación perfecta, admite soluciones para la clonación parcial. En esta no se copia el estado completo sino el valor esperado de un conjunto de observables que conmutan. La contribución original de esta tesis, en el campo de la clonación cuántica, es la generalización de un resultado previo de clonación cuántica parcial para dimensiones arbitrarias. Además, los autores se posicionan en el debate acerca del carácter clásico o cuántico del formalismo de clonación cuántica parcial.

En el Capítulo 3, se introduce un algoritmo para recrear un entorno de selección natural en una plataforma experimental cuántica. El ingrediente fundamental son los denominados *individuos*, que representan las entidades mínimas y autoconsistentes capaces de evolucionar según los procesos funda-

mentales del modelo: replicación, tiempo de vida finito, mutación e interacciones. Cada individuo consta de dos partes, genotipo y fenotipo, codificadas en un qubit cada una de ellas. El qubit genotipo es el registro físico de la información exclusiva de cada individuo, mientras que el fenotipo es el registro de la expresión del genotipo en el entorno. A posteriori, se explica la traducción de cada proceso fundamental del modelo de selección natural en su correspondiente operación cuántica. La replicación se realiza mediante clonación cuántica parcial, el tiempo de vida finito se simula con el tiempo transcurrido en la evolución del fenotipo hasta las cercanías de un estado asintótico en una dinámica disipativa, las mutaciones son rotaciones aleatorias en el qubit genotipo y las interacciones son operaciones controladas a cuatro qubits. Los datos en las simulaciones numéricas se extraen mediante los histogramas de posición, genotipo y fenotipo. Estos corroboran la correspondencia entre los procesos fundamentales y las operaciones cuánticas. Por último, se analiza la posible implementación experimental del protocolo en diferentes plataformas.

En la segunda parte de la tesis se incluyen algoritmos para simular evolución cuántica con memoria, entendida como dependencia no trivial en tiempos pasados de la variación del estado. Por tanto, esta parte guarda cierta relación con las líneas de retroalimentación cuántica y evolución cuántica no-Markoviana. El primer resultado en esta área, una simulación algorítmica de efectos de memoria, se expone en el Capítulo 4. El protocolo permite simular ecuaciones íntegro-diferenciales en las que la acción de un Lindbladiano es pesada con un kernel de memoria. Estas ecuaciones modelan fenomenológicamente un amplio conjunto de dinámicas con memoria con un potencial interés para el estudio de sistemas complejos. Definimos el concepto de simulación algorítmica como un protocolo mixto que requiere la implementación de evolución temporal junto con un procesamiento matemático paralelo, que va más allá del análisis de la medida, para obtener el resultado final. En este caso, el carácter mixto lo aporta la combinación de simulación eficiente de procesos markovianos con la integración numérica del kernel de memoria. El mecanismo consiste en codificar la ecuación a simular en una ecuación semi-Markoviana, cuyas propiedades permiten escribir la dinámica como una acción secuencial de un superoperador sobre el estado inicial, a través de dos estados auxiliares intermedios. El algoritmo se cierra con un cálculo de errores que permite evaluar la realización del protocolo en función de los parámetros que establecen la dinámica. El resultado es un comportamiento favorable en términos de recursos, que nos permite concluir el tra-

bajo afianzando la posible realización de aplicaciones cuánticas en las que los efectos de memoria sean cruciales.

En el Capítulo 5 se introduce un protocolo para simular ecuaciones diferenciales atrasadas y adelantadas empleando la evolución controlada de fotones en guías de ondas. En esta plataforma física cada guía de onda tiene un término de acoplo evanescente con sus vecinas, por tanto, al conectar los puertos de entrada y salida del chip con fibras ópticas se obtiene un acoplo entre el estado en una posición dada y el mismo estado en posiciones anteriores y posteriores. Existe además una analogía entre la propagación espacial de los fotones y la evolución temporal de un estado cuántico bajo influencia de la ecuación de Schrödinger. Es decir, la posición en las guías de onda se corresponde al tiempo en la evolución simulada. Modificando la naturaleza de las conexiones se alcanzan diversas familias de ecuaciones, sean ecuaciones de una sola variable, sistemas e incluso ecuaciones con múltiples términos atrasados y adelantados. Por último, se obtiene una estimación del error teórico mediante cálculo numérico y se mencionan las posibles causas de error experimental. De cara al diseño de aplicaciones cabe destacar que el protocolo permite resolver cuestiones de índole puramente matemática así como implementar dinámica cuántica con retroalimentación y posalimentación, lo que supone un hito en el desarrollo de la información cuántica.

En la tercera parte se incluyen algoritmos cuánticos relacionados con procesos de aprendizaje, se analizan tanto contribuciones de algoritmos clásicos para mejorar protocolos cuánticos, como algoritmos de aprendizaje exclusivamente cuánticos. En estos trabajos se entiende el concepto de aprendizaje como una optimización de una tarea bien definida. En el Capítulo 6 se explica una propuesta para el uso de algoritmos genéticos que aumenta la fidelidad de circuitos cuánticos. Se afrontan dos problemas diferentes, la corrección de una puerta lógica a partir de una arquitectura de puertas con error y el diseño de un circuito que reduzca el error de simulaciones digitales. En ambos casos coincide el procedimiento para plantear el problema, que consiste en escribir el circuito cuántico como una secuencia de instrucciones mediante una matriz. Esta tiene tantas columnas como número de puertas lógicas y cada fila especifica el tipo de puerta y los qubits sobre los que actúa. La información en la matriz hace las veces de código genético en el algoritmo genético, de forma que cada individuo tiene asociado un circuito cuántico. El funcionamiento del algoritmo genético es tal que a partir de individuos iniciales aleatorios encuentra soluciones óptimas mediante mutaciones y recombinaciones de individuos. Al final de cada ciclo del algoritmo se compara

la nueva generación de individuos con los integrantes de la generación previa mediante una función de evaluación, y se escogen los individuos mejor adaptados. La función empleada coincide con la fidelidad del circuito cuántico codificado en el individuo con respecto al circuito ideal.

En el Capítulo 7 se muestra un protocolo de aprendizaje cuántico capaz de encontrar el estado control adecuado de una operación unitaria controlada de estructura desconocida para la consecución de una puerta lógica. El protocolo incorpora un mecanismo de retroalimentación que sirve como motor del aprendizaje, ya que a partir de un control aleatorio inicial se incrementa la población en los subespacios que realizan la puerta deseada. Este efecto se consigue mediante un término en la ecuación de evolución proporcional a la diferencia entre los estados a dos tiempos diferentes, acompañado por un hamiltoniano que da lugar a la operación unitaria original. Además, no se requiere conocimiento alguno de la base natural de la operación unitaria, por lo que el protocolo adquiere un valor añadido al compararse con algoritmos clásicos destinados para la misma tarea. En el caso de existir múltiples soluciones, una dinámica disipativa diseñada según el criterio de eficiencia elegido permite hallar la solución óptima. La actuación conjunta de ambas fases, búsqueda de soluciones y búsqueda de la solución óptima, se analiza según las condiciones establecidas por el campo de aprendizaje en máquinas o *Machine Learning* para evaluar el resultado en un marco teórico apropiado.

En el Capítulo 8 se introduce el concepto de sumador cuántico, inspirado por la función de red en redes neuronales clásicas. El sumador se define como una operación cuántica que actua sobre dos estados iniciales desconocidos para obtener un estado final con la suma normalizada de los mismos. Los autores prueban la inexistencia de dicha operación invocando un argumento de invariancia bajo la acción de una fase global entre los estados iniciales y finales del sumador. Aportan además un argumento que clarifica una región de intersección entre el teorema de no clonación con el de no suma. Se muestran también propuestas de sumadores aproximados una vez eludida la prohibición mediante la restricción de los estados iniciales a determinados subconjuntos de estados, con la pérdida de generalidad que ello conlleva. Entre los sumadores aproximados destaca el sumador de base, que suma perfectamente elementos de la base y con una fidelidad elevada estados en superposición. Además, independientemente de la dimensión del estado a sumar basta con un solo qubit auxiliar para su realización. En paralelo, se estudian diferentes propuestas de implementación experimental de sumadores, optimizadas mediante la aplicación de algoritmos genéticos.

Abstract

Quantum Biomimetics is proposed as a research line devoted to the design of quantum information protocols inspired by properties exclusive of living systems. The goal behind this procedure of imitation is the search of quantum algorithms that encode significative features of macroscopic phenomena in a microscopic quantum registers for their use in reproducing biological complexity in the quantum realm. Our approach raises no contradiction since the quantum biomimetic protocols do not intend to capture every feature of the models describing living systems, but a simplified representation that can be accommodated in the space offered by controllable quantum platforms. In this sense, the algorithms we propose may be classified as emulators that aim at reproducing the input-output behavior of the targeted model. These emulators are different from simulators, which are machines that intend to imitate models as close as possible to the original system.

Depending on the behavior to mimic, the quantum protocols we present can be grouped in three main sets: natural selection, memory and intelligence. In each of them, we analyze the performance of our algorithms as compared to their closer classical counterparts. In parallel, we adapt our protocols to the limits imposed by the constant progress of current controllable quantum platforms. A common feature of our proposals is the consideration of both theoretical and experimental aspects for the development of realistic algorithms.

In conclusion, we think that the work presented here contributes to the improvement of the state of the art in quantum information via the introduction of new phenomena and regimes which resemble the ones of living systems.

Acknowledgments

While I am writing these words, I realize that this may well be the most read part of the thesis. This is almost a tradition. Either the content of the thesis is boring or interesting, the readers attention gets attracted by the acknowledgments, curious for knowing what kind of person the writer is.

The privilege of the first position is for my PhD supervisor Prof. Enrique Solano. Beyond his remarkable scientific guidance, I would like to thank Kike for a practical lesson he gives everyday that I will undoubtedly bring with me wherever I go. This is the capacity to do what you really believe in. Kike has carefully raised the oasis of QUTIS with a single seed, out of nowhere. It has taken me some time to realize that our origins and talents are irrelevant here, the secret of the permanent success of the group is no other than the passion that Kike shares with us in the form of discussions and decisions. When I landed in the group, I had the impression that I was not good enough to accomplish the task I was facing. Well, I was right. It is under the influence of the whole atmosphere of QUTIS that I have been able to capture at least some hints of how science is done.

Just after Kike is Dr. Lucas Lamata. He has been a constant support in my professional development and in the achievement of this thesis. I would like to thank Lucas for his patience and his academic and alchemic abilities in filtering and transmuting my outlandish ideas into reliable knowledge. He has usually been the first one to listen and criticize but also the first one to defend our work in front of other colleagues, being the greatest example of team spirit.

The Quantum Biomimetics team would not be complete without the presence of Dr. Mikel Sanz. His handling has been determinant to overcome different obstacles found along our journey. Besides, his communication skills have enabled to spread our ideas and gather people around them.

Let me also thank Prof. Iñigo Egusquiza who, more than once, has dedi-

cated his time and knowledge to help me.

I would like to extend my gratitude to the present and past members of the group for the unique experiences during these four years. Teammates, I like to believe that our discussions, travels, jokes, confusions, confessions, plans, etc., have shaped my personality, and probably yours, with beautiful lines and forms. It has been a nice time imagining new worlds with you.

I do not want to forget about my colleagues at the university, especially all those retired football players, the summer ping-pong addicts and the ones with whom I started this adventure almost ten years back. To all of you my friends, I hope you can find yourself in this list of names that I am avoiding but implicitly writing. Since we have come to an intersection where we separate, I want you to know that it has been a pleasure to share the same path with you. In the future, I will probably turn my head back expecting to hear my old companions, wondering about where you are.

I have had the opportunity of participating in scientific trips which has allowed me to interact with researchers all around the globe. I would like to thank Prof. Hartmut Häffner for hosting me in Berkeley, Dr. Frank Deppe for inviting me to Munich, Prof. Alexander Szameit and Dr. Armando Perez-Leija for their warm hospitality in Jena, Dr. David Zueco and all his group for giving me the chance of participating in their "Martes Cuanticos", and Prof. José Martín and Dr. Pablo Escandell for being so welcoming in my visit to Valencia. In my travel to Jena, the Jena-Bilbao collaboration was strengthened with the consolidation of multiple ideas. I want to specifically mention the friendly support of Alex and Armando, whose company and help have been crucial in the development of some of these chapters. In Valencia, the commitment and bravery of José and Pablo enabled us to overcome the initial difficulties and continue working in our nice project.

To finish the scientific part, thanks to all my collaborators, and in general to everyone with whom I have discussed. This exercise of creating, synthesizing and evaluating ideas has stylized my sailing across the sea of knowledge.

Happily, there is more. To drive back to reality at the end of each workday and be rewarded with the company of my friends and family is the main reason for getting in the car again the next day. This one is dedicated to my blood crew, to the birds of the night, to the fairy of the curly hair and her shiny companion, to Lord and Lady Alro and to the girl of the magical eyes.

List of Publications

Articles contained in this thesis

- U. Alvarez-Rodriguez, M. Sanz, L. Lamata, and E. Solano, Biomimetic Cloning of Quantum Observables, Sci. Rep. **4**, 4910 (2014).
- U. Alvarez-Rodriguez, M. Sanz, L. Lamata, and E. Solano, The Forbidden Quantum Adder, Sci. Rep. **5**, 11983 (2015).
- U. Alvarez-Rodriguez, M. Sanz, L. Lamata, and E. Solano, Artificial Life in Quantum Technologies, Sci. Rep. **6**, 20956 (2016).
- U. Las Heras, U. Alvarez-Rodriguez, E. Solano, and M. Sanz, Genetic Algorithms for Digital Quantum Simulations, Phys. Rev. Lett. **116**, 230504 (2016).
- U. Alvarez-Rodriguez, R. Di Candia, J. Casanova, M. Sanz, and E. Solano, Algorithmic Quantum Simulation of Memory Effects, arXiv:1604.02992 (2016).
- Unai Alvarez-Rodriguez, Armando Perez-Leija, Iñigo L. Egusquiza, Markus Gräfe, Mikel Sanz, Lucas Lamata, Alexander Szameit, and Enrique Solano, Advanced-Retarded Differential Equations in Quantum Photonic Systems, arXiv:1606.05143 (2016).
- U. Alvarez-Rodriguez, L. Lamata, P. Escandell, J. D. Martín, and E. Solano, Feedback-Induced Quantum Learning, *In preparation.*
-R. Li, U. Alvarez-Rodriguez, L. Lamata, and E. Solano, Quantum Adders with Genetic Algorithms, *In preparation.*

Other articles

- U. Alvarez-Rodriguez, J. Casanova, L. Lamata, and E. Solano, Quantum Simulation of Noncausal Kinematic Transformations, Phys. Rev. Lett. **111**, 090503 (2013).

- Xiao-Hang Cheng, Unai Alvarez-Rodriguez, Lucas Lamata, Xi Chen, and Enrique Solano, Time and spatial parity operations with trapped ions, Phys. Rev. A **92**, 022344 (2015).
- Tony E. Lee, Unai Alvarez-Rodriguez, Xiao-Hang Cheng, Lucas Lamata, and Enrique Solano, Tachyon physics with trapped ions, Phys. Rev. A **92**, 032129 (2015).

Contents

List of Figures

List of Tables

Chapter 1

Introduction

> Though human ingenuity may make various inventions which, by the help of various machines answering the same end, it will never devise any inventions more beautiful, nor more simple, nor more to the purpose than Nature does; because in her inventions nothing is wanting, and nothing is superfluous, and she needs no counterpoise when she makes limbs proper for motion in the bodies of animals. But she puts into them the soul of the body, which forms them that is the soul of the mother which first constructs in the womb the form of the man and in due time awakens the soul that is to inhabit it.
>
> *Leonardo da Vinci*

Quantum Technologies

Quantum theory, developed in the beginning of the twentieth century, allows for an accurate description of nature phenomena at the microscopic scale. The drawback is that analytical solutions to equations modeling realistic physical systems are elusive in general due to the involved mathematical complexity. Moreover, the exponential dependence of the Hilbert space dimension in the number of particles implies a poor scalability when treating these problems with classical computers. Therefore, although quantum mechanics provides powerful tools for describing physical phenomena, its use is restricted by our knowledge of analytical and numerical techniques. This situation motivates a quest towards efficient methods for working with quantum mechanics.

The contribution by Richard Feynman is considered nowadays as the precursor of the field of quantum simulations [1]. He proposed to use controllable quantum mechanical systems as registers for encoding the evolution of other systems. Later on, David Deutsch established the quantum computing framework by extending the Church-Turing thesis with the tools provided by quantum mechanics [2]. Each of these ideas represent the compass towards the consecution of the quantum simulator and the quantum computer, respectively.

Quantum Simulators Inspired by the original scope of Feynman a quantum simulator is a device allowing for the representation of a mathematical model describing the system of interest in a controllable quantum platform [3]. There are already several quantum simulators which enable the time evolution prediction in physical systems with increasing complexity [4, 5, 6]. Moreover, this scenario can also be exploited to study abstract models not being necessarily related with existing phenomena [7, 8]. Therefore, quantum simulators could be used for reproducing new regimes of consolidated physical models.

Inside quantum simulators, one often distinguishes between analog and digital methods. In analog simulators, the reproduced model is typically encoded in physical processes of a similar time scale. This is achieved by engineering Hamiltonians and measurements which effectively resemble the dynamics of the system to imitate. Sadly, there is not any known protocol for obtaining an analog simulation of an arbitrary process.

On the contrary, digital quantum simulations are based in the Suzuki-

Trotter formula which approximates the evolution of a combination of Hamiltonians in the product of the individual evolutions [9]. In practice, this means that a complex dynamics can be achieved by repeatedly implementing a sequence of simpler building blocks of an smaller time scale with a controllable error.

The difference between analog and digital simulations is similar to the one existing between conventional artistic paintings and digitally assembled images in CCD cameras. Although analog simulations usually require a more elegant design and can be more efficient in particular situations, at this moment digital techniques are more versatile. This is a convenient property because it guarantees that the same physical platform can be used for simulating radically different dynamics.

Quantum Computers An alternative approach arises, following the vision of Deutsch, towards the design of a universal quantum computer. Quantum computation is a research field oriented to the theoretical study and experimental modelling for the implementation of information processing encoded in quantum mechanical variables [10]. The ultimate goal is the realization of a scalable and universal quantum Turing machine, i.e., a device capable of efficiently carrying out any algorithm in the framework of quantum physics.

The quantum bit or qubit, encoded in a superposition of two quantum states, constitutes the minimal representative of information. While qubits serve as information registers, the information processing is realized with unitary operations. These are naturally provided as the time evolution operator solving Schrödinger equations. Additionally, the existence of a universal set of gates ensures that any unitary operation can be obtained as a product of the elements of the set, more precisely, single and two qubit gates. Therefore, in theory, any quantum platform supporting initialization and readout, an entangling gate and single qubit rotations is a valid candidate for the quantum computer. Nevertheless, when these ideas are experimentally expressed, the overall performance of the quantum computer is limited by scalability and errors in the computation.

Open Quantum Systems The errors are due to the fact that the model supporting the quantum computing framework is only achieved as an approximation. The complete system contains more degrees of freedom that affect

the physical registers and operations, producing imperfections in the qubits and quantum gates, respectively. These errors are studied within the theory of open quantum systems [11]. Its goal is to obtain an effective evolution for a subsystem of interest belonging to a higher dimensional system once the environment is traced out. Here, the environment groups every region of the Hilbert space that is not the subsystem of interest.

Although the evolution operator for the complete system is unitary, the effective one in the reduced subspace is not. Even so, the positivity and normalization and, thus, the notion of quantum state are preserved. Therefore, notice that unitary dynamics does not cover the complete spectra of possible processes. Instead, completely positive and trace preserving (CPTP) maps represent a more general class of dynamics. The main consequence is that this opens a new research line for directly implementing CPTP dynamics [12, 13, 14, 15]. In order to make it efficient, the goal is to avoid the cost in resources of increasing the Hilbert space until the reduced CPTP map is obtained with a unitary evolution on a larger space.

Present situation Currently, there are examples of advanced quantum algorithms in both simulation and computation categories for the leading quantum platforms. These are superconducting circuits [16, 17], trapped ions [18, 19, 20] and, integrated and bulk, quantum optics [21, 22, 23, 24]. An obvious aspect to mention is that each experimental platform has its own properties, traduced into advantages and disadvantages for accommodating specific quantum protocols.

The most successful applications in quantum computing are Shor's [25] and Grover's [26] algorithms, capable of outperforming classical computers, which have already been experimentally tested in Refs. [27, 28, 29, 30, 31], among others. In quantum simulations, one of the most active and promising research lines is the study of embedding quantum simulators, consisting on an enhanced encoding of the model to analyze in order to improve its efficiency [32]. Another raising trend is the design of quantum protocols combining the aforementioned digital and analog approaches, with the scope of exploiting the universality of digital and the efficiency of analog simulators [33, 34]. The expectation about these theoretical results is justified in the light of recent experiments reaching the order of 10^3 quantum gates [6], therefore achieving a first milestone in the route towards scalability.

In parallel, different approaches as the quantum annealer [35, 36] and

boson sampler [37, 38, 39, 40] are also capable of solving particular problems faster than ordinary computers. Thus, they offer an alternative for the encoding of other type of quantum algorithms.

Quantum Biomimetics

We have coined the concept of Quantum Biomimetics for denoting the research field oriented to the design of quantum protocols which mimic features that appear only in living systems. In order to clarify the idea, it is important to mention two important facts. The first one is that the properties of living systems constitute only the surface of complex phenomena that emerges from the interaction of multiple particles. The second one is that this complexity is in general unreachable with current theoretical or experimental knowledge from first principles in quantum mechanics. Therefore, instead of using the existing biological models, we create simpler ones in which the features we want to reproduce are directly introduced.

Beyond the intellectual exercise, our purpose is to improve the versatility of quantum protocols in the direction of complex biological phenomena and to study the possibility of employing these protocols for producing useful quantum algorithms.

The origin of Biomimetics lies at the beginning of human history. When our ancestors used animal skin to cover themselves, or understood the process of cultivating a tree from a seed they were being inspired by particular phenomena in nature around them. The modern idea is that natural creations are more efficient and flexible than human creations because they have been optimized generation after generation under the laws of natural selection.

Nowadays, biomimetic techniques are specially famous for their implementation in the design of new materials. Nevertheless, their influence covers a larger set of applications [41, 42]. In particular, when restricting our view to the field of classical computation we find examples of studies that could be classified under the label of classical biomimetics [43]. In other words, these well stablished research lines in classical computation have been used as source of inspiration for producing our quantum biomimetics protocols.

Consider the case of computational artificial life in which software encoded mechanisms undergo processes that try to reproduce the natural selection scenario [44, 45]. In a similar manner, the field of genetic algorithms aims at solving problems by encoding them in the genetic code of compet-

ing individuals [46]. With a similar spirit but different techniques, the area of Artificial Intelligence is oriented to the creation of algorithms that allow machines to show intelligent behavior, defining types of intelligence as the capacity to solve a particular problem or perform a given task [47].

In the quantum realm, there are already works that consider similar questions as the ones we ask in our quantum biomimetics approach [48]. More precisely, the field of quantum cellular automata and the field of quantum machine learning among others are good examples of it.

This Thesis

Following its definition, quantum biomimetics has the potential of accounting for a diverse set of quantum protocols, which for the same reason, makes the process of designing a common mathematical framework hard. Therefore, we have analyzed a selection of the most paradigmatic biological properties and reproduced some of their aspects independently in each of our works. The content of the thesis is divided in three main parts, each of them associated with a particular biological feature used as an inspiration: natural selection, memory and intelligence.

Before looking at them with more detail, it is convenient to clarify that the feature of memory, defined as the property of a system whose time evolution depends explicitly on previos times, is not exclusive of living systems. Even if this feature does not fit properly in the definition of quantum biomimetics, we have upgraded its status because quantum memory protocols can be employed as building blocks for simulating purely biomimetic dynamics, as we show in the thesis.

The first part, Quantum Artificial Life, contains two quantum protocols that offer a possibility for simulating individuals encoded in quantum states, whose dynamics is driven by natural selection processes implemented with quantum operations. In Chapter 2, we explain a mechanism for obtaining a partial quantum cloner for states of arbitrary dimension. In the partial quantum cloner, a unitary transformation acting on a given quantum state and a blank state achieves an output in which the expectation value of a chosen observable in the initial state is copied in every subsystem. At the same time, the expectation value of a different and non-commuting observable in the initial state is transported to a non-local observable. In Chapter 3, we show an algorithm for simulating individuals evolving according to the laws

dictated by their surrounding natural selection scenario. These individuals are encoded in two qubits, each representing the genotype and phenotype. The self-replication process is implemented via the partial quantum cloning protocol. The remaining aging, mutation, and inter-individual interaction processes that complete the natural selection model are developed in the language of unitary transformations and dissipative evolution. In both chapters, we give a basic experimental analysis showing the feasibility of our ideas.

The second part, Mnemonic Quantum Systems, is composed of two quantum algorithms that enable the simulation of quantum dynamics with memory. In Chapter 4, we present a method for retrieving the information of the evolution under an integro-differential equation modeling the memory effects. The protocol requires a combination of numerical and experimental solving techniques. These allow for calculations in which the dynamics are not CPTP maps. Our work is particularly interesting for the study and implementation of quantum non-Markovian processes. In Chapter 5, we show a quantum algorithm for realizing advanced-retarded differential equations in integrated photonics circuits. Beyond their mathematical interest, these equations enable the implementation of quantum feedback and feedforward driven dynamics. The proposed experimental setup exploits the analogy existing between spatial propagation and time evolution as well as the connectivity offered by optical waveguides and fibers in the context of integrated quantum photonics.

In the third and last part, Intelligent Quantum Systems, we study the possibility of merging quantum evolution with optimization techniques in three different projects. In Chapter 6 we analyze the possibility of employing Genetic Algorithms for improving quantum information protocols. The idea is to obtain high fidelity and efficient gate decomposition of a quantum protocol by using the genetic codes of competing individuals as a register for the sequence of gates. The algorithm makes that the survival probability of the individuals depends on the fidelity of the process they encode. We have used genetic algorithms in two situations, the optimization of a digital protocol and the annihilation of gate errors when concatenating imperfect operations. In Chapter 7 we present an algorithm for learning how to perform a given task in a controlled unitary operation of multiple possibilities. The protocol finds the optimal control state capable of driving input output connection into the target subspace. Instead of training the system several times, the goal is achieved by initializing the control state in a superposition

state and launching it in a time delayed equation. We analyze the performance of our algorithm in the context of machine learning and compare it with the process of directly measuring the action of the unitary controlled operation. Chapter 8 is about our work in the Quantum Adder. This is a hypothetical device creating the superposition of two unknown quantum states in a single output register. Even though we prove that it is forbidden by fundamental reasons in its most general form, we provide approximate quantum adders obtained when relaxing the conditions. The relation with the field of artificial intelligence is that quantum adders could be the basic building blocks behind quantum neural networks.

Part I

Quantum Artificial Life

Chapter 2

Biomimetic Cloning of Quantum Observables

> Life isn't about finding yourself.
> Life is about creating yourself.
>
> *George Bernard Shaw*

In this chapter, we propose a bio-inspired sequential quantum protocol for the cloning and preservation of the statistics associated to quantum observables of a given system. It combines the cloning of a set of commuting observables, permitted by the no-cloning and no-broadcasting theorems, with a controllable propagation of the initial state coherences to the subsequent generations. The protocol mimics the scenario in which an individual in an unknown quantum state copies and propagates its quantum information into an environment of blank qubits. Finally, we propose a realistic experimental implementation of this protocol in trapped ions.

2.1 Introduction

Quantum information is a research field that studies how to perform computational tasks with physical platforms in the quantum regime. Coping with complex quantum systems could give rise to an exponential gain in computational power and a new branch of possibilities as compared with classical computing [1, 3]. One of the turning points of quantum information

is the no-cloning theorem [49], which expresses the impossibility of copying an unknown state. Therefore, the notion of perfect universal quantum cloning was abandoned, and replaced by the cloning of restricted families of states or cloning with imperfect fidelities. A paradigmatic instance is the Buzek and Hillery universal quantum cloning machine [50], among other cases [51, 52, 53, 54, 55]. Another approach is *partial quantum cloning*, consisting in the copy of partial quantum information of a quantum state. In this sense, an interesting example is the cloning of the statistics associated with an observable [56]. However, these methods are limited due to the classical character of the information one replicates, since it is impossible to clone two non-conmuting observables with the same unitary [57, 58].

For a long time, human beings mimicked nature to create or optimize devices and machines, as well as industrial processes and strategies. In particular, biomimetics is the branch of science which designs materials and machines inspired in the structure and function of biological systems [41, 48, 59, 60, 61, 62]. Analogously, novel quantum protocols may be envisioned by mimicking macroscopic biological behaviors at the microscopic level, in what we call quantum biomimetics.

Living entities are characterized by features such as reproduction, mutations, interactions or aging. Among them, the ability to self-replicate is the most basic one. In fact, even though they are allowed to perfectly replicate classical information, biological systems only reproduce part of this information in the following generations. A paradigmatic example is DNA replication inside the nucleus of the cell, since only sequences of bases are copied, but not all of the information about the physical state of the molecule.

In this chapter, we propose a formalism for cloning partial quantum information beyond the restrictions imposed by the aforementioned no-go theorems. We use a family of increasingly growing entangled states [63, 64] in order to preserve and propagate the information of an initial state. In particular, we are able to transmit more than just classical information to the forthcoming generation, i.e., both the diagonal elements and coherences of the associated density matrix. Finally, we analyze the feasibility of a possible experimental implementation with trapped ions.

2.2 Biomimetic Cloning method

To introduce our protocol, let $\rho \in \mathfrak{B}(\mathbb{C}, n)$ and $\rho_e \in \mathfrak{B}(\mathbb{C}, n)$ be an arbitrary state and a blank state, respectively, and let θ be a Hermitian operator. We define the cloning operation $U(\theta, \rho_e)$ as

$$\langle \theta \rangle_\rho \equiv \mathrm{Tr}(\rho\theta) = \langle \theta \otimes \mathbb{1} \rangle_{U(\rho \otimes \rho_e)U^\dagger} = \langle \mathbb{1} \otimes \theta \rangle_{U(\rho \otimes \rho_e)U^\dagger}. \tag{2.1}$$

We denote each subspace as an *individual*, see Fig. 2.1. The expectation value of θ in the initial state is cloned into both subspaces of the final state. This is the cloning machine for observables introduced in Ref. [56]. Here, we extend their results to an arbitrary dimension and show the existence of an additional operator τ, which does not commute with θ, and whose statistics is encoded in the global state of the system

$$\langle \tau \rangle_\rho \equiv \mathrm{Tr}(\rho\tau) = \langle \tau \otimes \tau \rangle_{U(\rho \otimes \rho_e)U^\dagger}. \tag{2.2}$$

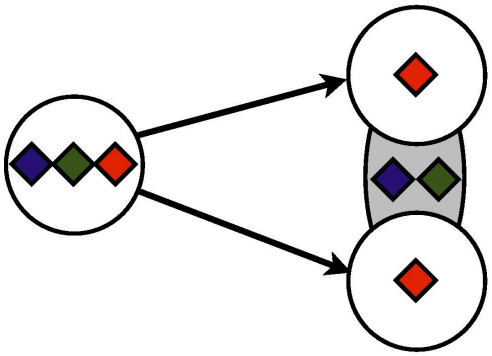

Figure 2.1: **Cloning and transmission of quantum information.** In this scheme of our protocol, the individuals are plotted with circles. The red diamond (centered inside each circle) represents the information that is cloned in every individual of the forthcoming generation, shown in Eq. (2.1). The other diamonds represent the information that is transmitted onto the global state of each generation relative to Eq. (2.2).

At this stage, it is convenient to point out the differences between both processes. On the one hand, Eq. (2.1) can be regarded as a replication of a characteristic from an individual into its progeny. In this sense, the

global state is traced out and the only important feature is the information of the individual. On the other hand, Eq. (2.2) can be considered as a spread of the quantum coherences of the initial individuals to the forthcoming generations as a whole. Our formalism combines the notions of cloning and preserving quantum information without contradicting the no-cloning and no-broadcasting theorems [65]. This allows the propagation of the statistics of two non-commuting observables in a controllable way.

The explanation of the cloning method requires a selection of the basis, provided here by an external environment. The dark state of an unknown environment dynamics is the blank qubit for the copying process, i.e., the state that we define as the $|0\rangle$. This point will be relevant later in the discussion about the quantumness of the process.

Let us work without loss of generality in a basis in which θ is diagonal. Then, we define the cloning operation $U_n(\theta, \rho_e)$ in terms of the generator of n-dimensional representation of the translation group $\{x_{ni}\}$ and the projectors into each subspace $\{s_{ni}\}$. We clarify that U_n, after all, does not explicitly depend on θ.

$$x_{ni}|k\rangle = \begin{cases} |k+i-1\rangle & \text{if} \quad k \leq n-i+1, \\ |k+i-1-n\rangle & \text{if} \quad k > n-i+1, \end{cases} \tag{2.3}$$

$$s_{ni} = |i\rangle\langle i|, \tag{2.4}$$

$$U_n = \sum_{i=1}^{n} s_{ni} \otimes x_{ni} = \bigoplus_{i=1}^{n} x_{ni}. \tag{2.5}$$

For example, for $n = 2$, $U_2 = U_{\text{CNOT}}$, and for $n = 3$, U_3 is given by

$$U_3 = \begin{pmatrix} 1 & 0 & 0 \\ 0 & 1 & 0 \\ 0 & 0 & 1 \end{pmatrix} \oplus \begin{pmatrix} 0 & 0 & 1 \\ 1 & 0 & 0 \\ 0 & 1 & 0 \end{pmatrix} \oplus \begin{pmatrix} 0 & 1 & 0 \\ 0 & 0 & 1 \\ 1 & 0 & 0 \end{pmatrix}. \tag{2.6}$$

We will demonstrate below that Eq. (2.5) fullfils Eq. (2.1). The forthcoming theorems are proved in Appendix A.

Theorem 1. *Let $\mathcal{H} \in \mathbb{C}^n$ be a Hilbert space of dimension n, $U \in \mathcal{H} \otimes \mathcal{H}$ the unitary operation defined in Eq.* (2.5)*, $\rho_e = |0\rangle\langle 0|$, and $\rho, \theta \in \mathfrak{B}(\mathcal{H})$ bounded Hermitian operators. Then, the unitary U satisfies Eq.* (2.1)*.*

We analyze now if the cloning unitary U transmits information from the initial individual to the progeny as a whole, apart from cloning its expectation value independently.

Theorem 2. *Let $U \in \mathcal{H} \otimes \mathcal{H}$ be the unitary transformation defined in Eq.* (2.5)*. Then, there exists a bounded antidiagonal operator τ, whose matrix elements are* 0 *or* 1*, fulfilling Eq.* (2.2)*.*

Notice that, in previous theorems, we have worked in a basis in which θ is diagonal. However, the cloning operation can be rewritten in any basis just by rotating the matrix with the proper unitary, $\theta' = R^\dagger \theta R$, transforming τ into $\tau' = R^\dagger \tau R$ and U into $U' = (R^\dagger \otimes R^\dagger) U (R \otimes \mathbb{1})$.

When the cloning operation is sequentially reapplied, it propagates the information of the initial state, i.e., it transmits the full statistics of the density matrix, $\mathrm{Tr}[\rho\sigma_i]$, $i = 1, 2, 3$. We show here how two-qubit operations are extended into m-qubit states,

$$U_{i,i+\frac{m}{2}} = x_1^{\otimes i-1} \otimes s_1 \otimes x_1^{\otimes m-i} + x_1^{\otimes i-1} \otimes s_2 \otimes x_1^{\otimes \frac{m}{2}-1} \otimes x_2 \otimes x_1^{\otimes \frac{m}{2}-i},$$

where the subscripts of U refer to the pair of qubits that is acted upon. The cloning for the subsequent generations, see Fig. 2.2, is constructed through the product of pairwise cloning operations, $U = \prod_{i=1}^{\frac{m}{2}} U_{i,i+\frac{m}{2}}$. For instance, the density matrices of the first and second generations reads

$$\rho_1 = (U_{1,2})(\rho_0 \otimes \rho_e)(U_{1,2})^\dagger, \tag{2.7}$$

$$\rho_2 = (U_{1,3}\, U_{2,4})(\rho_1 \otimes \rho_e \otimes \rho_e)(U_{1,3}\, U_{2,4})^\dagger. \tag{2.8}$$

Therefore, the mechanism is straightforwardly generalizable for obtaining sequential generations with the same information in each individual, in the spirit of a quantum genetic code. Moreover, although Eq. (2.7) holds only for qubits, it is noteworthy to mention that an extension to higher dimensions is possible. This can be achieved using as building block the unitary gate U_n defined in Eq. (2.5).

We will present now a counter-example showing that the cloning operation is not unique. When n is not a prime number, $n = kl$, there are other cloning unitaries apart from U_{kl}. For instance, an additional U'_{kl} is constructed via the solutions in each subspace, U_k and U_l, respectively,

$$U'_{kl} = \sum_{i=1}^{k} \sum_{j=1}^{l} s_{ki} \otimes s_{lj} \otimes x_{ki} \otimes x_{lj}. \tag{2.9}$$

This result shows that it is possible to mix information among subspaces of different dimensions. An example for $n = 6$ is depicted in Fig. 2.3.

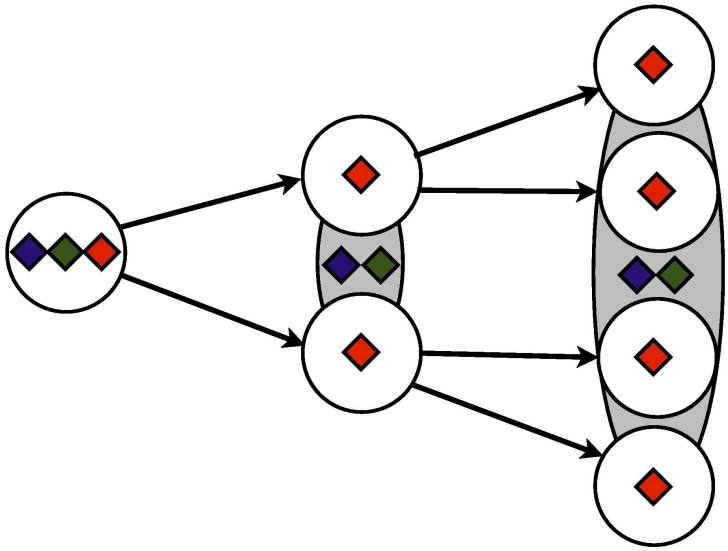

Figure 2.2: **Iteration of the cloning process.** Scheme of the sequential cloning of the information encoded in an initial state into individuals of subsequent generations.

Maximally Entangled States

We would like to point out that one of the possible applications of the cloning unitary is the generation of maximally entangled states. These, are defined as $|m\rangle = \frac{1}{\sqrt{n}} \sum_{i=1}^{n} |i\rangle|i\rangle$ for an arbitrary dimension n. The maximally entangled state is obtained when applying the cloning unitary to the tensor product of a uniformly superposed state, $|u\rangle = \frac{1}{\sqrt{n}} \sum_{i=1}^{n} |i\rangle$, and a blank qudit.

$$U|u\rangle|1\rangle = \frac{1}{\sqrt{n}} \sum_{i=1}^{n} \sum_{j=1}^{n} s_{nj} \otimes x_{nj}|i\rangle|1\rangle = \frac{1}{\sqrt{n}} \sum_{i=1}^{n} \sum_{j=1}^{n} \delta_{ij}|j\rangle|j\rangle = \frac{1}{\sqrt{n}} \sum_{i=1}^{n} |i\rangle|i\rangle \tag{2.10}$$

2.3 Quantumness and Classicality

In this section, we analyze the quantumness of the proposed biomimetic cloning protocol. In Ref. [66], Meznaric *et al.* recently introduced a criterion

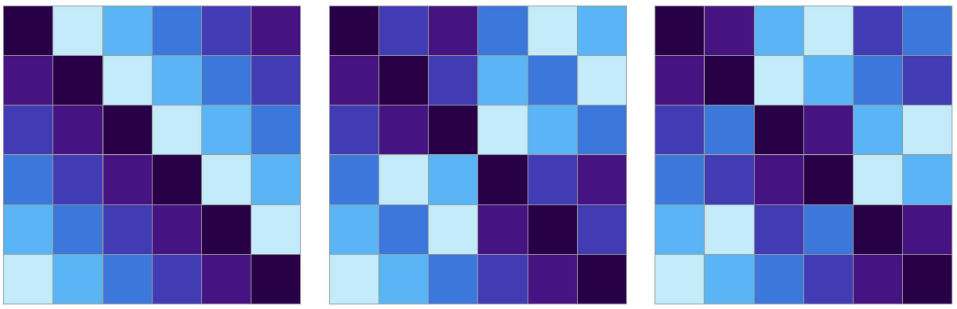

Figure 2.3: **Cloning unitary operations for n = 6.** In these graphics, each color represents a matrix of the translation group. Therefore, each of the three two-dimensional arrays groups the six matrices of the translation group for $n = 6$. The first array combines the x_{ni} operations of Eq. (2.5), while the second and third show $x_{ki} \otimes x_{lj}$ of Eq. (2.9) with $k, l = 2, 3$ and $k, l = 3, 2$, respectively.

to determine the nonclassicality of an operation Ω. This method is based on the distance between the outcome of the operation and the pointer basis einselected by the environment. The quantum operation Ω is composed with the completely dephasing channel Γ, provided by the environment. The measurement of nonclassicality is obtained by maximizing over all states the relative entropy of both operations acting on an arbitrary quantum state. The completely dephasing channel plays the role of an external environment that einselects the pointer basis, in which Ω is represented. Effectively, as deduced from Ref. [66], any operation is quantum whenever its column vectors are superpositions of the elements of the basis. On the contrary, the operation is classical if they are just permutations of the basis.

It is natural to identify the basis of the ancillary qudits, ρ_e, with the pointer states, since we assume that the system naturally provides blank qudits. By applying the classification formalism for qubits, the process of copying σ_z in the individual state and σ_x in the global state is classical, because the U_{CNOT} is written in terms of permutations of the pointer states.

Nevertheless, the complementary operation

$$U_x = \frac{1}{\sqrt{2}} \begin{pmatrix} 1 & 1 & 0 & 0 \\ 0 & 0 & 1 & -1 \\ 0 & 0 & 1 & 1 \\ 1 & -1 & 0 & 0 \end{pmatrix}, \tag{2.11}$$

which clones σ_x in the individual state and σ_z in the global state, is quantum.

Another possibility is to consider that the classical pointer basis is defined by the Ω operator itself. This means that we can construct the quantum channel $\mathcal{E}(\rho)$ which maps the initial state to any of the outcomes, considering the blank qudit and the other outcome as the environment. By construction, the unitary given by Eq. (2.5) leads to an injective channel, since the number of Kraus operators is the same as the square of the matrix dimension. Therefore, the only fixed point is the identity and the cloning operations are classical when written in the einselected basis [67].

According to these results, the cloning formalism copies classical information but preserves quantum correlations, which makes the global operation quantum. The interpretation of this property is that the quantum part of the information is encoded in the global state. By analogy with biological systems, the environment plays a fundamental role in the kind of information that, similar to quantum darwinism [68], is preserved and cloned through a pure quantum mechanism. In our work, the quantumness is only revealed when considering collectively all outcomes of the copying process.

2.4 Experimental Implementation

We consider that an experimental realization of our protocol in a quantum platform sets a significant step towards quantum artificial life. We propose an experimental setup of our formalism in trapped ions, arguably one of the most advanced quantum technologies in terms of coherence times and gate fidelities [18]. Current experimental resources would allow copying processes for qubits and qutrits of three and two generations, respectively. The number of logical gates and trapped ions required to perform the experiment is presented in Table 2.1. We point out that the only limitations for performing trapped-ion experiments with higher dimensions and larger number of generations are decoherence times and gate errors. None of these are fundamental and near future improvements may allow to reach the implementation of

higher dimensional individuals and many more generations with near perfect fidelities.

Qubit				
Sequential generation step	0	1	2	3
Total gates (2 qubit gates)	0	19(2)	57(6)	133(14)
Ions	1	2	4	8
Qutrit				
Sequential generation step	0	1	2	-
Total gates (2 qubit gates)	0	38(4)	114(12)	-
Ions	2	4	8	-

Table 2.1: **Technological and computational resources.** We show the number of quantum gates and trapped ions needed to perform the cloning experiment with qubits and qutrits, respectively. In the case of qutrits, this table shows de number of gates for producing the submatrices, and not the complete gate.

We encode the initial state in one of the ions, while the rest are initialized in the $|0\rangle$ state. The cloning operation for two qubits is the CNOT gate, which can be reproduced performing the Mølmer-Sørensen gate [69] and a sequence of single qubit gates [70], $U_{\mathrm{CNOT}} = -(\sigma_x \otimes \sigma_z) P_1 P_2^{-1} H_2 R P_1 H_1 P_1 R P_2$. Here, P is the phase gate, H is the Hadamard gate, R is the Mølmer-Sørensen gate, and the subindex denotes the ion number. We express the gates as products of carrier transitions R^c and a phase factor,

$$P = e^{-i3\pi/4} R^c(\pi, 0) R^c(\pi, \pi/4), \tag{2.12}$$

$$H = e^{-i\pi/2} R^c(\pi, 0) R^c(\pi/2, \pi/2), \tag{2.13}$$

$$\sigma_z = e^{-i\pi/2} R^c(\pi, 0) R^c(\pi, \pi/2). \tag{2.14}$$

The first and second generations of cloned qubits are obtained as indicated in Eq. (2.8). The next step in the copying process, i.e., the third generation, is given by $\rho_3 = (U_{1,5}\, U_{2,6}\, U_{3,7}\, U_{4,8})(\rho_2 \otimes \rho_e^{\otimes 4})(U_{1,5}\, U_{2,6}\, U_{3,7}\, U_{4,8})^\dagger$.

We consider now the implementation of the qutrit case in trapped ions. As there is no direct access to qutrit gates, we have to engineer a protocol with one and two-qubit gates. We suggest to add three ancillary levels that split the unitary operation into three subspaces of 4×4 matrices. To achieve

this, for the U_3 given in Eq.(2.6), the modified U_3' is

$$U_3' = \mathbb{1}_4 \oplus \begin{pmatrix} 1 & 0 & 0 & 0 \\ 0 & 0 & 0 & 1 \\ 0 & 1 & 0 & 0 \\ 0 & 0 & 1 & 0 \end{pmatrix} \oplus \begin{pmatrix} 1 & 0 & 0 & 0 \\ 0 & 0 & 1 & 0 \\ 0 & 0 & 0 & 1 \\ 0 & 1 & 0 & 0 \end{pmatrix}. \tag{2.15}$$

The first submatrix does not require any quantum gate. The second and third submatrices are the products of two CNOT gates, for which the role of control and target ions is interchanged. Hence, the implementation is reduced from qutrit to qubit operations.

2.5 Conclusions

In summary, inspired by replication in biological systems, we have brought concepts and applications into quantum information theory. For instance, our partial quantum cloning method makes use of global and local measurements in order to encode information of nonconmuting observables beyond the classical realm. Moreover, we prove that the information transmission is purely quantum for a certain kind of operators. In parallel, we show that it is possible to implement our ideas in an ion-trap platform with current technology.

Replication is the most fundamental property that one may require from a biological system. We leave to the following chapter the introduction of additional biological behaviors such as mutations, evolution and natural selection, englobed by the frame of quantum artificial life. This proposal should be considered as the first step towards mimicking biological behaviours in controllable quantum systems, a concept that we have called quantum biomimetics.

Chapter 3

Artificial Life in Quantum Technologies

> A human being is a part of the whole called by us universe, a part limited in time and space. He experiences himself, his thoughts and feeling as something separated from the rest, a kind of optical delusion of his consciousness. This delusion is a kind of prison for us, restricting us to our personal desires and to affection for a few persons nearest to us. Our task must be to free ourselves from this prison by widening our circle of compassion to embrace all living creatures and the whole of nature in its beauty.
>
> *Albert Einstein*

In this chapter, we develop a quantum information protocol that models the biological behaviours of individuals living in a natural selection scenario. The artificially engineered evolution of the quantum living units shows the fundamental features of life in a common environment, such as self-

replication, mutation, interaction of individuals, and death. We propose how to mimic these bio-inspired features in a quantum-mechanical formalism, which allows for an experimental implementation achievable with current quantum platforms. This study paves the way for the realization of artificial life and embodied evolution with quantum technologies.

3.1 Introduction

In the last decades, the novel field of artificial life has enabled researchers to recreate biological behaviours with controllable inanimate platforms in the laboratory [45]. Its goals are diverse, ranging from the comprehension of the emergence of life to the explanation of the appearance of dynamical hierarchies that give rise to complexity. Examples of the latter are consciousness at the single agent level or social organization at the group level. Self-replication and self-organization have already been achieved in this context based on fundamental interactions between the artificial living entities called *individuals* [71]. Moreover, techniques developed in artificial life have been applied into different research lines, e.g., by modeling the formation of biological tissues [72], and explaining the dynamical structure of fluids [73]. In particular, software-based artificial life consists of computational algorithms of evolving individuals. This area has produced some prominent models like the Game of Life [74] or Tierra [75], that in most cases were developed using classical techniques, with few examples in the quantum domain [48, 76, 77].

It is known that certain quantum information protocols [25, 26] can be performed efficiently in terms of speed or number of resources. Therefore, it seems natural to look for the consequences of introducing quantum mechanics in artificial life models, and establish analogies and connections between these two seemingly unrelated fields. There are already some preliminary results in the realm of quantum evolution [78] and quantum learning agents [79]. Here, we would like to focus on the concept of quantum biomimetics, namely, mimicking macroscopic biological behaviours at the quantum microscopic level, for the sake of quantum information fundamentals and applications.

In this chapter, in the context of quantum biomimetics, we propose a quantum model of artificial life that aims at reproducing fundamental biological behaviours with controllable quantum platforms. Along these lines, we define quantum *individuals* that can be born, evolve, interact, mutate, and die, while they propagate and decohere in a common environment. These

concepts are designed to be implementable with current quantum technologies. Hence, we discuss an experimental realization in trapped ions, superconducting circuits, and integrated quantum photonics. Related ideas have already been echoed by the scientific community [80].

It is noteworthy to mention that the proposed quantum biomimetic ideas should be considered as a free creation of a possible quantum evolution model at the microscopic quantum level. In this sense, while related to standard fields as artificial intelligence, machine learning, cellular automata, artificial living systems, and the like, these ideas cannot be framed uniquely in any of them.

3.2 Quantum Artificial Life Protocol

The individuals, which are our quantum artificial living units, are described by two-qubit states. Inspired in the biological mechanism of self-replication and evolution, one of the qubits in a quantum living unit represents its *genotype* and the other qubit corresponds to its *phenotype*. In our model, the information with the characteristics of the living unit is codified in the genotype, and is transmitted through generations. Additionally, the genotype encodes the lifetime of the individual and its role in the trophic chain. On the other hand, the phenotype is the expression of the genotype under the influence of an environment. Specifically, the phenotype carries information about the age of the individual, which is encoded in the time elapsed in the evolution of the qubit from its initial state to the dark state of the environment. The information exchange between the genotype and the phenotype is produced at the creation of a newborn individual during the self-replication process. Moreover, the analogy with biological mutation is provided by adding the possibility of modifying the genetic qubit or introducing errors in the replication stage. Finally, the individuals live in a discrete spatial grid in which they move by virtue of a random process, see Fig 3.1. When they share the same location, they interact with each other, in an operation that modifies the phenotype but preserves the genotype. In the following, we explain in detail the physical operations underlying the different aspects of our model.

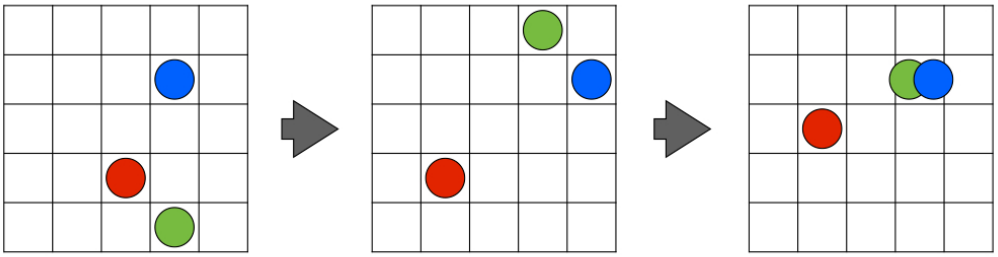

Figure 3.1: **Spatial Dynamics.** Coloured circles represent individuals that move in discrete time-steps along a periodic spatial grid. This schematically illustrates how two individuals can share the same location and interact.

Self-replication

The mechanism of self-replication is based on the cloning of partial quantum information explained on the previous chapter, Chapter 2. The qubit in which the information is encoded is coupled with an ancillary state that belongs to the environment. The information transmission consists in an entangling operation that distributes the information throughout the two-qubit quantum state. After the partial quantum cloning process, the information can be retrieved from both subspaces independently. Specifically, the expectation value of a desired operator θ in any quantum state ρ_0 can be propagated into the following generations ρ_1 with the use of an ancillary state ρ_A and a unitary operation U,

$$\langle\theta\rangle_{\rho_0} = \langle\theta\otimes\mathbb{1}\rangle_{\rho_1} = \langle\mathbb{1}\otimes\theta\rangle_{\rho_1}, \qquad \rho_1 = U(\rho_0\otimes\rho_A)U^\dagger. \tag{3.1}$$

In particular, we are using the expectation value of σ_z as the genotype of the individuals and the U_{CNOT} gate as the cloning operation. Different combinations of observables and cloning operations would also satisfy the partial quantum cloning criteria, but we have selected σ_z because it is diagonal in the basis given by the steady state of the environment. By construction, unlimited copies of the ancillary quantum state ρ_A are available in our model everywhere in the spatial grid, and they belong to the dark state of the dynamics that governs the interaction between individuals and environment. A new individual is produced in two steps. In the first one, the genotype belonging to the procreator individual is copied onto an ancillary state in

order to produce a new genotype. In the second step, the genotype of the new generation is copied onto another ancillary state in order to produce the phenotype. There is a fixed probability of self-replication that is equal for all individuals, since it does not depend on the genotype. The only requirement for the generation of a newborn individual via the self-replication process is that the procreator individual is alive. This property is encoded in the phenotype and depends on the interaction of the individual with the environment, as we describe below.

Environment

When the new individual is created, its genotype and phenotype exactly contain the same information. However, they progressively differentiate as the system evolves due to the coupling of the phenotype with the environment. This mechanism mimics a crucial feature in natural selection, namely, the preservation of the genetic information throughout successive generations. At the same time, the phenotype is degraded due to the interaction with the environment, which concludes with the death of the quantum living unit.

The dissipation is modeled with a Lindblad master equation, whose steady state corresponds to the ancillary state of the copying process, ρ_A. We define the Lindblad operators as acting in the natural basis of the environment, given by the σ_z basis of the self-replication process, i.e.,

$$\dot{\rho} = \mathcal{L}\rho = \gamma(\sigma\rho\sigma^\dagger - \frac{1}{2}\sigma^\dagger\sigma\rho - \frac{1}{2}\rho\sigma^\dagger\sigma), \qquad \sigma = |0\rangle\langle 1|, \qquad \rho_A = |0\rangle\langle 0|. \quad (3.2)$$

By evolving the system under this Lindbladian $\mathcal{L}$, all individuals end up in the state ρ_A. Therefore, we use this physical register to simulate the death of the quantum living unit. The cycle closes since the dead individuals serve as ancillary states for the new generations.

We can illustrate the processes of self-replication and aging with a generic example in which an individual and its progeny are created out of a precursor genotype. Let us suppose that, initially, there is a single genetic qubit ρ_g copied into a phenotype qubit in order to create an individual ρ_0,

$$\rho_g = \begin{pmatrix} a & b - ic \\ b + ic & 1 - a \end{pmatrix}, \qquad \rho_0(t = 0) = U(\rho_g \otimes \rho_A)U^\dagger. \quad (3.3)$$

The individual evolves under the dissipative dynamics with $\sigma = \mathbb{1} \otimes |0\rangle\langle 1|$,

$$\rho_0(t) = \begin{pmatrix} a & 0 & 0 & (b-ic)e^{-\frac{1}{2}\gamma t} \\ 0 & 0 & 0 & 0 \\ 0 & 0 & (1-a)(1-e^{-\gamma t}) & 0 \\ (b+ic)e^{-\frac{1}{2}\gamma t} & 0 & 0 & (1-a)e^{-\gamma t} \end{pmatrix} \quad (3.4)$$

The expectation value of σ_z remains constant in the genotype subspace, but exponentially decays in the phenotype subspace,

$$\langle \sigma_z \rangle_g = 2a - 1, \qquad \langle \sigma_z \rangle_p = 1 - 2e^{-\gamma t}(1-a). \quad (3.5)$$

The expectation value $\langle \sigma_z \rangle_p(t)$ measuring the age of the individual depends on a single genetic parameter a, and on the elapsed time in the evolution from the birth of the quantum living unit until its death. The death age t_d of the individual is achieved when $\langle \sigma_z \rangle_p(t_d) = 1 - \epsilon$, for fixed ϵ.

The individual continues its evolution until the self-replication protocol begins, as described in Fig. 3.2. This protocol consists in coupling an ancillary state ρ_A with the individual ρ_0 and performing the U operation between the genotypes of the two individuals. The next step is to use another ancillary state from the environment and perform the U gate between the genotype and phenotype of the new individual. We denote the self-replication time by t_1, after which the whole system is coupled with the environment via the Lindblad master equation for a time t_2. The expectation values of σ_z for the genotype and phenotype of the two individuals are given by

$$\begin{aligned} \langle \sigma_z \rangle_{g1} &= 2a - 1, \qquad \langle \sigma_z \rangle_{p1} = 1 - 2e^{-\gamma(t_1+t_2)}(1-a), \\ \langle \sigma_z \rangle_{g2} &= 2a - 1, \qquad \langle \sigma_z \rangle_{p2} = 1 - 2e^{-\gamma t_2}(1-a). \end{aligned} \quad (3.6)$$

Mutations

The mutation process enhances diversity in biological systems, which is a fundamental property of Darwinian evolution. The system adaptability to a changing environment is closely related to its mutation capacity. In our model, the mutation is a physical operation upon the individuals, which changes their genotype. We distinguish between two types of mutations, implemented with a small probability. On the one hand, there are spontaneous

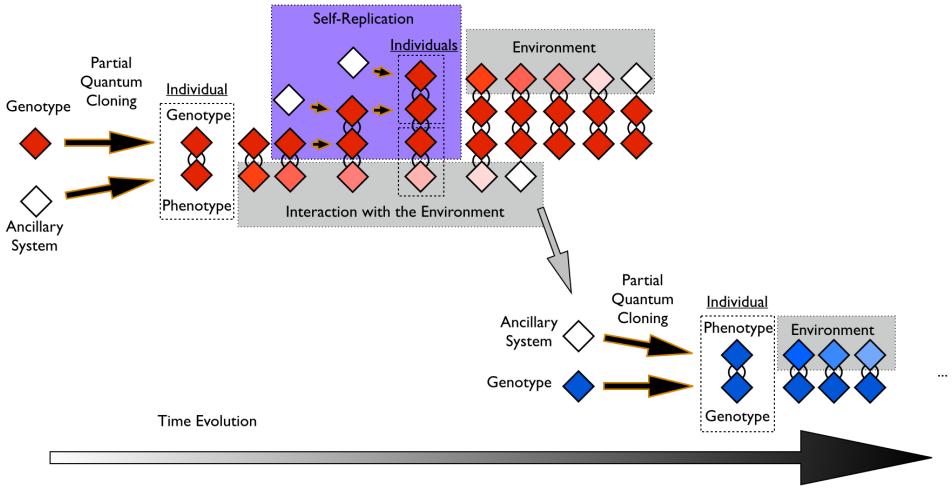

Figure 3.2: **Self-replicating Individuals.** We schematize a timeline in the evolution of individuals. Firstly, an individual is created out of a primordial genotype by combining it with an ancillary system. Then, the individual interacts with the environment which produces a gradual loss in the information of the phenotype, until the death of the individual. In the mean time, the living unit generates a new individual via the self-replication process. Additionally, the remaining phenotype can be used as a new ancillary state for the creation of another individual.

mutations upon the genotype subspace of an individual, given by the unitary matrix M,

$$M = \begin{pmatrix} \cos\theta & \sin\theta \\ \sin\theta & -\cos\theta \end{pmatrix}. \tag{3.7}$$

The mutation parameter θ is random and different for every mutation event in order to maximize the Hilbert space region spanned by the quantum states, and therefore maximize the biological diversity. On the other hand, there are mutations associated with errors in the copying process, modeled by imperfect cloning unitary operations U_M,

$$U_M(\theta) = \mathbb{1}_4 + \frac{1}{2}\begin{pmatrix} 0 & 0 \\ 0 & 1 \end{pmatrix} \otimes \begin{pmatrix} -1 & 1 \\ 1 & -1 \end{pmatrix} (\cos\theta + i\sin\theta + 1). \tag{3.8}$$

The difference between these mutation operations relies on the fact that M does not affect the phenotype of the mutated individual, while U_M changes both the genetic information and the lifetime.

Interactions

In the formalism explained so far, the natural selection mechanism is completely biased towards the long-living individuals, corresponding to $a \sim 0$ and $\langle \sigma_z \rangle \sim -1$. As the self-replicating probability is equal for all of them, the long-living individuals dominate the system due to the generation of a larger offspring. On the contrary, the possibility of interactions between pairs of individuals favors the short living individuals, and restores the equilibrium between long and short life genotypes. The idea behind the process is that individuals conditionally interchange their phenotype when meeting each other. The conditionality depends on the genotype, namely, the interaction is minimal for equal genotypes $a_1 = a_2$ and maximal for opposite ones, $a_1 = 1$, $a_2 = 0$ and viceversa. The physical operation U_I that performs the interaction between two individuals is

$$\begin{aligned} U_I =& k_1 \otimes (\mathbb{1} \otimes k_1 \otimes \mathbb{1} + k_1 \otimes k_4 \otimes k_1 + k_4^{\otimes 3} + k_2 \otimes k_4 \otimes k_3 + k_3 \otimes k_4 \otimes k_2) + \\ & k_4 \otimes (\mathbb{1} \otimes k_4 \otimes \mathbb{1} + k_1^{\otimes 3} + k_4 \otimes k_1 \otimes k_4 + k_2 \otimes k_1 \otimes k_3 + k_3 \otimes k_1 \otimes k_2), \end{aligned} \tag{3.9}$$

with $k_1 = |0\rangle\langle 0|$, $k_2 = |0\rangle\langle 1|$, $k_3 = |1\rangle\langle 0|$, $k_4 = |1\rangle\langle 1|$. See Fig. 3.3 for a graphical representation.

Here, U_I is a logical gate acting on two control qubits and two target qubits, which is defined in the computational basis as follows. When the control qubits are equal, the target qubits remain unchanged. On the contrary, when the control qubits are different, the target qubits are exchanged. In particular, we have selected the first and the third subspaces as control qubits. A direct implication of the interaction process is that, when a short-living individual encounters a long-living one, the lifetime of the former increases, while the lifetime of the latter decreases. Therefore, to have a genotype parameter $a \sim 1$ is more advantageous in this case, because it corresponds to the role of a predator in our model. According to this, every individual is a combination of predator and prey depending on its instantaneous phenotype and the local environment. Notice that the role of predator and prey can be completely interchanged in consecutive events for individuals that have

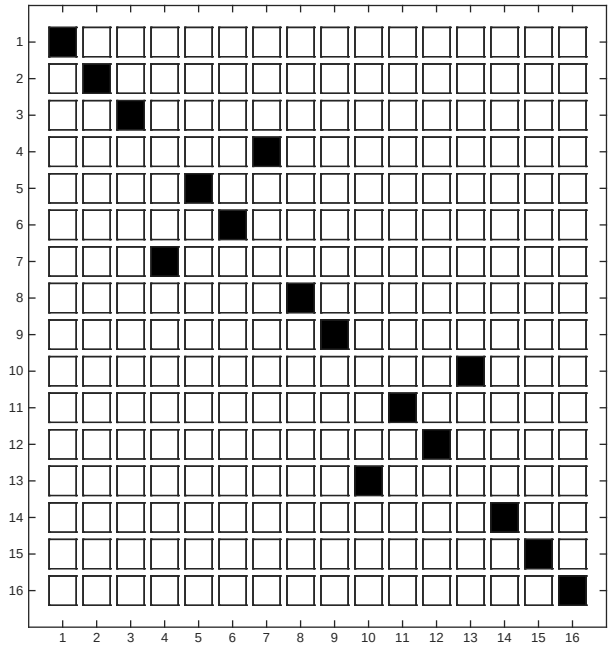

Figure 3.3: **Interaction unitary.** U_I matrix is represented in this figure, where the color of the squares denotes the value of the corresponding matrix component, white for 0 and black for 1.

previously interacted. The probability of this second-order event is low, and it depends on the interaction rate, which at the same time depends on the spatial distribution of the individuals and the grid geometry. Therefore, for each initial state of a particular individual, there are a grid geometry and distribution of the other quantum living units, which respectively optimize the survival probability and the interaction rate for the system of individuals.

Spatial Dynamics

In our model, the individuals live in a two-dimensional grid divided into cells, as seen in Fig. 3.1. The spatial distribution of the individuals determines the interaction rate, because they only interact when occupying the same cell. The displacement along the grid is a random process, and the proposed model allows for two or more individuals occupying the same cell.

Furthermore, the grid can be split into distinct spatial regions with different properties: mutation rate, self-replication probability, and coupling constant with the environment. These are basic properties of the model associated with physical processes encoded in the genotype and phenotype, as we show in Fig. 3.4.

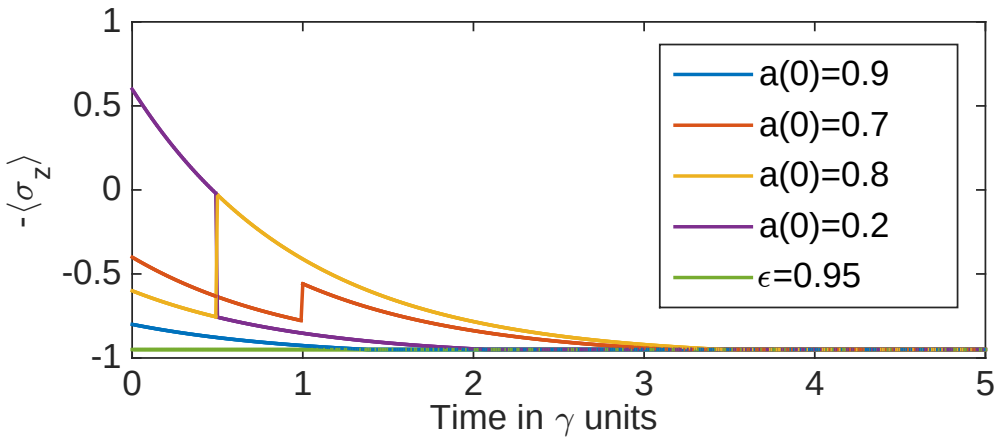

Figure 3.4: **Processes in the artificial life model.** We plot a combination of the genotype and phenotype of the individuals that depends on the genotype parameter a and the time t in which the individual has been in contact with the environment. The life quantifier is $\langle\sigma_z\rangle_p$, whose asymptotic value represents the death of the individual in the bottom of the figure. Each colour is associated with a basic process in the model: the blue line ($a = 0.9$) shows the dissipation of the phenotype due to the environment, the orange line ($a = 0.7$) depicts a mutation process event, and the yellow and purple lines, $a_1 = 0.8$ and $a_2 = 0.2$ respectively, illustrate an interaction process.

3.3 Numerical Simulations

In this section, we explain the dynamical numerical simulations based on our model. Classical artificial life models may address relevant questions about the properties of the self-replicating units: Which kind of individuals have maximized their survival probability by adapting to the environmental characteristics and the presence of other individuals? Is this an asymptotic

behaviour or on the contrary is a part of a cycle in populations? In the case in which more than one species dominates how distinct are their genotypes, and has any complex spatial organization emerged? In our case, the time evolution is computationally hard due to the exponential growth of the Hilbert space dimension with the number of individuals. Therefore, answering these questions in our context may motivate the realization of our proposal in an experiment on a controllable quantum platform, as discussed below. In our current analysis, we numerically examine other interesting properties, such as the information spreading and the genotype and phenotype diversities.

In order to study the information spreading and the mean path of the individuals, we generate a position histogram of the quantum living units for a large number of realizations, with fixed initial conditions. Moreover, the density in each cell is related to the probability of finding a single individual in that particular position. Therefore, we can estimate the interaction and self-replication rates by comparing position histograms corresponding to different parameters in the model, as shown in Fig. 3.5. Larger values of the position histogram peaks indicate the presence of additional individuals, and therefore, a larger amount of self-replicating events.

Additionally, we have produced genotype and phenotype histograms that show the expectation value of σ_z in each subspace of every individual, providing a snapshot of the final state of the simulation. These histograms evidence the preservation of the initial genotypes, the decay of the phenotypes, as well as the mutations and interactions which give origin to diversity, see Fig. 3.6. The deviation of the initial information in the genotype is related to mutation events. In contrast, the deviation from the initial peak in the phenotype histogram is related to interaction events, when simultaneously produced in two individuals. Otherwise, the change in the phenotype is due to a mutation followed by a self-replication event.

Quantumness

The entanglement among different individuals allows us to clone the classical information and propagate the quantum coherences of the initial quantum living units to the successive generations. Nevertheless, the fact that our model requires the solution of a Lindblad master equation for a large number of entangled qubits, restricts the solution of the model to a small number of individuals and short times. Some of the features of our model are purely quantum, for instance, the entanglement among individuals with the same

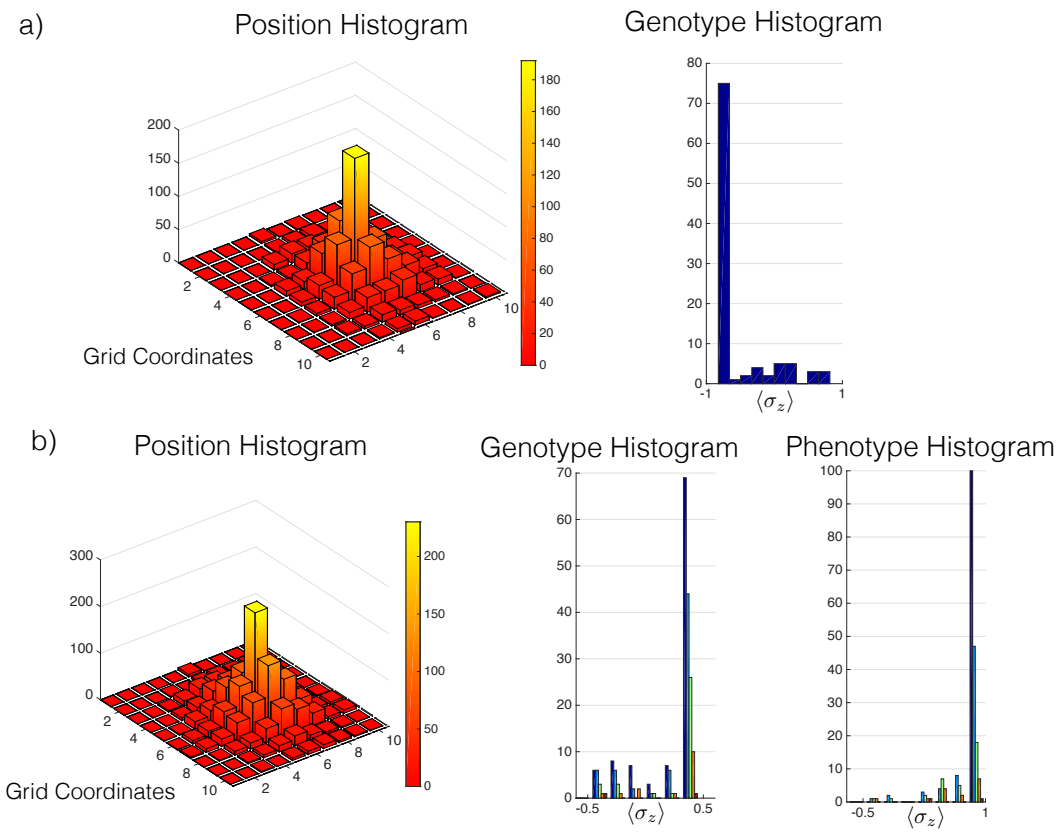

Figure 3.5: **Numerical simulation of replicating and non-replicating individuals.** These plots are obtained evolving an individual with a random genotype at a given initial position during a time $\gamma t = 10$. The position histogram shows the accumulation of the paths covered by the living unit for all runs of the simulation. The genotype histogram shows the expectation value of σ_z in the genotype subspace after each simulation. The initial individual does not self-replicate in (a), while it does self-replicate in (b), therefore the secondary peaks in the genotype and phenotype histograms appear in (b) as a consequence of the newborn individuals.

origin permits to measure collective correlations of the whole family. In this way, we can both distinguish between individuals with the same or different genotype, and individuals with the same or different origin. The physical mechanism in which we are basing our claim is the propagation of the collec-

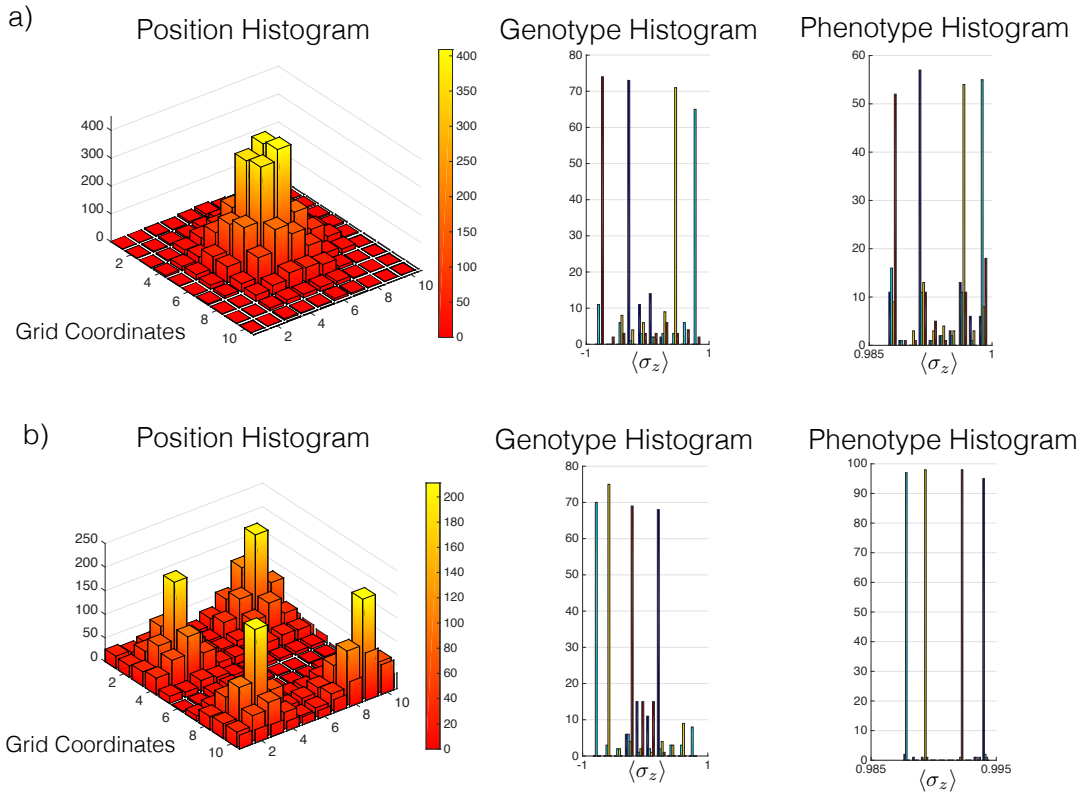

Figure 3.6: **Numerical simulation of interacting and non-interacting individuals.** We have limited the simulation of our model to 4 initial individuals until a maximum time of $\gamma t = 10$. No self-replicating events are allowed, and therefore, the diversity in the phenotype is due to interaction events. (a) The interaction rate is increased because of the short distances among the living units. (b) The interaction rate is small because of the long distances among the living units. Therefore, the secondary peaks in the phenotype histogram (a) are associated with interaction events which exchange the phenotype of individuals.

tive expectation value $\langle\tau\rangle$ in the previous chapter, see Fig. 3.7. Additionally, the individuals are in a superposition of a prey and predator, which allows us to simulate a trophic chain behaviour encoded in the two qubits that conform each individual.

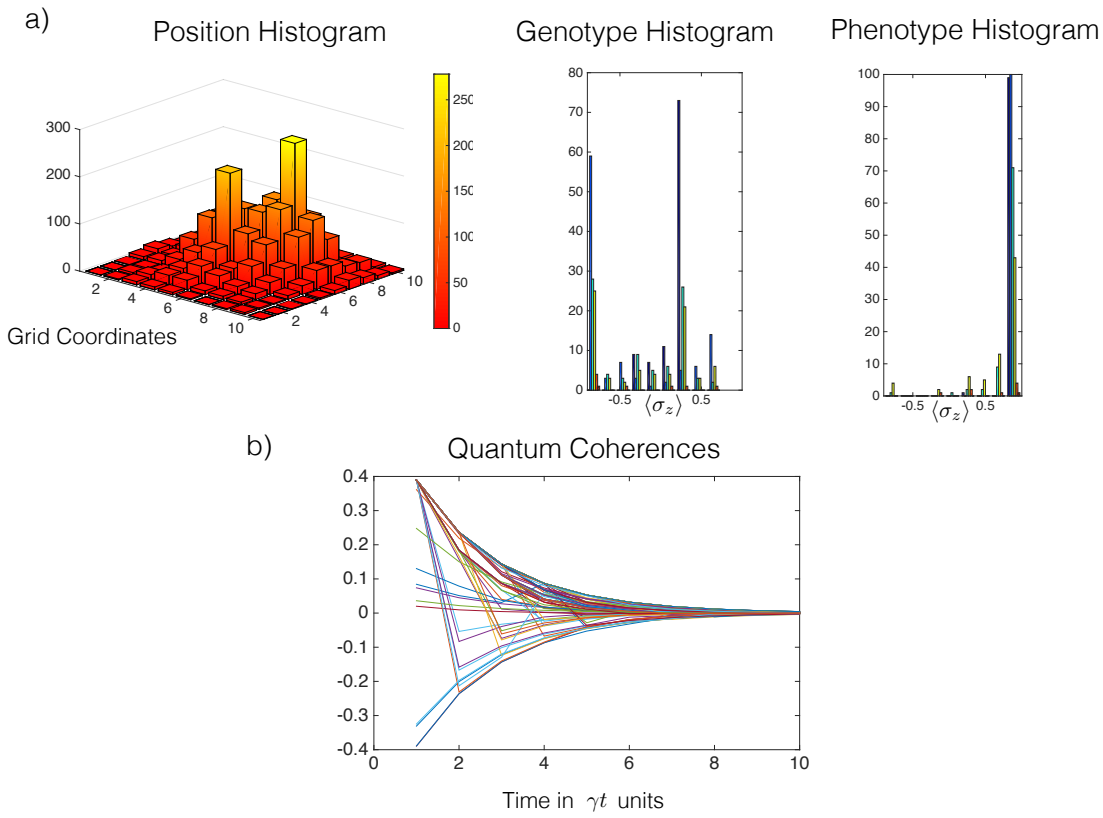

Figure 3.7: **Numerical simulation with quantum coherences.** Data compilation for 100 simulations of the time evolution of two initial individuals allowed to self-replicate. (a) The position histogram shows two peaks of the initial spatial distribution and the spread of the individuals as time increases. The effects of the copying process are illustrated in the genotype histogram with the presence of secondary peaks behind the principal one that corresponds to the original individual. The small peaks in the phenotype histogram represent the newborn individuals. In (b), we have depicted the expectation value of σ_x in all subspaces, $\langle\sigma_x^{\otimes 2n}\rangle$, where n is the number of individuals. These quantum coherences give us information about the history of the individual. Therefore, we can infer the mutation and interaction events as well as the dissipative dynamics.

Connections with other fields

In the same way that classical artificial life models can be applied in other areas of science, we think that our protocol is closely related with some aspects of quantum information theory. One can understand the model as a naturally emergent maximization problem of survival under the rules imposed by the environment, mutation rate, grid geometry and self-replication rate. The rules are external and tunable, which means that we could encode optimization problems and solve them by using an artificially-engineered natural-selection quantum mechanism. Furthermore, our model of natural selection can be related to quantum game theory and quantum learning, if we consider that each of the genotypes encodes a strategy, and the environment together with the aforementioned elements establish the rules of the game. Typically, the players with winning strategies survive, a fact that makes the rewarding mechanism an intrinsic part of the game. Under these analogies, it may also be possible to analyze the robustness of the optimization process or the strategy by changing the parameters describing the proposed model.

From all existing quantum protocols those in the line of quantum cellular automaton are the ones that lie closer to the ideas presented here. Nevertheless, we point out that our quantum biomimetic model is not a particular case of a quantum cellular automaton (QCA). In a QCA, the information is encoded in the spatial grid, while in our model the information is stored in individuals that displace along the spatial grid. Therefore, the time evolution in the QCA system is by construction different to the time evolution in our model. In a QCA, the spatial lattice state at time t is obtained by updating the one at $(t-1)$ according to the automaton transition function [48].

3.4 Quantum Artificial Life in Different Experimental Platforms

Our model may be implemented on a variety of quantum platforms, which would be justified due to the theoretical interest and the computational difficulty of classical simulations to answer several relevant questions. Here, we provide an encoding of the information in the respective qubits and the sequences of gates implementing our dynamics for superconducting circuits [16, 17], trapped ions [18, 19, 20] and quantum photonics [21, 22, 23].

The U_{CNOT} implements the self-replication process as explained in Eq.

(3.1), the aging of the individual is simulated with the dissipation given by the Lindblad dynamics in Eq. (3.2), and the mutations may be modelled with single qubit rotations as in Eq. (3.7). Finally, the interaction among individuals given in Eq. (3.9) involves a four-qubit operation, which can be decomposed in terms of the Toffoli gate, U_{CCNOT}, by relabeling the levels encoding the quantum state. We point our that this relabeling is also a non-trivial quantum gate,

$$\{|4\rangle, |7\rangle\} \to \{|7\rangle, |8\rangle\}, \;\; \{|10\rangle, |13\rangle\} \to \{|15\rangle, |16\rangle\} \implies U_I \to \mathbb{1} \otimes U_{\mathrm{CCNOT}}. \tag{3.10}$$

Trapped Ions

In trapped ion devices, chains of ions are spatially confined by using time dependent electromagnetic fields. The physical system is described with a model that results in a set of internal (electronic) and collective (motional) quantized energy levels. Laser fields tuned in the frequencies of the desired transitions provide a good control of the system allowing for the implementation of several physical operations that can be translated into logical ones. In particular, we show the trapped-ion control Hamiltonian for a single spin and a single mode,

$$H = \Omega\sigma^{+}\left[1 + i\eta\left(ae^{-i\nu t} + a^{\dagger}e^{i\nu t}\right)\right]e^{i(\phi-\delta t)} + \mathrm{H.c.} \tag{3.11}$$

Therefore, trapped ions can be used as quantum information processing experimental platforms. Here, Ω is the Rabi frequency, σ^{+} the spin raising operator, η the Lamb-Dicke parameter, a and $a^{\dagger}$ the motional annihilation and creation operators, ν the trap frequency, ϕ the initial phase of the laser field and δ the detuning between the laser and qubit frequencies.

In our proposal, each quantum living unit, composed of two qubits, can be encoded either in four metastable levels of a single ion or two levels of a pair of ions, and ancillary levels enable the readout of the state [18]. The U_{CNOT} can be implemented with the Mølmer-Sørensen gate and a sequence of single-qubit gates [81]. We rely on previous proposals [82] for simulating the dissipative dynamics. Mutations as single qubit rotations could be done with controlled Rabi oscillations between the levels that encode the genotype. The interaction among individuals can be realized with the Toffoli gate, that has already been implemented in a trapped-ion setup [83].

Superconducting Circuits

The superconducting circuits are designed with inductors, capacitors and Josephson junctions as building elements. The main properties of the circuits are the superconductivity that allows the flow of electrical current without energy dissipation, and the nonlinear separation of the quantized energy levels introduced by the Josephson junctions. The effective equation that describes the time evolution of the charge and phase, the degrees of freedom in the superconducting circuit, can be manipulated by rearranging the disposition of the circuit elements. The system can be controlled by coupling it with resonant photons, which allows for the implementation of several physical models, including the Jaynes-Cummings model,

$$H = \omega_r a^\dagger a + \epsilon \sigma^+ \sigma^- + g(a\sigma^+ + a^\dagger \sigma^-). \tag{3.12}$$

Here, ω_r is the photon frequency, g is the coupling constant, and ϵ is the qubit frequency, which is encoded in the quantum excitations of the circuit.

For the particular aspects of our proposal, the transmon is the most appropriate superconducting qubit, because of its long coherence time. The single and two qubit gates used for implementing self-replication and mutations can be realized with high fidelities [84]. The controlled dissipation necessary for encoding the evolution of the phenotype can be realized with current technology [85]. The Toffoli gate performing the interaction processes among individuals is feasible in superconducting circuits [86].

Quantum Photonics

In quantum photonics devices, quantum information processing tasks are implemented with linear optical elements: beam splitters, phase shifters, single photon sources and photodetectors. The qubit is encoded in the coherent superposition of two modes in a photon. The variation in the refractive index, and the interaction between the modes are the physical mechanism introduced by the phase shifters and beam splitters respectively. These operations allow for the realization of deterministic single qubit gates, and are modeled with the following Hamiltonians

$$H_{ps} = \phi a_{in}^\dagger a_{in}, \qquad H_{bs} = \theta e^{i\phi} a_{in}^\dagger b_{in} + \theta e^{-i\phi} a_{in} b_{in}^\dagger. \tag{3.13}$$

Here, a and b are the modes in which the qubit is encoded, ϕ is the relative phase and θ the phase associated with the transmission amplitude. Moreover,

two qubit gates are performed probabilistically, employing the Hong-Ou-Mandel effect as a computational resource.

These techniques provide a complete set of single and two qubit gates, that can be extended for particular logical operations, like the Toffoli gate [87]. Therefore, the self-replication, mutations and interactions in our model can be realized in an experimental protocol with photons. Finally, a technique for the implementation of stochastic quantum walks [23] could be used to simulate the evolution of the phenotype.

3.4.1 Proof of Principle

More precisely we would like to discuss the implementation of an experimental proof of principle about the Quantum Artificial Life model in an integrated photonics architecture. The goal is to reproduce the first steps in the timeline of a given individual. These involve a self-replication event and the environment induced aging for both living units. In physical terms, the realization of three consecutive U_{CNOT} gates is required together with the engineering of dissipation in the phenotype-encoding qubits. Inspired by the result in bulk optics, [88], the U_{CNOT} gate can be implemented in path encoded qubits, supported in pairs of waveguides [24]. The U_{CNOT} is achieved with three generations of directional couplers, aided by two auxiliary waveguides, after post selecting in the coincidence basis.

The proposed theoretical idea is experimentally challenging for three main reasons. Firstly, the number of gates is bounded by the physical limitation of the length of the chip allowing for a fixed number of directional couplers generations. Secondly, the total number of qubits requires the simultaneous generation of four photons, which is technologically demanding. Thirdly, the concatenation of post selected operations, like the U_{CNOT} gate, makes the rate of successful events decrease, and therefore requires an increasing number of resources.

Nevertheless, there is an ongoing collaboration for the design and realization of the Quantum Artificial Life experiment in which the author of this thesis is involved.

3.5 Conclusions

We have developed a quantum information model for mimicking the behaviour of biological systems inspired by the laws of natural selection. Our protocol is hardly tractable with classical simulations, leaving many relevant questions coming from the classical models without answer in our quantum analogue. Simultaneously, we have analyzed several figures of merit, which provide partial information about the quantum features of the model for small systems. Finally, we have studied the feasibility of the protocol in different physical systems, which enables the realization of artificial life in quantum technologies.

Part II

Mnemonic Quantum Systems

Chapter 4

Algorithmic Quantum Simulation of Memory Effects

> Life can only be understood backwards; but it must be lived forwards.
>
> *Søren Kierkegaard*

In this chapter, we propose a method for the algorithmic quantum simulation of memory effects described by integro-differential evolution equations. It consists in the systematic use of perturbation theory techniques and a Markovian quantum simulator. Our method aims to efficiently simulate both completely positive and non-positive dynamics without the requirement of engineering non-Markovian environments. Finally, we find that small error bounds can be reached with polynomially scaling resources, evaluated as the time required for the simulation.

4.1 Introduction

Fundamental interactions in nature are described by mathematical models that frequently overcome our analytical and numerical capacities. This problem is especially challenging in the quantum realm, due to the exponential growth of the Hilbert space with the number of particles involved. Richard Feynman proposed that the desired calculations may be experimentally realised by codifying the model of interest into the degrees of freedom of another

more controllable quantum system [1]. Along these lines, in the last decade, this approach has been employed to simulate the dynamics of many-body quantum systems. A machine performing this task is called quantum simulator, and it has been studied with increasing interest, theoretically and experimentally, in controlled quantum systems [5, 89]. It is expected that quantum simulators will solve relevant problems unreachable for classical computers. Among them, we could mention complex spin, bosonic, and fermionic many-body systems [4, 5], entanglement dynamics [32, 90], and fluid dynamics [91], among others.

In quantum mechanics, realistic situations in which the quantum system is coupled to an environment are modeled in the framework of open quantum systems. In this description, an effective evolution equation for the system of interest is obtained by disregarding the environmental degrees of freedom [11]. The resulting dynamics can be classified as Markovian or non-Markovian [92, 93, 94, 95, 96, 97]. In the former, the time evolution depends solely on the current state of the system, and there are several results concerning its quantum simulation [12, 13, 14, 15]. On the contrary, the non-Markovian evolution depends on the history of the system, and it is more challenging to treat both analytically and numerically [13]. In this sense, despite some recent results [98, 99, 100, 101, 102, 103, 104, 105, 106, 107, 108, 109], including a work on the sufficient conditions for a CPTP non-Markovian dynamics [100], a general non-Markovian quantum simulator has not been fully developed yet. A paradigmatic feature of non-Markovian dynamics is the existence of quantum memory effects as an extension of the classical history-dependent dynamics to the quantum domain. Moreover, a number of key applications in the quantum domain can be envisioned, such as quantum machine learning [110, 111], neuromorphic quantum computing [112, 113] and quantum artificial life in Chapters 2 and 3. These can be implemented by mirroring the already existing results in memcomputing devices [114], intelligent materials [115] and population dynamics [116]. Therefore, the simulation of quantum memory effects would be a significant step forward to understand open quantum systems and, consequently, to employ them in the development of the aforementioned research fields.

In this chapter, we provide an efficient and general framework for an algorithmic quantum simulation of memory effects modeled by integro-differential evolution equations [1]. The protocol algorithmically combines a Markovian

[1]Our concept of algorithmic quantum simulation is not equivalent to the one presented

quantum simulator with perturbation theory techniques in order to retrieve the time evolution of an arbitrary initial state. Our method does not require the engineering of any additional environment, avoiding the challenging task of developing first-principle non-Markovian quantum simulators. Moreover, the protocol works even when the evolution does not correspond to a completely positive and trace preserving (CPTP) map, which is the case of most of time-delayed Lindblad master equations. Indeed, although the CPTP character is not guaranteed, our approach circumvents this issue by splitting the simulation in two CPTP parts. Finally, we prove polynomial scaling error bounds for the proposed method.

4.2 Description of the Quantum Algorithm

The model describing the memory effects we aim to simulate is based on the integro-differential equation

$$\partial_t \rho(t) = \int_0^t ds\, K(t,s) \mathcal{L}\, \rho(s). \tag{4.1}$$

Here, $K(t,s)$ is a memory Kernel modeling how the evolution of the state at a certain time is affected by its history, and $\mathcal{L}$ is a general time-independent Lindblad operator. Notice that $K(t,s) = 2\delta(t-s)$ corresponds to the standard Markovian master equation written in the Lindblad form. As noticed for instance in Refs. [13] and [101], it is not conceivable to simulate a general non-Markovian dynamics efficiently. The reason is that one could then imagine simulating a highly inefficient calculation in the environment, retrieving afterwards this information into the system due to the non-Markovian information backflow, in an efficient manner. However, Equation (4.1) includes in the Kernel $K(t,s)$ the non-Markovian aspects of the evolution, which gives only an effective description of the environment contribution.

In order to simulate Eq. (4.1), we use as a tool the quantum simulation of the equation

$$\partial_t \rho(t) = \int_0^t ds\, H(t,s) \left[\mathcal{E} - \mathcal{I}\right] \rho(s), \tag{4.2}$$

by D. Wang [117], even if both approaches involve a combination of classical processing and quantum simulation. While in the protocol of D. Wang, the classical part is used for optimizing the design of quantum circuits, in our protocol the classical processing involves the numerical integration of certain functions depending on the measurement outcomes and memory kernels.

where $H(t,s)$ is a memory Kernel, $\mathcal{E}$ is a general CPT map and $\mathcal{I}$ is the identity map. Equation (4.2) describes the dynamics of a *semi-Markovian* process [118]. It is noteworthy to mention that while Eqs. (4.1) and (4.2) preserve the trace of the density matrix, they do not generally preserve positivity. However, sufficient conditions for Eq. (4.2) to determine a CPT map have been studied when $H(t,s) = H(t-s)$. Indeed, if the Laplace transform of the memory kernel $H(\tau)$ satisfies the relation $\tilde{H}(u) = \frac{u\tilde{w}(u)}{1-\tilde{w}(u)}$ for some waiting distribution $w(t)$, then Eq. (4.2) corresponds to a CPT process [119]. Moreover, if this condition is fulfilled, then the solution of Eq. (4.2) can be written as $\rho(t) = \sum_{i=0}^{\infty} p_i(t)\mathcal{E}^i\rho(0)$, where $0 \leq p_i(t) \leq 1$ [119]. In this case, by truncating the series, we can simulate Eq. (4.2) assuming that an efficient quantum simulator of $\mathcal{E}$ and its powers is available. In the following, we will consider processes $\mathcal{E}$ corresponding to Markovian evolutions, whose efficient quantum simulator has been already designed, e.g. k-local Lindblad equations [13]. We will show how to simulate a general kernel $H(t,s)$, including the case in which Eq. (4.2) does not correspond to a CPT process. Finally, we illustrate how to employ this result to simulate Eq. (4.1).

4.2.1 Simulation of Semi-Markovian Dynamics

Let us consider the Volterra version of Eq. (4.2),

$$\rho(t) = \rho(0) + \int_0^t ds\, h(t,s)\,[\mathcal{E} - \mathcal{I}]\,\rho(s), \tag{4.3}$$

where $h(t,s) \equiv \int_s^t d\tau\, H(\tau,s)$. We assume that $H(t,s) \geq 0$ and $h(t,s) \leq c$, for a given constant c, for all $t \geq s \geq 0$. Moreover, we quantify the results in terms of the trace norm for matrices, defined as the sum of their singular values $\|\sigma\|_1 \equiv \sum_i \sigma_i$, and the respective induced superoperator norm $\|\mathcal{A}\| \equiv \max_\sigma \frac{\|\mathcal{A}\sigma\|_1}{\|\sigma\|_1}$. Then, Eq. (4.3) can be iteratively solved, via the series $\rho(t) = \sum_{i=0}^{\infty} \rho_i(t)$, where

$$\rho_0 = \rho(0), \quad \rho_{i\geq 1} = \int_0^t ds\, h(t,s)\,[\mathcal{E} - \mathcal{I}]\,\rho_{i-1}(s). \tag{4.4}$$

This expansion can be truncated at order n, $\tilde{\rho}_n(t) = \sum_{i=0}^{n} \rho_i(t)$, with a small truncation error given by the following estimation.

Proposition 1 (Truncation error)**.** $\|\rho(t) - \tilde{\rho}_M(t)\|_1 \leq \varepsilon$ *provided that* $M \geq at + \log 1/\varepsilon - 1$, *with* $a = (e+1)c\,\|\mathcal{E} - \mathcal{I}\|$.

Proof. First, we notice that $\tilde{\rho}_n(t)$ respects the relation

$$\tilde{\rho}_n = \rho(0) + \int_0^t ds\, h(t,s)\,[\mathcal{E} - \mathcal{I}]\,\tilde{\rho}_{n-1}(s), \quad \tilde{\rho}_{-1} \equiv 0. \tag{4.5}$$

From Eqs. (4.3)-(4.5) we directly see that, for $n \geq 1$, $\|\rho(t) - \tilde{\rho}_n(t)\|_1 \leq yc \int_0^t ds\, \|\rho(s) - \tilde{\rho}_{n-1}(s)\|_1$, where we have denoted $y \equiv \|\mathcal{E} - \mathcal{I}\|$, and we have used that $h(t,s) \leq c$. For $n = 0$ we have that $\|\rho(t) - \tilde{\rho}_0(t)\|_1 \leq y \int_0^t ds\, h(t,s) e^{y\int_0^s d\tau\, h(s,\tau)} \leq e^{cyt} - 1$, where we have used that $h(s,\tau) \leq h(t,\tau)$ for $s \leq t$, and Grönwall's inequality in order to bound $\|\rho(s)\|_1 \leq e^{y\int_0^s d\tau\, h(s,\tau)}$, see Appendix B. One can prove by induction that

$$\|\rho(t) - \tilde{\rho}_M(t)\|_1 \leq \sum_{i=M+1}^{\infty} (cyt)^i / i!, \tag{4.6}$$

which is bounded by $e^{cyt}(cyt)^{M+1}/(M+1)!$ The last expression is bounded by ε provided that $M \geq (e+1)cyt + \log(1/\varepsilon) - 1$, which concludes the proof. □

This truncation allows us to write the approximated solution of Eq. (4.2) by a finite sum, with a number of terms growing linearly with the simulated time. Indeed, we have that

$$\tilde{\rho}_n(t) = \sum_{i=0}^{n} d_i(t)\,[\mathcal{E} - \mathcal{I}]^i\,\rho(0), \tag{4.7}$$

with the corresponding parameter values $d_0(t) = 1$ and

$$d_{i\geq 1}(t) = \int_0^{s_0 \equiv t} \cdots \int_0^{s_{i-1}} ds_1 \cdots ds_i\, h(t,s_1) \cdots h(s_{i-1}, s_i). \tag{4.8}$$

This truncated sum can be rewritten as $\tilde{\rho}_n(t) = \sum_{i=0}^n c_i(t)\mathcal{E}^i\rho(0)$, with $c_i(t) = \sum_{k=i}^n \binom{k}{i}(-1)^{k-i} d_k(t)$. Proposition 1 tells us that we can directly simulate a semi-Markovian dynamics by just implementing powers of the process $\mathcal{E}$, and numerically integrating the memory kernel. As we need a number of terms which increases linearly with the simulated time, we have that this step is efficient if the implementation of the $\mathcal{E}$ is efficient. Notice that, by construction, $\tilde{\rho}_n$ has trace one, but it is not necessarily a density matrix, since it can have negative eigenvalues. However, we can write $\tilde{\rho}_n(t)$ as a

weighted sum of two density matrices and introduce the quantities $c_i^+(t) \equiv \max\{c_i(t), 0\}$ and $c_i^-(t) \equiv \min\{c_i(t), 0\}$. In consequence, we have that

$$\tilde{\rho}_n(t) = C_n^+(t)\rho_n^+(t) + C_n^-(t)\rho_n^-(t), \tag{4.9}$$

where the parameter values $C_n^\pm(t) = \sum_{i=0}^n c_i^\pm(t)$ and

$$\rho_n^\pm(t) = \frac{1}{C_n^\pm(t)} \sum_{i=0}^n c_i^\pm(t)\mathcal{E}^i\rho(0), \tag{4.10}$$

while $C_n^-(t) = 1 - C_n^+(t)$ holds due to trace preservation. Notice that $\rho_n^\pm(t)$ are two density matrices, as their trace is one and they are, by construction, positive. Indeed, we have approximated the dynamics $\Lambda(t)$ corresponding to Eq. (4.2) as a weighted sum of two CPT maps: $\Lambda(t) \simeq \Lambda_n(t) = C_n^+(t)\Lambda_n^+(t) + C_n^-(t)\Lambda_n^-(t)$, with $\Lambda_n^\pm(t) = \frac{1}{C_n^\pm(t)} \sum_{i=0}^n c_i^\pm(t)\mathcal{E}^i$. The form of the resulting CPT maps allows us to simulate Eq. (4.2) by making use of a Markovian quantum simulator and numerical techniques. In fact, all $c_i(t)$, and thus also $c_i^\pm(t)$, can be classically computed, and the states $\rho_n^\pm(t)$ can be prepared assuming that the Markovian operations $\mathcal{E}^i$ $(0 \leq i \leq n)$ are available.

Proposition 2 (Simulation of semi-Markovian processes)**.** *Let us consider the simulating dynamics* $\Lambda_{sim}(t) = C_M^+(t)\tilde{\Lambda}_M^+(t) + C_M^-(t)\tilde{\Lambda}_M^-(t)$*, where* $\tilde{\Lambda}_M^\pm(t) = \frac{1}{C_M^\pm(t)} \sum_{i=0}^M c_i^\pm(t)\tilde{\mathcal{E}}^i$*,* $\tilde{\mathcal{E}}$ *denotes an efficient quantum simulation of* $\mathcal{E}$*, and* $M \geq at + \log 1/\tilde{\varepsilon}$*. If* $\|\mathcal{E}^i - \tilde{\mathcal{E}}^i\| \leq \delta$ *requires a simulation time* $\bar{t} = O\left(\text{poly}(i, 1/\delta)\right)$*, then we can simulate the semi-Markovian process in Eq.* (4.2) *within an error* $\|\Lambda(t) - \Lambda_{sim}(t)\|_1 \leq \tilde{\varepsilon}$ *by using a simulation time* $\tilde{t} = O\left(\text{poly}(t, C_M^+(t)/\tilde{\varepsilon})\right)$*.*

Proof. We have that $\|\Lambda(t) - \Lambda_{sim}(t)\| \leq \|\Lambda(t) - \Lambda_M(t)\| + \|\Lambda_M(t) - \Lambda_{sim}(t)\|$. The first term is bounded by $\tilde{\varepsilon}/2$, as $M \geq at + \log 1/\tilde{\varepsilon}$. The second term can be bounded by $\|\Lambda_M(t) - \Lambda_{sim}(t)\| \leq C_M^+(t)\|\Lambda_M^+(t) - \tilde{\Lambda}_M^+(t)\| - C_M^-(t)\|\Lambda_M^-(t) - \tilde{\Lambda}_M^-(t)\|$. We have that $\|\Lambda_M^\pm(t) - \tilde{\Lambda}_M^\pm(t)\| \leq \tilde{\varepsilon}/4|C_M^\pm(t)|$, assuming $\|\mathcal{E}^i - \tilde{\mathcal{E}}^i\| \leq \tilde{\varepsilon}/4|C_M^\pm(t)|$. This requires a simulation time $\bar{t} = O(\text{poly}(t, C_M^+(t)/\tilde{\varepsilon})$, where we have used that $C_M^-(t) = 1 - C_M^+(t)$. □

Proposition 2 allows us to compute approximately the evolution of expectation values of observables under the dynamics of Eq. (4.2). It is noteworthy to mention that our method does not require the engineering of any bath corresponding to a semi-Markovian dynamics. Instead, we have written the

formal solution of Eq. (4.2), and exploit the availability of a Markovian quantum simulator generating $\mathcal{E}$ and its powers. This is possible due to the fast convergence of the exponential series, which limits the number of terms to be classically computed. Moreover, the truncation provided in Proposition 1 implies also that an efficient Markovian simulation is sufficient to generate approximatively the solution of Eq. (4.2).

Notice that while in the CPT semi-Markovian case we can directly sample from the probability distribution of a given observables, since we are implementing directly the solution, for more general non-Markovian equations we have only access to expectation values, as this time the process is split into two parts. A consequent question is whether we can compute interesting quantities beyond mere observables with our algorithmic quantum simulator. In the following, we study the example of the two-time correlation function of unitary operators, i.e. $D_{\rho,U}^{\Lambda(t)} = \mathrm{Tr}[U(t)U(0)\rho]$. In the last expression, $U(t) \equiv \Lambda^*(t)U$, where $\Lambda^*(t)$ is the dual of $\Lambda(t)$, defined as $\mathrm{Tr}[A(\Lambda(t)\cdot\sigma)] \equiv \mathrm{Tr}[(\Lambda^*(t)\cdot A)\sigma]$ for arbitrary A and σ. First, let us notice that $D_{\rho,U}^{\Lambda(t)} \simeq C_n^+(t)D_{\rho,U}^{\Lambda_n^+(t)} + C_n^-(t)D_{\rho,U}^{\Lambda_n^-(t)}$ for a sufficiently large n. Each resulting term can be computed with an extension to unitary dynamics of the protocol for the two-time correlation function proposed in Ref. [120]. Indeed, we add a two-dimensional ancilla and initialize the joint system in the state $\tilde{\rho} = \frac{1}{2}(|0\rangle + |1\rangle)(\langle 0| + \langle 1|) \otimes \rho$. First, we implement a controlled operation $U_c = |0\rangle\langle 0| \otimes U + |1\rangle\langle 1| \otimes \mathbb{1}$, then the evolution $\Lambda_n^{\pm}(t)$ on the original system, and finally U_c again. In the end, $D_{\rho,U}^{\Lambda_n^{\pm}(t)}$ is retrieved by measuring the operator $\sigma_x + i\sigma_y$ in the ancilla. Notice that this protocol shows the same efficiency as the one in Proposition 2. Moreover, the method can be straightforwardly extended to multi-time correlation functions of unitary operators by iterating the aforementioned steps. Lastly, the multi-time correlation functions of observables O can be computed by decomposing it into $O = U_a + \gamma U_b$, with $\gamma \in \mathbb{R}$ and $U_{a,b}$ unitary matrices [91].

4.2.2 Simulation of Quantum Memory Effects

Now, we are ready to show how to use the quantum simulation of Eq. (4.2) to simulate Eq. (4.1). Let us consider $\mathcal{E} = e^{\lambda\mathcal{L}}$, where $\lambda \in \mathbb{R}^+$ is a control parameter and $\mathcal{L}$ an arbitrary Lindblad operator, as in Eq. (4.1). In the following, we prove that the solution of Eq. (4.2), describing a semi-Markovian process, approximates the solution of the memory process in Eq. (4.1) provided that

λ is small.

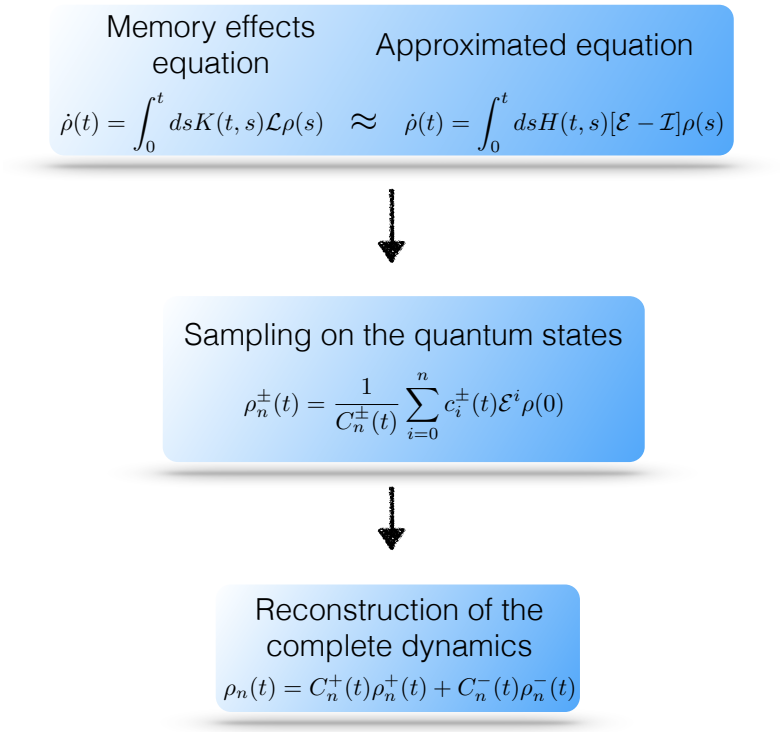

Figure 4.1: **Scheme of the algorithmic quantum simulator.** We approximate the equation underlining the memory effects with a semi-Markovian equation. We then split the solution of the semi-Markovian process into two CPT parts, implementing each part separately. This process is accompanied by the integration of products of the memory kernel in a number which increases linearly with the simulated time.

Proposition 3 (Simulation of Memory Effects)**.** *Let* $\rho_1(t)$ *and* $\rho_2(t)$ *be the solutions of Eq.* (4.1) *and Eq.* (4.2) *respectively, with* $\mathcal{E} \equiv \mathcal{E}_\lambda = e^{\lambda\mathcal{L}}$ $(\lambda \in \mathbb{R}^+)$*,* $H(t,s) = K(t,s)/\lambda$ *with* $\int_s^t d\tau\, K(\tau,s) \leq c$*, and* $\rho_1(0) = \rho_2(0)$*. Then,* $\|\rho_1(t) - \rho_2(t)\|_1 \leq \varepsilon$ *holds if* $\lambda \leq \frac{e^{-(2+o(\varepsilon))c\|\mathcal{L}\|t}}{c\|\mathcal{L}\|^2 t}\varepsilon$*, when* $c\|\mathcal{L}\|t > 1/e$*, and if* $\lambda \leq \log\left(\frac{1}{c\|\mathcal{L}\|t}\right)\frac{\varepsilon}{\|\mathcal{L}\|}$*, when* $c\|\mathcal{L}\|t \leq 1/e$*, provided that* $\varepsilon \leq 1/2$*.*

Proof. Using the Volterra version of Eqs. (4.1) and (4.2), together with the Taylor expansion of the exponential function, we see that

$$\|\rho_1(t) - \rho_2(t)\|_1 \leq \|\mathcal{L}\| \int_0^t ds\, k(t,s) \|\rho_1(s) - \rho_2(s)\|_1 + \frac{\lambda^2 \|\mathcal{L}\|^2 e^{\lambda \|\mathcal{L}\|}}{2} \int_0^t ds\, h(t,s) \|\rho_2(s)\|_1, \tag{4.11}$$

where we have introduced $k(t,s) \equiv \int_s^t d\tau\, K(\tau, s)$. To derive Eq. (4.11), we have used the triangle inequality and the Lagrange bound for the Taylor series truncation $\sum_{i=2}^{\infty} \frac{\lambda^i \|\mathcal{L}\|^i}{i!} \leq \frac{\lambda^2 \|\mathcal{L}\|^2}{2} e^{\lambda \|\mathcal{L}\|}$. Now, we can use the Grönwall's inequality in order to find the general bound $\|\rho_2(s)\|_1 \leq e^{\int_0^s d\tau\, h(s,\tau) \|\mathcal{E}_\lambda - \mathcal{I}\|}$, and the fact that $h(s,\tau) \leq h(t,\tau)$ for $s \leq t$. This allows us to bound the second term in Eq. (4.11) by $\frac{\lambda^2 \|\mathcal{L}\|^2 e^{\lambda \|\mathcal{L}\|}}{2\|\mathcal{E}_\lambda - \mathcal{I}\|} \left(e^{\int_0^t ds\, h(t,s) \|\mathcal{E}_\lambda - \mathcal{I}\|} - 1 \right)$. By applying Grönwall's inequality to Eq. (4.11) and setting $h(t,s) = k(t,s)/\lambda$, we conclude that $\|\rho_1(t) - \rho_2(t)\|_1 \leq \frac{\lambda \|\mathcal{L}\|^2 e^{\lambda \|\mathcal{L}\|}}{2\|\mathcal{E}_\lambda - \mathcal{I}\|/\lambda} \left(e^{ct \|\mathcal{E}_\lambda - \mathcal{I}\|/\lambda} - 1 \right) e^{ct\|\mathcal{L}\|}$, where we have used that $k(t,s) \leq c$. Now, if $c\|\mathcal{L}\|t > 1/e$, the last expression is bounded by ε if we choose $\lambda \leq \frac{e^{-(1+e^\varepsilon)c\|\mathcal{L}\|t}}{c\|\mathcal{L}\|^2 t} \varepsilon$, provided that $\varepsilon \leq 1/2$. Otherwise, if $c\|\mathcal{L}\|t \leq 1/e$, the same bound holds if we choose $\lambda \leq \log\left(\frac{1}{c\|\mathcal{L}\|t}\right) \frac{\varepsilon}{\|\mathcal{L}\|}$, see Appendix B. □

The result of Proposition 3 provides the error bound for a general simulation of a complex environment described by Eq. (4.1), and it is rather general as it holds for any $\mathcal{L}$. The algorithm consists in implementing the states defining the solution of the approximated semi-Markovian process, together with the numerical integration of the memory kernel, as schematically depicted in Fig. 4.1. The method can be generalized to even more complicated dynamical equations. For instance, the case of higher-order derivatives, as

$$\partial_t \rho(t) = \int_0^t \int_0^{s_1} ds_2\, ds_1\, K(s_1, s_2) \mathcal{L}\, \rho(s_2). \tag{4.12}$$

The solution of Eq. (4.12) can be approximated analogously to Eq. (4.1), and Proposition 3 extended in order to find similar bounds. A further generalization consists in introducing additional terms, increasing the versatility of the proposed algorithmic quantum simulator. For instance, let us consider

the equation

$$\partial_t \rho(t) = \sigma + \int_0^t ds\, K(t,s) \mathcal{L}\, \rho(s), \tag{4.13}$$

where σ can be an arbitrary matrix. Then, Eq. (4.13) can be simulated by approximating it with the equation $\partial_t \rho(t) = \sigma + \int_0^t ds\, K(t,s) \left[e^{\lambda \mathcal{L}} - \mathcal{I}\right] / \lambda\, \rho(s)$, which can be rewritten and simulated similarly to Eq. (4.2).

Regarding the possible implications of this algorithms beyond the direct application in simulating quantum memory effects we would like to mention that the results in this chapter can be exploited for the classical simulation of memory effect equations. In fact, if the Markovian process used as tool is decomposed efficiently by gates with positive Wigner function, then expected values of observables can be estimated by using Montecarlo techniques [121, 122].

Lastly, we are aware of other works with a similar spirit of our algorithmic quantum simulator. In this sense, a similar approach oriented mainly to quantum machine learning has been realized in Ref. [123]. The authors use a D-Wave quantum annealer as analog simulator on top of a classical algorithm, which proves the power of these algorithmic quantum simulators.

4.3 Conclusions

In conclusion, we have developed a flexible and efficient quantum algorithm for the solution of integro-differential evolution equations describing quantum memory effects, including the case of non-Markovian dynamics. The proposed algorithmic quantum simulation is useful for mimicking the effective action of complex environments. Alternative situations that our approach may cover include quantum feedback [124, 125, 126], quantum machine learning and neuromorphic quantum computation.

Chapter 5

Advanced-Retarded differential equations in quantum photonics

> They who dream by day are cognizant of many things which escape those who dream only by night.
>
> *Edgar Allan Poe*

In this chapter, we propose the realization of photonic circuits whose dynamics is governed by advanced-retarded differential equations. Beyond their mathematical interest, these photonic configurations enable the implementation of quantum feedback and feedforward without requiring any intermediate measurement. We show how this protocol can be applied to implement positive and negative delay effects in the classical and quantum realms. Our results elucidate the potential of the protocol as a promising route towards integrated quantum control systems on a chip.

5.1 Introduction

In advanced-retarded (A-R) differential equations, also known as mixed functional differential equations, the derivative of the associated function explicitly depends on itself evaluated at different advanced-retarded values of the *time variable* [127, 128, 129, 130, 131]. In order to solve such A-R equations

either analytically or numerically, we require the knowledge of the solution history out of the domain of the equation. In many scientific disciplines A-R differential equations are used to describe phenomena containing feedback and feedforward interactions in their evolution [132, 133, 134]. In physics, for instance, A-R equations can be used to model systems exhibiting *temporal symmetries* in the dynamics. As a prominent example one may mention the application of A-R equations [135] in Wheeler-Feynman absorber theory [136, 137].

In the context of quantum mechanics, the implementation of feedback is more intricate than in the classical case due to the sensitivity of quantum systems to measurements. In this regard, a set of techniques has been developed for the realization of feedback-dependent systems, each of them employing different resources such as dynamical delays [138, 139], machine learning optimization [140], weak measurements [141, 142], including quantum memristors [112, 113], and projective measurements for digital feedback [143] among others. Certainly, the inclusion of feedback or memory effects in quantum dynamical systems has extended the scope of quantum protocols, and it has allowed for the study and reproduction of more complex phenomena. Therefore, devising schemes for engineering Hamiltonians that display advanced-retarded dynamics is of great relevance. Along these lines, the field of non-Markovian quantum dynamics focuses on the study of effective equations that govern the evolution of systems interacting with state-dependent environments [92, 93, 96, 97]. As a result, the estimation of non-Markovianity sheds light on the memory content of the systems under study.

In this chapter, we show that photonic lattices can be used to effectively tailor the dynamics of classical and quantum light fields in an advanced-retarded fashion. Our strategy is to exploit the duality between light propagation in space and time. More specifically, we use the existing mapping between time and the propagation coordinate [144]. Our A-R photonic approach utilises the isomorphism existing between the steady state of judiciously designed photonic waveguide circuits and solutions of A-R differential equations. We foresee that the inherent versatility of the proposed system will make the implementation of feedback and feedforward noticeably simple, in both classical and quantum frameworks, and thus may open the door to many interesting applications in integrated quantum technologies.

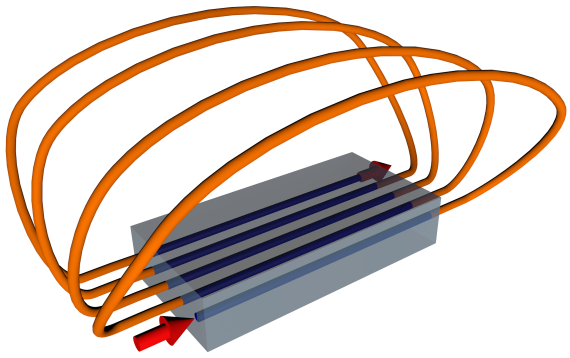

Figure 5.1: **Photonics chip representation.** Illustration of the chip for implementing the photonic simulator in Eq. (5.2), where the arrows represent the input and output ports, while the lines inside and outside the chip represent the waveguides and fiber connections, respectively.

5.2 Description of the Advanced-Retarded Protocol

To introduce our protocol, we start by considering the following first-order linear and non-autonomous A-R differential equation [127]

$$i\frac{dx(t)}{dt} = \beta(t)x(t) + \kappa^{-}(t)x(t-\tau) + \kappa^{+}(t)x(t+\tau), \tag{5.1}$$

with $\kappa^{+}(t) = \kappa^{-}(t+\tau)$, and boundary conditions $\kappa^{-}(0 < t < \tau) = \kappa^{+}((N-1)\tau < t < N\tau) = 0$. We associate the functions $x(t)$, $x(t \pm \tau)$ with the mode amplitude of classical monochromatic waves traversing the j-th and $j \pm 1$-th waveguides, $a_j(z)$ and $a_{j\pm1}(z)$, of an array of N evanescently coupled waveguides, each supporting a single mode and having a *time-dependent* propagation constant $\beta(z)$. This physical system is governed by a set of N differential equations [145]

$$i\frac{da_j}{dz} = \beta(z)a_j(z) + \kappa_{j,j+1}(z)a_{j+1}(z) + \kappa_{j,j-1}(z)a_{j-1}(z), \tag{5.2}$$

with $j \in [1, N]$. In quantum optics, the dynamics of single photons traversing this type of devices is modeled with a set of Heisenberg equations isomorphic to Eq. (5.2), which are achieved by replacing the classical mode amplitudes

a_j by the corresponding annihilation bosonic operators $\hat{a}_j$ [24, 146]. In order to make Eq. (5.2) isomorphic to Eq. (5.1), we must impose a continuity condition $a_j(0) = a_{j-1}(\tau)$ within the interval $j \in [2, N]$. Physically, this condition implies that the mode field a_{j-1}, at the propagation distance of $(j-1)\tau$ (τ being the length of the waveguides), has to be fed back into the input of the j-th waveguide. Furthermore, the finiteness of the waveguide array imposes the boundary conditions $\kappa_{1,0} = \kappa_{N,N+1} = 0$. Additionally, we establish the aforementioned mapping of the independent variable t into the spatial coordinate z. Therefore, our protocol requires the implementation of waveguide lattices endowed with input-output connections as illustrated in Fig. 5.1.

Physically, the initial condition $a_1(0)$ is implemented by continuously injecting light into the system. This condition is crucial to establish the isomorphism between the light dynamics in the waveguide array and the solution of Eq. (5.1). As a result, this solution is obtained in the stationary regime of our photonic system. Once the intensity is measured, the modulus square of the solution is obtained by joining the intensity evolution of each waveguide in a single variable. See Fig. 5.2 for a demonstration of the potentiality of our protocol, where we analyze the setup depicted in Fig. 5.1 with $N = 6$ and constant lattice parameters, $\beta(z) = 1$, $\kappa = \sqrt{\beta + N}$ and $\tau = 1$. The light dynamics occurring in such an array is governed by Eq. (5.2). See Fig. 5.3 for an scheme of the error depending on the distance from the stationary state.

An interesting point to highlight is the existence of a z reversal symmetry in the simulation with respect to the central point of the evolution, $z_c = N\tau/2$, for constant lattice parameters. This relation holds for the modulus square of the solution, $aa^*(z_c + z) = aa^*(z_c - z)$. Consequently, after the system reaches the steady state, it simultaneously fulfills the periodic boundary condition, $a(0) = a(N\tau)$, where we have neglected a global phase factor. Moreover, the preservation of the norm is a common feature in all our simulations because it is the footprint of how we have defined the stationary state. Therefore, our intuition suggest that from all the possible solutions our technique is finding those which preserve the input-output norm. This property combined with the space-time analogy open a possible framework for the study and implementation of closed timelike curve (CTC) gates [147, 148, 149].

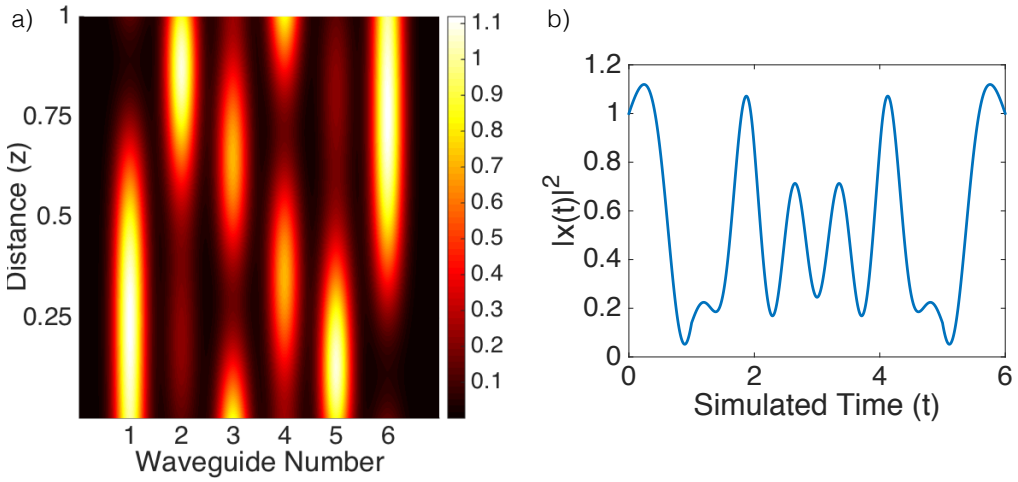

Figure 5.2: **Proof of principle.** a) Intensity evolution for an array having $N = 6$ waveguides and constant lattice parameters $\beta = 1$, $\kappa = \sqrt{\beta + N}$ and $\tau = 1$. b) Intensity of all the waveguides concatenated in a single curve, which represents the absolute square of the solution of Eq. (5.2).

5.3 Numerical Simulations of Paradigmatic Equations

Dynamical Parameters

A more flexible scenario arises when considering space dependent parameters in Eq. (5.2), which in the context of photonic lattices means that the system acquires dynamics. The dynamical character is achieved with modulations of the refractive index of individual waveguides. We consider an implementable system conformed by a periodic variation $\beta(z) = \beta_0 + \epsilon \cos(\omega z)$, where β_0 is a constant, ϵ is the modulation amplitude, and ω stands for the modulation frequency along z. It is noteworthy to mention that in the context of advanced-retarded equations the time dependence allows us to encode non-autonomous equations, which are hard to compute in general. For illustration purposes, Consider the oscillatory time dependence of the propagation constant, β, for the single variable A-R equation, Eq. (5.1). We numerically simulate this system for a lattice of $N = 6$ waveguides, $\beta = 1$, $\kappa = \sqrt{7}$, $\epsilon = 1$ and $\omega = 2$, see Fig. 5.4. We have selected these parameters to show

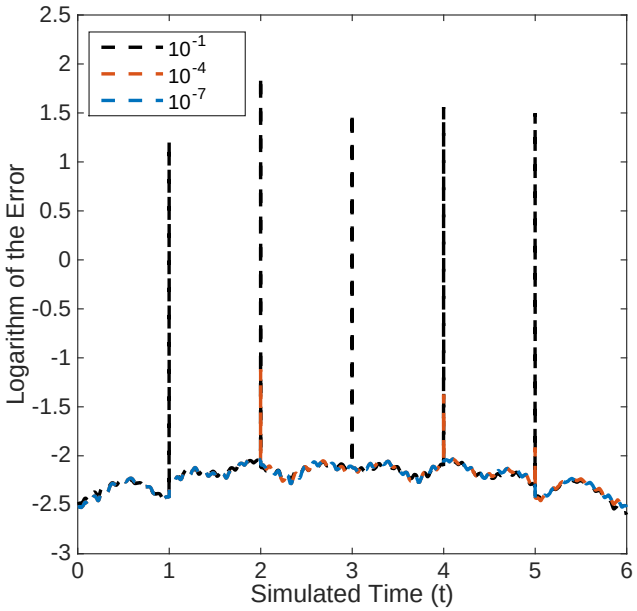

Figure 5.3: **Theoretical Error.** We depict the decimal logarithm of the error as a function of time for three runs of the simulation with different distances with respect to the stationary state. The fact that the effective interaction between photons is zero makes possible the analogy between the stationary state solution and the accumulation of solutions for an initial excitation combined until the initial population has escaped from the output port. Therefore, the distance is calculated as the norm of the population that remains in the chip. The dynamical constants of the system are equivalent to the ones in Fig. 5.2.

the existence of resonant solutions, in which a high amount of light gets trapped in the chip. Notice that, although a high population is achieved in the stationary state, the theoretical error is still small.

Systems of Equations

We now turn our attention to demonstrate how our protocol can be extended to provide solutions of systems of classical and quantum A-R equations. To this end, we encode every unknown variable in a family of waveguide arrays, and place all the families involved close to each other in such a way that light fields traversing the system can tunnel from array to array. In this manner, all the functions are self-coupled and coupled to others, enriching the dynamics

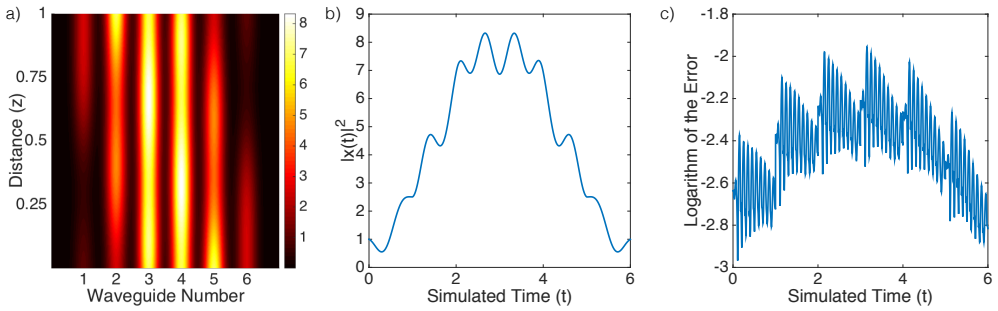

Figure 5.4: **Dynamical Parameters.** Numerical Simulation of Eq. (5.1) with $N = 6$, $\beta = 1$, $\epsilon = 1$, $\kappa = \sqrt{7}$, $\omega = 2$. (a) Intensity in the stationary state in the waveguides array. (b) Modulus square of the solution as a function of time. (c) Decimal Logarithm of the error of the simulation with respect to the solution of the A-R equation.

of the systems. In order to explain the operation principle of the protocol, we focus on the simplest case of two variables. Note that in this case, we can relate each array x and y to a component of a qubit, $|\psi\rangle = (a_x, a_y)^{\mathrm{T}}$, where T denotes the transpose. Thereby, we mold its dynamics to evolve according to an effective A-R differential equation. As a first possibility, we can put together two lattices in which the feedback takes place as depicted in Fig. 5.5 a. In this scenario, the light can hop to its neighboring sites as well as to the sites of the adjacent array. This arrangement enables the time evolution simulation of a single qubit Hamiltonian combined with two terms corresponding to advanced and retarded couplings

$$i|\dot{\psi}(t)\rangle = H(t)|\psi(t)\rangle + H^{+}(t)|\psi(t+\tau)\rangle + H^{-}(t)|\psi(t-\tau)\rangle, \tag{5.3}$$

$$H(t) = \begin{pmatrix} \beta_x(t) & q(t) \\ q(t) & \beta_y(t) \end{pmatrix}, H^{+}(t) = \begin{pmatrix} \kappa_x^{+}(t) & d_{xy}^{+}(t) \\ d_{yx}^{+}(t) & \kappa_y^{+}(t) \end{pmatrix},$$
$$H^{-}(t) = \begin{pmatrix} \kappa_x^{-}(t) & d_{xy}^{-}(t) \\ d_{yx}^{-}(t) & \kappa_y^{-}(t) \end{pmatrix}. \tag{5.4}$$

A second configuration arises by mixing the fibers as shown in Fig. 5.5 b. In this case, we flip the qubit in the advanced and retarded times. Even though the equation exhibits the same structure as Eq. (5.3), the forward

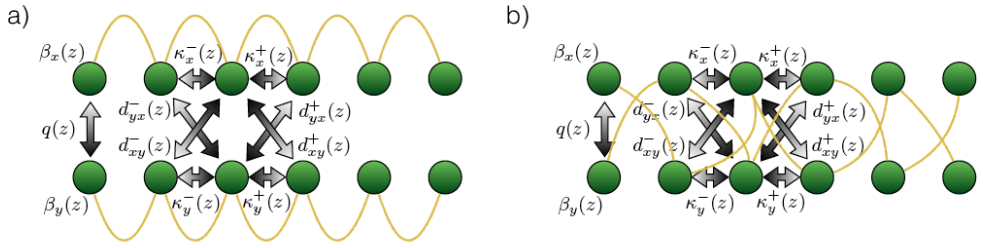

Figure 5.5: **Chip connections.** Front side view of the chip showing the input-output connections and the parameters of the simulation. Here β is the propagation constant, q is the vertical coupling constant, κ is the horizontal coupling constant and d the diagonal coupling constant. a) The scheme in which each plane is associated with a component of the qubit simulates Eq. (5.3). b) The crossed links allow for a stronger temporal mixing of the qubit components in the derivative. This situation corresponds to the second example of Eq. (5.3).

and backward Hamiltonians, H^+ and H^- are the same matrices given in Eq. (5.4) multiplied on the left by σ_x. Here $H(t)$, $H^+(t)$, and $H^-(t)$ depend on the parameter β and on the coupling between waveguides belonging to different arrays and the coupling between the guides of the same array. While the vertical, transversal and diagonal couplings are denoted with q, κ and d respectively, the (x, y) labels represent the plane in which the arrays are located. In addition to the conditions for each array in Eq. (5.1), the following consistency and boundary conditions are fulfilled,

$$\begin{aligned} H^+((n-1)\tau < t < n\tau) = H^-(0 < t < \tau) = 0, \\ d_{yx}^+(t) = d_{xy}^-(t+\delta), \qquad d_{xy}^+(t) = d_{yx}^-(t+\delta). \end{aligned} \tag{5.5}$$

In Fig. 5.6, we plot a numerical simulation of the array proposed to simulate systems of A-R equations given by Eq. (5.3). The dynamical parameters are $N = 5$, $\beta_x = 1$, $\beta_y = 2$, $\kappa_x = 3$, $\kappa_y = 1$, $q = 1$, $d = 1$ and $\tau = 1$ for an initial state $|\psi(0)\rangle = |0\rangle$. The theoretical error is smaller than 10^{-2} for the complete time evolution. We have selected these parameters to show that highly asymmetric solutions are also possible for time independent equations even with the limitation induced by the physical constrains in the coupling constants κ.

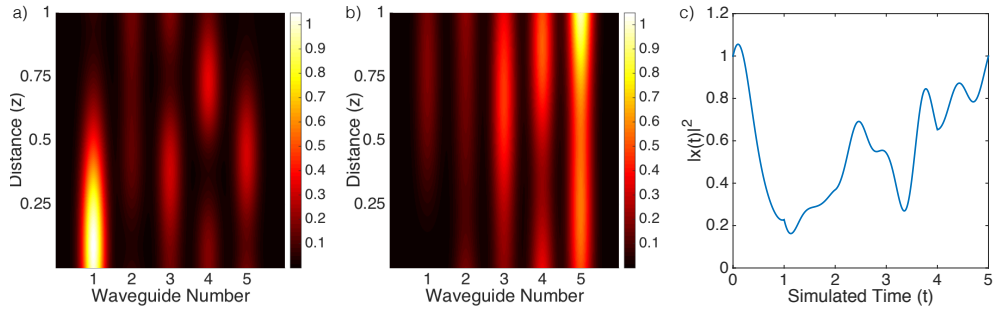

Figure 5.6: **Systems of Equations.** Numerical simulation of Eq. (5.3) with $N = 5$, $\beta_x = 1$, $\beta_y = 2$, $\kappa_x = 3$, $\kappa_y = 1$, $q = 1$, $d = 1$, $\tau = 1$ for the initial state $|\psi(0)\rangle = |0\rangle$. (a) Waveguide intensity in the x plane corresponding to the first component of the qubit. (b) Waveguide intensity in the y plane corresponding to the second component of the qubit. (c) Modulus square of the quantum state as a function of time.

Multiple Delays

We next consider a variant of Eq. (5.1) with multiple delays. This configuration arises when we allow each waveguide to couple to multiple neighbors and after reordering the feedback connectors. The first non-trivial example is a two-time A-R equation

$$\begin{aligned} i\dot{x}(t) &= \beta(t)x(t) + \kappa^{+}(t)x(t+\tau) + \kappa^{++}(t)x(t+2\tau) \\ &+\kappa^{-}(t)x(t-\tau) + \kappa^{--}(t)x(t-2\tau). \end{aligned} \tag{5.6}$$

Experimentally, the arrangement can be engineered by fabricating the waveguides in a zig-zag configuration. The resulting equation shares the structure of an A-R differential advanced-retarded with additional feedback and feedforward terms. For this particular system, the coupling coefficients are related as

$$k^{++}(t) = k^{--}(t+2\tau), \qquad k^{+}(t) = k^{-}(t+\tau), \tag{5.7}$$

See Fig. 5.7 for a numerical simulation of Eq. (5.6) with $N = 5$, $\beta = 1$, $\kappa = 5$ and $\tau = 1$.

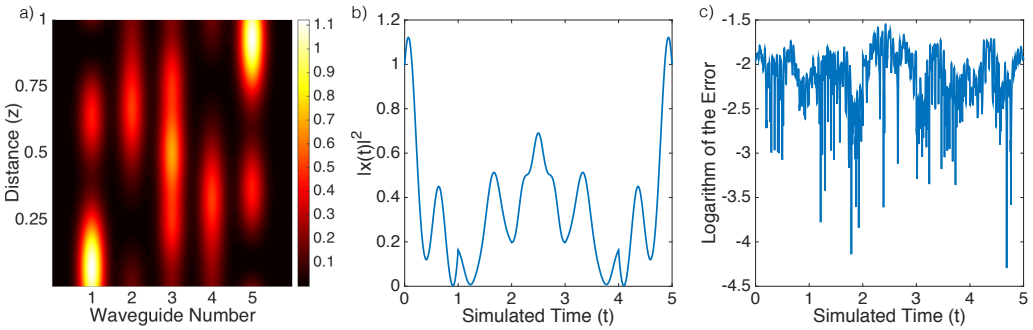

Figure 5.7: **Multiple delays.** Numerical simulation of Eq. (5.6) with $N = 5$, $\beta = 1$, $\kappa = 5$ and $\tau = 1$. (a) Intensity in the stationary state in the waveguide array. (b) Modulus square of the solution as a function of time. (c) Decimal logarithm of the simulation error with respect to the solution of the A-R equation.

Complex Parameters and High Order Equations

One last generalization of the A-R simulator consists in introducing complex dynamical parameters. This can be achieved by combining our feedback technique with Bloch oscillator lattices [150, 151, 152]. These types of arrays can be implemented by including a transverse ramping on the potential of the waveguides or by curving the waveguide arrays. Provided the evolution equations for the Bloch oscillator array, $i\dot{a_n} + n\beta z a_n + \kappa^+ a_{n+1} + \kappa^- a_{n-1} = 0$, and making the formal transformation $a_n = \tilde{a}_n(z)\exp(in\phi(z))$, with $\phi(z) = \int_0^z \beta(z')dz'$, one can show that it is formally equivalent to a system endowed with complex coefficients, $i\dot{\tilde{a}}_n + \exp(in\phi(z))\kappa^+\tilde{a}_{n+1} + \exp(-in\phi(z))\kappa^-\tilde{a}_{n-1}$. The inclusion of arbitrary complex parameters could be used to enhance the versatility of the protocol. Furthermore, a complete control of the coupling constants would allow to simulate higher-order equations via systems of first-order equations.

Mathematical Generalization

Even though the toolbox we present here is valid for simulating diverse physical configurations, it can be generalized by an appropriate mathematical treatment. Let $M(t)$ be the matrix containing the information about the propagation constant and couplings among the waveguides defined by

$i\dot{a}(t) = M(t)a(t)$, F the matrix encoding the input-output connections, and α the initial state independent of the feedback and feedforward mechanism, such that $a(0) = Fa(\tau) + \alpha$. Consider now that the dynamical equation is solvable in terms of the evolution operator $U(t)$, $a(t) = U(t)a(0)$. Our goal is to determine the complete initial condition $a(0)$ in terms of the independent initial condition α, evolution operator $U(t)$ and input-output matrix F. The consistency relations at $a(\tau)$ impose that $a(0)$ has to fulfill, $a(\tau) = U(\tau)a(0)$,

$$\begin{aligned} &a(0) = Fa(\tau) + \alpha \Rightarrow a(0) = \left(\mathbb{1} - FU(\tau)\right)^{-1}\alpha, \\ &a(t) = U(t)(\mathbb{1} - FU(\tau))^{-1}\alpha. \end{aligned} \tag{5.8}$$

Notice that this relation holds for any α, allowing the input of quantum states superposed in more than one waveguide, and is also valid for different configurations of couplings U and connections F, limited by the existence of the inverse of $(\mathbb{1} - FU(\tau))$. Moreover, we can think of different experimental conditions in which the connections happen at distinct evolution times τ_i, $a(0) = \sum_i F_i a(\tau_i) + \alpha$, resulting in $a(t) = U(t)(\mathbb{1} - \sum_i F_i U(\tau_i))^{-1}\alpha$.

At this point the protocol enables to implement systems of multiple delay advanced-retarded differential equation of first or higher orders, therefore allowing to address a variety of mathematical models along different branches in the tree of science. In the remainder, in order to make the algorithm realistic, we analyze the main limitations of the protocol regarding its interpretation and experimental realization.

If we interpret the solution of the qubit equation, Eq. (5.3), as a quantum particle we obtain a particle whose probability is not always normalized, associated with the forward and backward jumps of the particle. Although this effect excludes in principle the particle interpretation, absorbing potentials [153] account for this kind of kinematics. Moreover, the solution can always be divided by a constant, and the advanced-retarded equation will still be fulfilled. We can then calculate the non-Markovianity measurement, and see that quantum memory effects are present in the time evolution.

5.4 Experimental Considerations

An important source of errors is given by the decoherence of the quantum state in the time elapsed until the equilibrium situation in the system is achieved. This time is related with the population in the equilibrium situation, which is unknown before the experiment is realized. Identifying the re-

lation between the resonances and the dynamical parameters could be helpful for estimating the population in the stationary state, and therefore the total experimental time for achieving this state. Another possible approach is to employ the analogy explained in Fig. 5.3 for obtaining the complete solution as a combination of snapshots of the chip at different times. This is specially useful in the quantum case, because it allows to implement the experiment using a single photon instead of a constant supply of energy. While both methods provide the solution to the advanced-retarded differential equation, only the stationary state technique allows to obtain the physical state of the system at $t = n\tau$, which has the same norm as the initial state in $t = 0$.

We have to take into account the losses introduced by the fiber connections that will break the continuity condition allowing us to simulate Eq. (5.1) in terms of Eq. (5.2). The length and propagation constant of this fibers have to be tuned so that no phase is introduced in the evolution. Additionally, the space dependence of propagation and coupling constants is limited by the experimentally realizable functions. The degrees of freedom to consider are the writing precision for modifying the propagation constants and the spatial path of each waveguide for modifying the coupling constants.

5.5 Conclusions

In conclusion, we have developed a flexible and realistic toolbox for implementing advanced-retarded differential equations in integrated quantum photonics circuits. We have shown that our analogy enables the simulation of time-dependent systems of advanced-retarded equations in the classical and quantum realms, which in the context of quantum information can be employed to realize feedback and feedforward driven dynamics. Therefore, we consider that our work enhances the versatility of quantum simulators in the abstract mathematical direction and in terms of applications for retrospective and prospective quantum memory.

Part III

Intelligent Quantum Systems

Chapter 6

Genetic Algorithms for Digital Quantum Simulations

> Live as if you were to die tomorrow. Learn as if you were to live forever.
>
> Attributed to *Isidore of Seville*

In this chapter, we propose genetic algorithms, which are robust optimization techniques inspired by natural selection, to enhance the versatility of digital quantum simulations. In this sense, we show that genetic algorithms can be employed to increase the fidelity and optimize the resource requirements of digital quantum simulation protocols, while adapting naturally to the experimental constraints. Furthermore, this method allows us to reduce not only digital errors, but also experimental errors in quantum gates. Indeed, by adding ancillary qubits, we design a modular gate made out of imperfect gates, whose fidelity is larger than the fidelity of any of the constituent gates. Finally, we prove that the proposed modular gates are resilient against different gate errors.

6.1 Introduction

Optimization problems, a prominent area in computer science and machine learning [154], are focused on finding, among all feasible solutions, the best

one in terms of efficiency and resource requirements. In particular, genetic algorithms (GAs) [46], an especially flexible and robust set of optimization methods, are inspired by ideas of evolution and natural selection. In this sense, GAs optimize among different strategies, which are codified in the genetic information of an individual. Their evolution is given by genetic recombination over a group of individuals, together with random mutations. Natural selection is represented according to the optimization criteria, codified in an evaluation or fitting function. This process is repeated until the individuals satisfy a condition of adaptation. As the solutions to the problem are encoded in the genetic information of the individuals, the information of the survival corresponds to the optimal solution.

A variety of applications have been designed utilizing these methods: mirrors that funnel sunlight into a solar collector [155], antennas measuring the magnetosphere of Earth from satellites [156], walking methods for computer figures [157] and efficient electrical circuit topology [158, 159]. The resilience against changes in the initial conditions of the problem is based on the overheads in the resources.

One of the most important limitations in the field of quantum computing [2] is the fidelity loss of quantum operations. Quantum error correction protocols [160, 161], which codify logical qubits in several physical qubits, have been proposed and implemented in different quantum technologies, such as linear optics [162], trapped ions [163] and superconducting circuits [84, 164]. It is noteworthy to mention that quantum error correction have been designed for gate-based quantum computing and, in principle, they are also meant to be adaptable to digital quantum simulations [3]. However, experimental implementations of quantum error correction protocols applied to specific quantum algorithms are still to come in the expected development of quantum technologies.

Here, we propose a protocol based on genetic algorithms for the suppression of errors ocurring within digital quantum simulations, along the general lines of bioinspired algorithms in quantum biomimetics. First, we prove that GAs are able to decompose any given unitary operation in a discrete sequence of gates inherently associated to the experimental setup. Moreover, we numerically demonstrate that this sequence achieves higher fidelities than previous digital protocols based on Trotter-Suzuki methods [3, 9]. Second, we show that GAs can be used to correct experimental errors of quantum gates. Indeed, architectures combining a sequence of imperfect quantum gates with ancillary qubits generate a modular gate with higher fidelity than any of

the components of the sequence. We exemplify this with a possible implementation of a high-fidelity controlled-NOT (CNOT) modular gate, which is made out of several imperfect CNOTs. Additionally, these architectures show resilience against changes in the gate error. Therefore, by combining the concept of digital quantum simulation with GA, it is possible to design robust and versatile digital quantum protocols.

6.2 Genetic Algorithms for Digital Quantum Simulations.

In the following, we explain how GAs can improve the fidelity of digital quantum simulations. Up to now, the standard technique for realizing digital simulations is Trotter-Suzuki expansion [9], which has been proven to be efficient [101, 165, 166]. This method consists in executing a series of discretized interactions, resulting in an effective dynamics similar to the ideal dynamics of the simulated system. Associated with the unitary evolution of Hamiltonian $H = \sum_j^s H_j$, Trotter formula reads

$$U_I = e^{-iHt} = \lim_{l\to\infty} \left(e^{-iH_1 t/l} \cdots e^{-iH_s t/l}\right)^l, \tag{6.1}$$

where U_I is the ideal unitary evolution, t is the simulated time, l is the number of Trotter steps, and H_i are the Hamiltonians in the simulating system. On one hand, for a fixed total execution time, the larger the number of Trotter steps is, the lower the digital error of the simulation. On the other hand, the execution of multiple gates in a quantum system can introduce experimental errors due to decoherence and imperfect gate implementation. Therefore, there is a compromise between the number of Trotter steps and quantum operations that can be performed by the quantum simulator [167, 168].

GAs can be employed for outperforming current techniques of digital quantum simulations. The first step of a digital quantum simulation is the decomposition of the simulated Hamiltonian into interactions implementable in the quantum platform, which is a tough task in general. However, by using GAs, it is possible to find a series of gates adapted to the constraints imposed by the quantum simulator, whose resulting interaction is similar to the one of Hamiltonian H. For this purpose, we need neither to satisfy the condition $H = \sum_j^s H_j$, nor to use the same execution time for every involved gate. This not only relaxes the conditions for simulating the dynamics, but also

allows us to control the number of gates involved, permitting the possibility of minimizing the experimental error.

Let us assume the situation in which is not possible to compute the ideal dynamics of a short-range interacting Hamiltonian, since, for instance the number of particles is too large. By using the Trotter-Suzuki formula, it is possible to decompose the interaction into α local blocks of k-interacting particles each, out of N total particles. Let us denote by U_j the ideal unitary evolution of the Hamiltonian acting on the jth local block of k qubits. Once the total dynamics is decomposed into blocks, each U_j has to be implemented employing the resources available in the experimental platform, as depicted in Fig. 6.1. Here, GAs play an important role, since they provide an architecture for efficiently approximating each U_j by W_j:

$$U_T = \left(\prod_{j=1}^{\alpha} U_j\right)^l = \left(\prod_{j=1}^{\alpha} e^{-iH_j t/l}\right)^l, \tag{6.2}$$

$$U_{GA} = \left(\prod_{j=1}^{\alpha} W_j\right)^l, \tag{6.3}$$

where $\alpha = \left\lceil \frac{N-1}{k-1} \right\rceil$. We assume that k is sufficiently small to allow the minimization of the error associated with the approximation in a standard computer. Therefore, the evaluation function has access to an approximate version of the complete system dynamics, because this is solvable in terms of the Trotter expansion. In our algorithm, as an evaluation function, we compare Trotter unitary evolution, U_T, for a given number of Trotter steps l with the unitary evolution obtained from GAs, U_{GA}. The evaluation function is then given by $R_j = ||U_j - W_j||$[1]. The result, for all the examples analyzed, is that the number of gates involved in the GA protocol is lower than in the Trotter expansion, which gives positive perspectives for experimental realizations of digital quantum simulations based on this approach.

The upper bound for the total error ξ of the protocol, is obtained by combining the Trotter error with the error of the GA optimization $\xi =$

[1]Notice that a global phase in the unitary W_j does not affect the evolution but it affects the value of R_j, so we should consider $\inf_\phi ||U_j - e^{i\phi} W_j||$. As we normally have access to the initial state of the evolution, the evaluation function $R_j = |\langle\Psi|U_j^\dagger W_j|\Psi\rangle|^2$, in which the global phase is irrelevant, can be chosen.

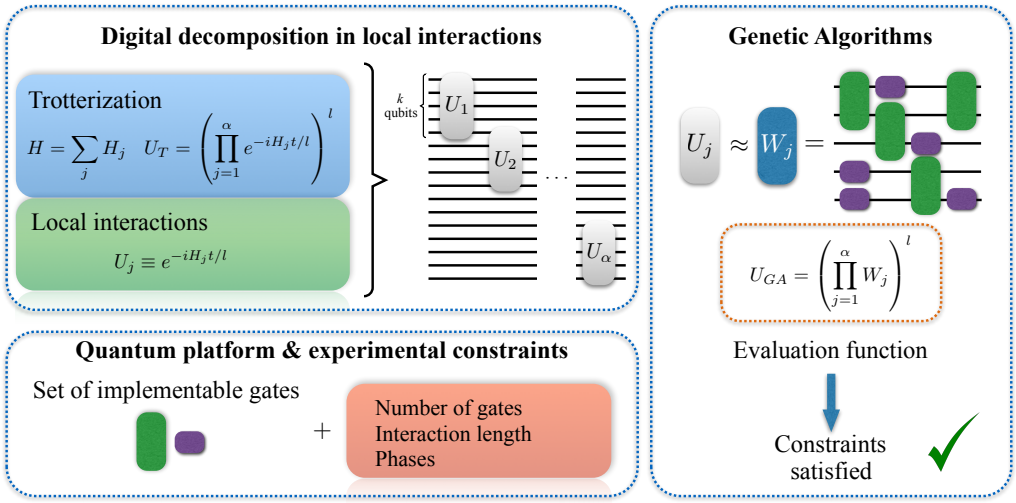

Figure 6.1: **Scheme of the GA-based protocol for digital quantum simulations.** Firstly, the simulated Hamiltonian is decomposed in local interaction blocks, separately implemented in different unitary evolutions U_j which act on a subset of k particles of the system. Secondly, the set of gates is selected according to the constraints of the simulating quantum technology: total number of gates to avoid experimental gate error, interactions restricted to adjacent physical qubits, and implementable phases of the Hamiltonian, among others. Once the set of gates is determined, GAs provide a constraint-fulfilling sequence of gates, which effectively perform the resulting dynamics U_{GA} similar to U_T.

$||U_I - U_{GA}|| \leq ||U_I - U_T|| + ||U_T - U_{GA}||$. The first term is nothing but the digital error [9], so we analyze the second term. Consider that W_j, the unitary provided by the GA, has a matrix error η_j, $W_j = U_j + \eta_j$. Let us denote by $\tilde{U}_j = \mathbb{1}^{\otimes j-1} \otimes U_j \otimes \mathbb{1}^{\otimes \alpha - j}$, the operations when extending to the whole Hilbert space, where α is the number of blocks. The same relation holds for $\tilde{W}_j$ and $\tilde{\eta}_j$, therefore, $\tilde{W}_j = \tilde{U}_j + \tilde{\eta}_j$. We are now able to compute the error of the GA optimization for a single Trotter step, given by $||U_T - U_{GA}|| = ||\prod \tilde{W}_j - \prod \tilde{U}_j|| = ||\prod(\tilde{U}_j + \tilde{\eta}_j) - \prod \tilde{U}_j||$. We approximate this expression to a first order in $\tilde{\eta}_j$, $||\sum \tilde{W}_1 ... \tilde{W}_{j-1}\tilde{\eta}_j \tilde{W}_{j+1} ... \tilde{W}_\alpha|| \leq \sum ||\tilde{W}_1|| ... ||\tilde{W}_{j-1}|| ||\tilde{\eta}_j|| ||\tilde{W}_{j+1}|| ... ||\tilde{W}_\alpha||$. By computing the norm of the unitary matrices $\tilde{W}_j$, we obtain $\sum ||\tilde{\eta}_j||$, which coincides with the error in each

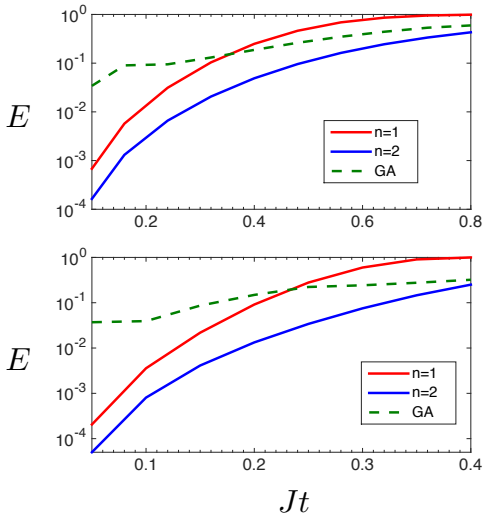

Figure 6.2: **Logarithmic plot of the error.** We depict the error, $E = 1-|\langle\Psi|U_I^\dagger\tilde{U}|\Psi\rangle|^2$, in the evolution of (a) Ising and (b) Heisenberg spin models for $N = 5$ qubits, $J = 2$, $B = 1$, and $|\Psi\rangle = |0\rangle^{\otimes 5}$. Here, U_I is the ideal unitary evolution, while $\tilde{U}$ refers to the unitary evolution using either a digital expansion in 1 (blue line) and 2 (red line) Trotter steps, or GA (dashed green). The GA protocol requires fewer gates than the digital method for a single Trotter step achieving similar fidelities to two Trotter steps.

of the subspaces, $||U_T - U_{GA}|| = \sum ||\eta_j||$. Therefore, the GA error, at first order, is given by the sum of the errors in each unitary block, which is linear in the number of qubits for the simulation of a short-range interacting Hamiltonian. As a final remark, since both W and U are unitaries, we would like to point out that the error could also be parametrized by a multiplicative unitary matrix. However, both approaches are equivalent for small errors in the sense that $V_\mu = \exp(i\mu H) \approx 1 + i\mu H + O(\mu^2||H||^2)$ for a small μ, so $W \approx U + iUH\mu = U + \eta$.

We now illustrate the protocol for simulating digitally the isotropic Ising and Heisenberg spin models with a magnetic field in a superconducting circuit

architecture [4, 167, 169]. The Hamiltonians of these models are

$$\begin{aligned} H_I &= J\sum_{\langle i,j\rangle}^{N}\sigma_i^z\sigma_j^z + B\sum_{i}^{N}\sigma_i^x, \\ H_H &= J\sum_{\langle i,j\rangle}^{N}(\sigma_i^x\sigma_j^x + \sigma_i^y\sigma_j^y + \sigma_i^z\sigma_j^z) + B\sum_{i}^{N}\sigma_i^x, \end{aligned} \tag{6.4}$$

where J is the coupling between nearest-neighbor spins $\langle i, j\rangle$, B is the strength of the magnetic field, and σ_i^γ are the Pauli operators acting on the ith spin with $\gamma = x, y, z$. We decompose the interactions in terms of single-qubit rotations and controlled-phase (CPHASE) gates between nearest-neighbor superconducting qubits [5, 6, 33]. Following the approach of Ref. [169], simulating the Ising Hamiltonian requires $N-1$ CPHASE and $3N-2$ single-qubit gates, while Heisenberg Hamiltonian demands 3(N-1) CPHASE and $11N-6$ single-qubit gates. In this simulation, we consider a chain of $N = 5$ spins. The GA computes a digitalized unitary evolution for a concrete time t, constituted by the previous gates in a local subspace of $k = 2$ qubits. Then, this unitary evolution W_1 is repeated following Eq. (6.3) with l=1 over all adjacent qubits due to the translation invariance . The resulting unitary process U_{GA} is compared with the ideal dynamics of the model. This protocol employs 4 CPHASE and 8 single-qubit gates for the Ising model, and 4 CPHASE and 16 single-qubit gates for the Heisenberg model. Moreover, fidelities are enhanced when compared with the corresponding to pure digital methods for a single Trotter step, even using less gates, as shown in Fig. 6.2. This approach can be applied in other quantum technologies just by adding the constrains of their implementable quantum gates to the genetic algorithm. In this protocol, we have considered gates with perfect fidelity. Let us now focus on how to employ GA to improve the experimental error of quantum gates.

6.3 Experimental Error in a CNOT Gate.

Besides outperforming protocols for digital quantum simulations, GAs are also useful for suppressing experimental errors in gates. We propose a protocol to perform an effective quantum gate by using ancillary qubits and a set of imperfect gates, and we illustrate it for the CNOT. A CNOT gate is

given by a unitary $U_{\text{CNOT}} = \exp(i\frac{\pi}{2}H_{\text{CNOT}})$, with

$$H_{\text{CNOT}} = \frac{1}{2}\left[(\mathbb{1}+\sigma^z)\otimes\mathbb{1} + (\mathbb{1}-\sigma^z)\otimes\sigma^x\right]. \tag{6.5}$$

Let us consider imperfect gates modeled by $W_{\text{CNOT}} = \exp(i\frac{\pi}{2}H_{\text{CNOT}} + \delta H_R)$, with $\delta << 1$ and H_R a random matrix, such that $||H||_2 = 1$. These unitaries define unital quantum channels $\mathbb{E}_U = U\otimes\bar{U}$ and $\mathbb{E}_W = W\otimes\bar{W}$ respectively, and we define the error of the gate as the distance $\eta = ||\mathbb{E}_W - \mathbb{E}_U||_2$.

Let us now consider $q-2$ ancillary qubits in the state $|0\rangle$ in addition to the control and target of the integrated CNOT. Let us also consider n imperfect CNOT gates $\vec{W} = \{W_1, \ldots, W_n\}$ acting on any possible pair of the q qubits, with errors $\vec{\eta} = \{\eta_1, \ldots, \eta_n\}$ respectively, and denoted by $\eta = \min_i \eta_i$. The integrated circuit is defined by a set of n ordered pairs $IG_{\vec{\eta}} = \{(i_k, j_k)|1 \leq i_k, j_k \leq q, k = 1, \ldots, n\}$, where the indices indicate the control and target qubits, respectively. In order to calculate the fidelity of the protocol, we compute the Kraus operators of the integrated CNOT, by tracing out the $q-2$ ancillary qubits, and compare the resulting channel $\mathbb{E}_{IG_{\vec{\eta}}}$ with the unital channel $\mathbb{E}_U$, $\epsilon_{IG_{\vec{\eta}}} = ||\mathbb{E}_{IG_{\vec{\eta}}} - \mathbb{E}_U||_2$. If $\epsilon_{IG_{\vec{\eta}}} < \eta$, then the CNOT gate is implemented with higher fidelity than any of the original CNOT gates, showing this GA-based architecture resilience against quantum errors.

The set $IG_{\vec{\eta}}$ codifies the genetic information of the individuals which conform the population evolving into successive generations. During the reproduction, the individuals recombine their genetic code, which is also allowed to mutate. The survival probability depends on the fidelity of the effective CNOT encoded in $IG_{\vec{\eta}}$ and, therefore, only individuals associated with a small error succeed.

The number of possible architectures involving n different CNOT gates and q ancillary qubits is $P = (q^2-q)^n n!$, see Appendix C. The factor $(q^2-q)^n$ is due to all possible CNOT configurations in a given order between qubits i and j for n gates, while $n!$ comes from reordering imperfect gates $\{W_1, ..., W_n\}$. When q and n are small, the optimal architecture can be found by analyzing all cases. However, when we increase these parameters, this brute-force optimization method turns out to be inefficient. GAs allow us to optimize the protocol in this unreachable regime, being moreover robust, as presented below.

This CNOT case has been analyzed involving three, five and seven gates. Notice that, when one considers $q = 4$ and $n = 7$, the number of possible architectures is larger than 1.8×10^{14} for a fixed set of imperfect gates. We

have chosen a set of gates and find the optimal architecture by GA. Then, we analyze the resilience or robustness of this architecture by changing the set. In Fig. 6.3, we have depicted the results for a sampling of 1000 sets of random imperfect CNOT gates. The pie charts show the percentage of cases with a lower error than any CNOT performed in the protocol, which are 6% for three qubits, 87% for five, and 96% for seven. Furthermore, the bar charts show the average improvement of the error for the integrated CNOT with respect to the best implementing CNOT, which is -39%, $+18\%$, and $+30\%$, respectively. For completeness, in Fig. 6.4, we show the optimal architecture for $q = 4$ and $n = 5$, obtained from a fixed set of imperfect gates $\vec{W}$, and proven to be robust, see Appendix C.

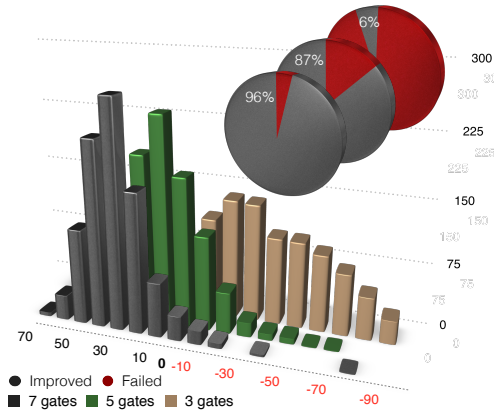

Figure 6.3: **Error resilience for architectures with $n = 3, 5, 7$ imperfect CNOT gates using 1000 runs.** Pie charts show the percentage of cases in which the fidelity of the effective CNOT overmatches the best CNOT employed in the architecture. Bar charts show the distribution of cases according to the relative improvement in the error, again when compared with the best CNOT.

Additionally, we have studied the behavior of the protocol with respect to the number of ancillary qubits. The results show no significant improvement when the number of performed gates is small, see Appendix C. For instance, architectures up to $n = 7$ do not overcome fidelities shown above when adding a third ancillary qubit, $q = 5$. However, we expect that architectures with a larger number of gates would actually take advantage of using more ancillary qubits in order to suppress the error.

The same protocol can be applied in the realization of more general uni-

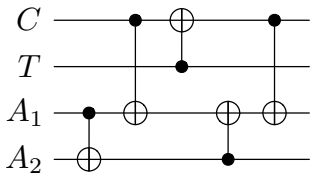

Figure 6.4: **Quantum circuit.** Scheme of the optimal architecture for constructing a CNOT gate with 5 imperfect gates, by using two ancillary qubits initialized in state $|0\rangle$. Here, C is the control, T is the target, and A_1 and A_2 are the ancillary qubits.

tary operations. Additionally, the gates conforming the building blocks can be arbitrary, which facilitates the adaptation of the protocol to any experimental platform.

6.4 Conclusions

In summary, in this work we proposed a new paradigm based on GAs to enhance digital quantum simulations and face different types of quantum errors. We showed that they can be used to improve the fidelity of quantum information protocols by effectively reducing digital errors produced in Trotter-Suzuki expansions. Our method allowed us to correct experimental errors due to imperfect quantum gates, by using ancillary qubits and optimized architectures. We also argued that solutions provided by GAs manifest resilience against digital and experimental quantum errors. From a wide perspective, we expect that GAs will be part of the standard toolbox of quantum technologies, and a complementary approach to analog [170, 171] and digital [172] optimal-control techniques.

Chapter 7

Feedback-Induced Quantum Learning

> It's the questions we can't answer that teach us the most. They teach us how to think. If you give a man an answer, all he gains is a little fact. But give him a question and he'll look for his own answers.
>
> *Patrick Rothfuss*

In this chapter, we present a quantum learning algorithm for determining the optimal state in controlled unitary operations. The underlying physical mechanism of the protocol is the iteration of a quantum time delayed equation that introduces feedback in the dynamics and eliminates the necessity of intermediate measurements. The performance of the algorithm is analyzed by comparing the results obtained in numerical simulations with the outcome of Machine Learning methods for the same problem.

7.1 Introduction

One of the main consequences of the revolution in computation sciences, started by A. Turing, K. Zuse and J. Von Neumann among others [173, 174],

is that computers are capable of substituting us and improving our performance in an increasing number of tasks. This is due to the advances in the development of complex algorithms and the technological refinement allowing for faster processing and larger storage. One of the golden dreams in this area, in the frame of the biomimetic ideas, is the design of algorithms that provide computers human-like capacities such as image or speech recognition, and creativity. These achievements would enable us to interact with computers in our own language.

This research, together with other projects with similar spirit, is carried out in the field of Artificial Intelligence [47]. In particular, researchers in the area of Machine Learning inside Artificial Intelligence are devoted to the design of algorithms responsible of training the machine with data so that is able to find a given optimal relation according to the desired criteria [154]. More precisely, the area is divided in three main lines depending on the nature of the protocol. In supervised learning the goal is to teach the machine a known function without explicitly introducing it in its code. In unsupervised learning the goal is that the machine develops the ability to classify data by grouping it on a different subset depending on its properties. In reinforcement learning, the goal is that the machine selects a sequence of actions so that the transition from the initial to the final state is optimal.

These techniques have also been studied in the quantum regime, under the flag of quantum machine learning [79, 110, 111, 175, 176, 177], with two main motivations. The primary one is to exploit the promised speedup of quantum protocols for improving the already existing classical ones. The secondary one is to develop unique quantum machine learning protocols for combining them with other quantum computational tasks. Apart from quantum machine learning, fields like quantum neural networks, or the more general quantum artificial intelligence, have also addressed similar problems [178, 179, 180, 181, 182].

7.2 Quantum Learning Algorithm

Here, we introduce a quantum algorithm for finding the optimal control state of a multitask controlled unitary operation. It is based on a sequentially applied time delayed equation that allows to implement feedback driven dynamics. The purely quantum encoding allows to speedup the training process by evaluating all the possible choices in parallel. Finally, we analyze the per-

formance of the algorithm with a figure of merit defined as the trace of the matrix product between the ideal and the real quantum states.

The first step in the description of the algorithm is the clarification of the concept of multitask controlled unitary operations U. In essence, these do not differ from ordinary controlled operations, but the multitask label is selected to emphasize that more than two operations on the target subspace are in principle possible. Mathematically, we define them as

$$U = \sum_{i=1}^{d} |c_i\rangle \langle c_i| \otimes s_i, \tag{7.1}$$

where $|c_i\rangle$ denotes the control state, and s_i is the reduced or effective unitary operation that U does on the target subspace when the control is on $|c_i\rangle$.

Our algorithm is useful when U is experimentally implementable but its internal structure, $|c_i\rangle$ and s_i are unknown. The goal is to find the optimal $|c_i\rangle$ for fixed input and output states, $|in\rangle$ and $|out\rangle$, in the target subspace. The protocol consists on sequentially reapplying the same dynamics in such a way that the initial state in the signal subspace is always $|in\rangle$, while the initial state in the control subspace is the output of the previous cycle. The equation modeling the dynamics is

$$\frac{d}{dt}|\psi(t)\rangle = -i\left[\theta(t-t_i)\theta(t_d-t)\kappa_1 H_1 |\psi(t)\rangle + \kappa_2 H_2 \left(|\psi(t)\rangle - |\psi(t-\delta)\rangle\right)\right]. \tag{7.2}$$

In this equation θ is the Heaviside function, H_1 is the Hamiltonian giving rise to U with $U = e^{-i\kappa_1 H_1 (t_d - t_i)}$, H_2 is the Hamiltonian connecting the input and output states, with κ_1 and κ_2 as the coupling constants of each Hamiltonian.

The first thing to comment is that this evolution cannot be realized with ordinary unitary or dissipative techniques. Nevertheless, recent studies in time delayed equations could be the key for simulating processes of this kind [138, 139], together with the results shown in Chapter 5. Another important feature of Eq. (7.2) is that it only acquires physical meaning once the output is normalized. Regarding the behavior of the equation, each term has an specific role in the learning algorithm. The mechanism is inspired in the most intuitive classical technique for solving this problem, which is the comparison between the input and output states together with the correspondent modification of the control state. Here, the first Hamiltonian produces the input-output transition while the second Hamiltonian produces the reward by populating the control states responsable of the desired modification of

the target subspace. The structure of H_2 guarantees that only the population in the control $|c_i\rangle$ associated with the optimal s_i is increased,

$$H_2 = \mathbb{1} \otimes (-i\,|in\rangle\,\langle out| + i\,|out\rangle\,\langle in|)\,. \tag{7.3}$$

Notice that while this Hamiltonian does not contain explicit information about $|c_i\rangle$, the solution of the problem, its multiplication with the feedback term, $|\psi(t)\rangle - |\psi(t-\delta)\rangle$, is responsible for introducing the reward as an intrinsic part of the dynamics. This is a convenient approach because it eliminates the measurements required during the training phase. Additionally, we would like to point out the similarity existing between the effect of this term in our quantum evolution and gradient ascent techniques in algorithms for Artificial Intelligence [47].

A possible strategy would be to feed the system with random control states, measure each result, and combine them to obtain the final solution. But, we have discovered that it is enough to initialize the control subspace in a superposition of the elements of the basis. We would like to remark that this purely quantum feature reduces dramatically the number of resources, because a single initial state replaces a set of random states large enough to cover all possible solutions.

The specific problem we solve is given by the excitation transport produced by the controlled swap gate. In this scenario, the complete system is an n node network, each of them composed by a control and a target qubit. The control states are in a superposition of open and close, $|o\rangle$ and $|c\rangle$, while the target qubits are written in the standard $\{|0\rangle, |1\rangle\}$ basis denoting the absence of presence of excitations. We define U, the multitask controlled unitary operation, to implement the swap gate between connected nodes only if all the controls of the corresponding nodes are in the open state, $|o\rangle$. See Fig. 7.1 for a graphical representation of the most simple cases, the two and three node line networks. The explicit formula for U_2 is given by

$$U_2 = (|cc\rangle\,\langle cc| + |co\rangle\,\langle co| + |oc\rangle\,\langle oc|) \otimes \mathbb{1} + |oo\rangle\,\langle oo| \otimes s_{12}. \tag{7.4}$$

Here s_{ij} represents the swap gate between qubits i and j. Although we have employed unitary operations for illustration purposes, the equation requires the translation to Hamiltonians. In order to do so, we first select $t_d - t_i$ to be $\pi/2$ and calculate the matrix logarithm,

$$\begin{aligned} &n = 2, \qquad H_1 = (|oo\rangle\,\langle oo|) \otimes h_{12}, \\ &n = 3, \qquad H_1 = (|ooc\rangle\,\langle ooc|) \otimes h_{12} + (|coo\rangle\,\langle coo|) \otimes h_{23} + (|ooo\rangle\,\langle ooo|) \otimes h_{13}. \end{aligned} \tag{7.5}$$

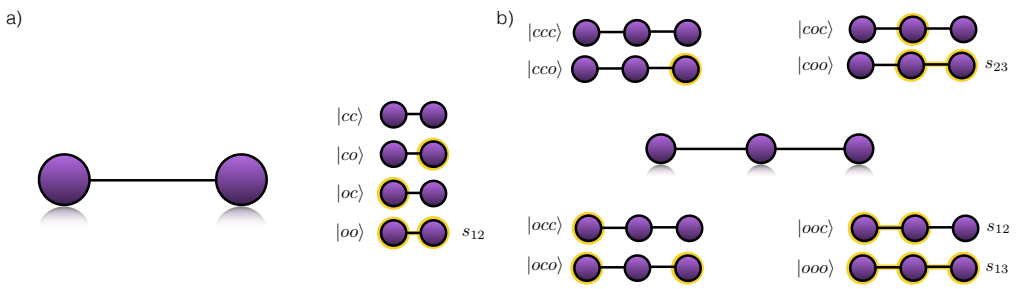

Figure 7.1: **Node line networks.** We show the graphical representation of the two, a), and three, b), node line networks. The circle around the node represent that the control is in the open state. The effective operation that the control performs on the target subspace is the s_{ij} swap gate between nodes i and j.

Here, being σ_k the Pauli matrices, h_{ij} for $i < j$ is obtained with

$$h_{ij} = \frac{1}{2}\left(\sum_{k=1}^{3} \mathbb{1}^{\otimes i-1} \otimes \sigma_k \otimes \mathbb{1}^{\otimes j-i-1} \otimes \sigma_k \otimes \mathbb{1}^{\otimes n-j} - \mathbb{1}^{\otimes n}\right). \tag{7.6}$$

7.3 Numerical Simulations of Learning Curves

In this work we have not proved the general character of the algorithm, but we have numerically tested it in a selection of examples covering diverse situations. Before looking at the results it is convenient to mention a technicality involving the the vector or matrix representation of quantum states. In order to recover the solution of the problem we need to trace out the target degrees of freedom, obtaining a density matrix. Additionally, the fact that Eq. (7.2) written for density matrices, Eq. (7.7), has non-local terms makes it harder to solve,

$$\begin{aligned}\frac{d}{dt}|\psi(t)\rangle\langle\psi(t)| = &-i\left[\theta(t-t_i)\theta(t_d-t)\kappa_1 H_1 + \kappa_2 H_2, |\psi(t)\rangle\langle\psi(t)|\right] \\ &+ i\kappa_2(H_2|\psi(t-\delta)\rangle\langle\psi(t)| - |\psi(t)\rangle\langle\psi(t-\delta)|H_2).\end{aligned} \tag{7.7}$$

Therefore, we have decomposed each density matrix in a sum of pure states and solve the vector equation for each of them separately, retrieving the total solution as a linear superposition of the individual ones. This method is consistent due to the linearity of Eq. (7.7).

Unique Solution The first family of problems we face are are the *n line networks*, which have a unique solution, given by the control state with all the nodes open, $|o\rangle^{\otimes n}$. The parameters we have selected, common for all simulations, are $\delta = 1$, $\kappa_1 = 100$, $\kappa_2 = 10$ and $T = 2$, where T represents the total duration of each episode. In Fig. 7.2 we represent graphically the results together with the required resources. These examples show how the algorithm is working for this family of problems independently of the natural basis of U.

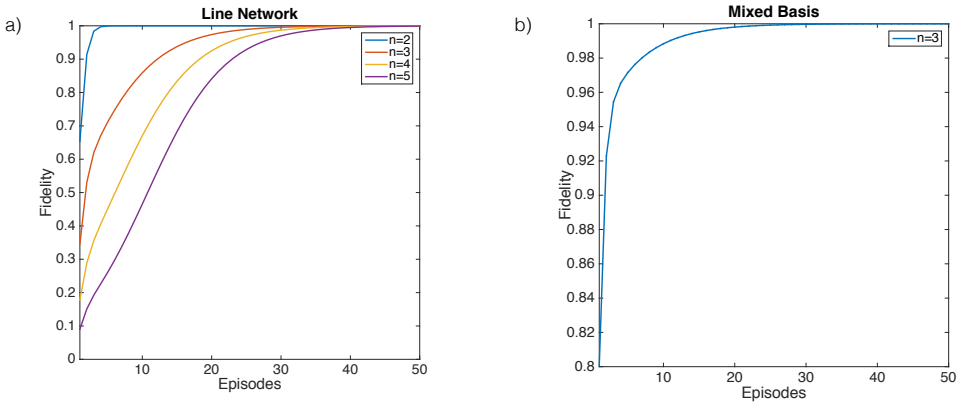

Figure 7.2: **Learning curves for single solutions.** a) We plot the fidelity of the learning process as a function of the number of episodes for the first examples of n node line networks. We have selected the open state, $|o\rangle = |1\rangle$ of the $\{|0\rangle, |1\rangle\}$ basis. b) We plot the fidelity for a different selection of $|o\rangle$ in the $n = 3$ case. Here the solution, $|ooo\rangle$, is given by $\frac{1}{\sqrt{2}}[|0\rangle + |1\rangle] \otimes |1\rangle \otimes [\cos(\pi/3)|0\rangle + \sin(\pi/3)|1\rangle]$.

Multiple Solutions

We address now a set of more complicated networks which will allow us to clarify how the algorithm behaves when solving problems with multiple

solutions. These are the *triangle* network for three nodes and the *bell* and *radiation* networks for four nodes, depicted in Fig. 7.3. These networks accept two pure states and their superpositions as solutions, a feature that is reflected in the result obtained with the algorithm. The asymptotic state achieved under the feedback induced learning equation is an equally weighted quantum superposition of both solutions, see Fig. 7.4.a for the numerical simulations. In this case, the previous definition of the fidelity is not valid, therefore we provide a new one in terms of the input and output states and the Hamiltonian. The new fidelity corresponds to the trace of the product between the ideal output and the output obtained with the control state achieved by the algorithm.

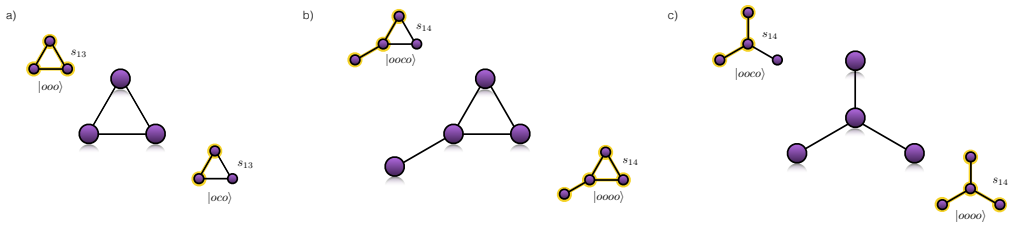

Figure 7.3: **Networks with two solutions.** We show the graphical of the triangle, bell and radiation networks in a), b) and c) respectively. In each of them we write the solution control state, that corresponds to the control performing the s_{14} gate in the target subspace.

For the cases studied, the complete set of solutions is obtained encoded in the result of the algorithm. This is convenient because it allows to design a protocol to select a specific optimal solution according to a given criteria. In the networks we are analyzing, one might want to obtain the most efficient solution, defining efficiency as achieving the transmission of the excitation while minimizing the number of open nodes. In order to accomplish this task a dissipative term has to be included in the evolution equation. Our idea is that a control dependent dissipation affects the target subspace. We explicitly write the Lindblad operators σ_i and dissipation constants γ_i for a two-node case. This technique allows us to find the shortest path between two nodes in a network once the natural basis of the unitary is known.

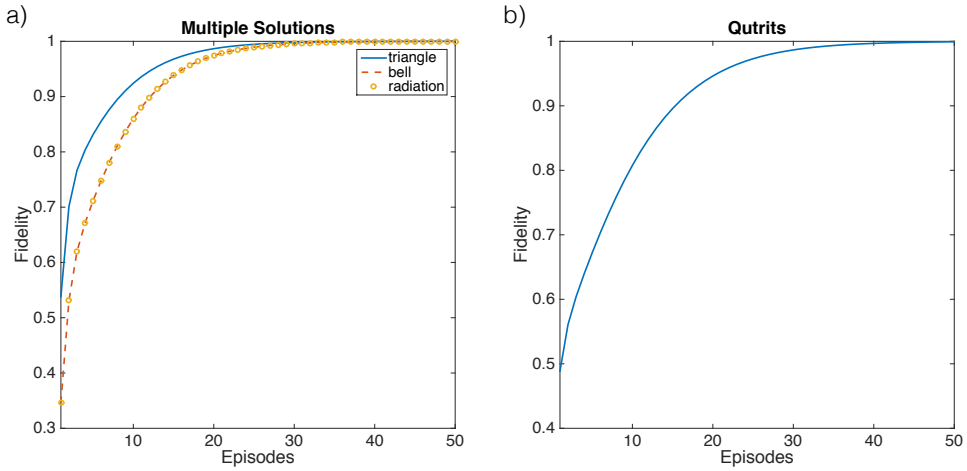

Figure 7.4: **Learning curves for two solution and qutrit problems.** a) We depict the learning curve for the triangle, bell and radiation networks as a function of the number of episodes. Notice that the curves for the bell and radiation networks are identical. b) We depict the learning curve for the multitask controlled unitary acting on two qutrits as a function of the number of episodes. Here $|in\rangle = |0\rangle$, $|out\rangle = |2\rangle$ and the solution is given by $|c_2\rangle = |1\rangle$, where the control states coincide with the basis of the qutrit space.

$$\begin{aligned}
&\sigma_1 = |co01\rangle\langle co11| + |co00\rangle\langle co10|\,, \quad \sigma_2 = |co00\rangle\langle co01| + |co10\rangle\langle co11|\,,\\
&\sigma_3 = |oc00\rangle\langle oc10| + |oc01\rangle\langle oc11|\,, \quad \sigma_4 = |oc10\rangle\langle oc11| + |oc00\rangle\langle oc01|\,,\\
&\sigma_5 = |oo00\rangle\langle oo10| + |oo01\rangle\langle oo11|\,, \quad \sigma_6 = |oo00\rangle\langle oo01| + |oo10\rangle\langle oo11|\,,\\
&\gamma_1 = \gamma_2 = \gamma_3 = \gamma_4, \quad \gamma_5 = \gamma_6 = 2\gamma_1. \qquad (7.8)
\end{aligned}$$

Qudits

Another interesting aspect to study is the extension of the algorithm to higher dimensional building blocks. We provide an example in which the optimal control state for a multitask controlled unitary operation acting on qutrits is

obtained. This operation U_3 is defined in terms of the control states $|c_i\rangle$ as

$$U_3 = |c_1\rangle\langle c_1| \otimes \mathbb{1} + |c_2\rangle\langle c_2| \otimes \begin{pmatrix} 0 & 1 & 0 \\ 0 & 0 & 1 \\ 1 & 0 & 0 \end{pmatrix} + |c_3\rangle\langle c_3| \otimes \begin{pmatrix} 0 & 0 & 1 \\ 1 & 0 & 0 \\ 0 & 1 & 0 \end{pmatrix}. \quad (7.9)$$

Although no network is defined in this case, the goal of the algorithm is to find the control state that realizes the input-output transition in the target subspace. In this problem, the system consist of a single control qutrit and a single target qutrit. See Fig. 7.4.b for a numerical simulation of the learning process.

7.4 Efficiency of the Quantum Learning Algorithm

It is important to mention that the simulations and techniques we provide here only constitute a proof of principle of our learning algorithm. It would be convenient to analytically solve Eq. (7.2) to rigorously analyze the scope of the algorithm and be able to obtain information about its scalability for general problems. Since we have not solved the dynamics analytically, we evaluate the performance by comparing our results with the ones obtained via different methods. In particular, we follow two different strategies to determine the structure of the controlled unitary operation, measure it and analyze it by using machine learning techniques. Here, the resources are represented by the number of times the unitary operation has to be applied and the output measured in order to be able to determine its structure.

7.4.1 Machine Learning

We show the results achieved for three different networks, the two node line, and two different instances of the three node line, all of them previously studied with our algorithm in Fig. 7.2. For each network, three data sets were used (small, medium, large) with a different number of instances.

It must be emphasized that all results are referred to test sets, i.e., obtained with data not used to train the models. Therefore, they must be taken as a good estimation of the prediction capability of the models for new (not previously seen) data. Cross-validation was implemented by means of a

k-fold approach [154] (k=10 for all data sets, except for the small data set of the two line network whose value was k=5 due to the very limited number of instances).

All results were achieved by using Support Vector Regressor (SVRs) [183], whose characteristics make it especially adequate when dealing with sparse data sets (few instances and high dimensions). SVRs work by creating a transformed data space in which the problem is more easily resolvable (ideally the problem is transformed into a linear one). That transformation between spaces is carried out by the so-called kernels (Gaussian and polynomial kernels have been used in this experimentation). The data used for training the models has been randomly selected from a set of multiple pairs of control state and fidelity.

Tables 7.1, 7.2 and 7.3 report the results achieved by the SVR in the three analyzed networks. For each case, the state with the best fidelity is shown, together with the Mean Error (ME) and the Root Mean Square Error. ME is a measure of bias that represents the difference between the real and the predicted efficiencies, i.e., gives information about whether the model tends to make overestimations (negative values) or underestimations (positive values). On the other hand, RMSE is a well-known robust measure of accuracy.

Number of Instances	Small (10)	Medium (75)	Large (500)
ME	0.0029	-1.3 10^{-4}	-8.6 10^{-5}
RMSE	0.0493	0.0012	0.0026
Best Fidelity	0.874	0.962	0.987

Table 7.1: **Two node line.** The optimal control state for this network is $|1\rangle \otimes |1\rangle$, while the best result obtained with this analysis is $(0.0535\,|0\rangle + 0.9986\,|1\rangle) \otimes (0.0786\,|0\rangle + 0.9969\,|1\rangle)$.

7.4.2 Measurement of the Unitary Operation

A different method would be to measure the input-output relation of the controlled unitary operation when strategically, and not randomly, exploring the control subspace. Let us denote by $|c_i\rangle$ the natural basis of the unitary operation, and by $|b_i\rangle$ our guess for this basis in a Hilbert space of dimension n. The measurement protocol consists on applying the unitary operation to

Number of Instances	Small (50)	Medium (200)	Large (1000)
ME	$7.2\ 10^{-4}$	$2.4\ 10^{-5}$	$3.2\ 10^{-4}$
RMSE	0.0054	0.0017	0.0039
Best Fidelity	0.6840	0.8836	0.8872

Table 7.2: **Three node line A.** The optimal control state for this network is $|1\rangle \otimes |1\rangle \otimes |1\rangle$, while the best solution that the machine learning protocol provides is $(0.1785\,|0\rangle + 0.9839\,|1\rangle) \otimes (0.2063\,|0\rangle + 0.9785\,|1\rangle) \otimes (0.1754\,|0\rangle + 0.9845\,|1\rangle)$.

Number of Instances	Small (50)	Medium (200)	Large (1000)
ME	$-9.3\ 10^{-4}$	$-7.8\ 10^{-5}$	$-9.6\ 10^{-5}$
RMSE	0.0082	0.0018	0.0014
Best Fidelity	0.9227	0.9188	0.9709

Table 7.3: **Three node line B.** The optimal control state for this network is $\frac{1}{\sqrt{2}}[|0\rangle + |1\rangle] \otimes |1\rangle \otimes [\cos(\pi/3)\,|0\rangle + \sin(\pi/3)\,|1\rangle]$., while the result of the analysis is $(0.7512\,|0\rangle + 0.66\,|1\rangle) \otimes (0.1599\,|0\rangle + 0.9871\,|1\rangle) \otimes (0.4936\,|0\rangle + 0.8697\,|1\rangle)$.

$|b_i\rangle \otimes |in\rangle$, project this result on $|out\rangle\langle out|$ and trace out the target subspace achieving ρ_i for each b_i. This operation has to be repeated at least n times to guarantee that the populations, but not the internal phases, of the solutions are found. Afterwards, one has to find the appropriate basis $|c_i\rangle$ as a linear combination of the proposed one $|b_i\rangle$. Another approach is to determine each component of the unitary operation and change to a basis in which the unitary is expressed as a direct sum of the s_i operations. This particular strategy highlights the relation between our algorithm and the field of quantum process tomography.

Summarizing, the purely random approach analyzed with ML techniques requires in principle more resources than the feedback algorithm. Nevertheless, the fact that ML techniques are independent of the basis guarantees their success in any possible situation. Regarding the complete measurement approach, recent studies suggest its scalability in the order of n^2 being n the dimension of the Hilbert space [184, 185], or even a linear bound [186]. On the other hand, the measurement protocol does not provide the solution in a physical register, is the analysis of the unitary operation that provides the knowledge of it. Moreover, each implementation of the controlled unitary operation is associated with a measurement, while in the learning algorithm

intermediate measurements are not required, because they are included as an intrinsic part of the dynamics, in contrast to the tomography approach. Additionally, when measuring, one needs to perform a search for the convenient basis along the Hilbert space to retrieve the correct structure of U.

This raises an important question about the scalability of resources in the feedback learning algorithm. We have observed that the number of episodes for reaching the solution depends on the distance between both, the initial control state and the solution. A direct consequence is that the protocol only works when the initial control state is not ortogonal to the solution. This is the most important drawback of the protocol because the only way to notice the failure is to validate the result by measuring the outcome of the unitary operation. In the simulations considered here we have employed $|+\rangle^{\otimes n}$ as the initial control state, but this choice is not unique.

In some sense, our protocol can also be understood as a search algorithm, therefore the comparison with Glover's result [26] is inescapable. Regarding the similarities, the conditional phase rotation in Grover's algorithm requires the use of an oracle, whose role is played by the combination of a controlled unitary operation and the time delay terms in our formalism. On the contrary, the main difference between both protocols is that on Grover's algorithm the basis in which the states to optimize are described is known, while in ours, the search is performed without previous knowledge of the basis.

7.5 Conclusions

In conclusion, we have developed a quantum learning algorithm in which the implementation of time-delayed dynamics allows to avoid the intermediate measurements required in traditional machine learning algorithms. We have shown how the framework of multitask controlled unitary operations is flexible enough to address different problems such as efficient excitation transport in networks. We leave for future works the analysis about the limits of the algorithm in terms of complexity and scalability, and the design of a suitable experimental protocol. For the moment, our study represents the first proof of principle for exploiting feedback induced effects in quantum learning algorithms.

Chapter 8

The Forbidden Quantum Adder

> There is no quantum world.
> There is only an abstract
> quantum physical description.
> It is wrong to think that the
> task of physics is to find out
> how nature is. Physics concerns
> what we can say about nature...
>
> *Niels Bohr*

In this chapter, we prove that there is no unitary protocol able to add unknown quantum states belonging to different Hilbert spaces. This is an inherent restriction of quantum physics that is related to the impossibility of copying an arbitrary quantum state, i.e., the no-cloning theorem. Moreover, we demonstrate that a quantum adder, in absence of an ancillary system, is also forbidden for a known orthonormal basis. We also discuss the distinct character of the forbidden quantum adder for quantum states and the allowed quantum adder for density matrices. Finally, we propose a family of approximate quantum adders whose gate sequence is optimized with the use of genetic algorithms for their experimental implementation.

8.1 Introduction

Addition plays a central role in mathematics and physics, while adders are ubiquitous devices in the fields of computation [174] and electronics [187].

In this sense, usual sum operations can be realized by classical Turing machines [173] and also, with a suitable algorithm, by quantum Turing machines [2, 188]. Furthermore, the sum of known state vectors in the same Hilbert space, i.e. quantum superposition, is at the core of quantum physics. In fact, entanglement and the promised exponential speed-up of quantum computing are based on such linear combinations. Here, we consider the existence of a quantum adder, defined as a unitary operation mapping two unknown quantum states encoded in different quantum systems onto their sum codified in a single system. The surprising answer is that this quantum adder is forbidden and it has the quantum cloner as a special case [49]. This no-go result, as other prohibited operations [49, 189, 190, 191], is of fundamental nature and its implications should be further studied. Furthermore, we consider a high-fidelity approximate quantum adder involving ancillary systems.

Recently, a quantum superposer was introduced [192], an operation allowing for an arbitrary superposition and different from the quantum adder to avoid the global phase limitation, but also forbidden by quantum mechanics on its most general form. Beyond the initial prohibition there is space for approximate versions of both adders. In particular, proposals of the quantum superposer [192] has been experimentally realized recently [193, 194]. Moreover, a third variant of the protocol was defined for creating a superposition of two unknown states from a given finite set in the presence of closed timelike curves [195].

8.2 Definition of the Quantum Adder

Let $|\Psi_1\rangle, |\Psi_2\rangle \in \mathbb{C}^d$ be two quantum states of a finite-dimensional Hilbert space. The conjectured quantum adder, sketched in Fig. 8.1, would be a mathematical operation defined as the unitary $U : \mathbb{C}^d \otimes \mathbb{C}^d \to \mathbb{C}^d \otimes \mathbb{C}^d$, for every pair of unknown $|\Psi_1\rangle \otimes |\Psi_2\rangle$ and ancillary vector $|\chi\rangle \in \mathbb{C}^d$,

$$U|\Psi_1\rangle|\Psi_2\rangle \propto (|\Psi_1\rangle + |\Psi_2\rangle)|\chi\rangle, \tag{8.1}$$

where the ancillary state $|\chi\rangle$ may depend on the input states. There are several ways of proving the unphysicality of Eq. (8.1). The simplest one is to note that the unobservable global phase on its l.h.s. could be distributed in infinite forms on its r.h.s., $Ue^{i\phi}|\Psi_1\rangle|\Psi_2\rangle = Ue^{i\phi_1}|\Psi_1\rangle e^{i\phi_2}|\Psi_2\rangle \propto (e^{i\phi_1}|\Psi_1\rangle + e^{i\phi_2}|\Psi_2\rangle)|\chi\rangle$, with $\phi = \phi_1 + \phi_2$, yielding an observable relative

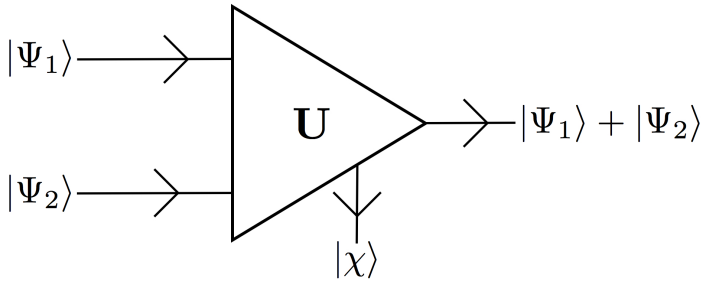

Figure 8.1: **Scheme of the conjectured quantum adder.** The inputs are two unknown quantum states, $|\Psi_1\rangle$ and $|\Psi_2\rangle$, while the outputs are proportional to the sum, $|\Psi_1\rangle + |\Psi_2\rangle$ with an ancillary state $|\chi\rangle$.

phase. When the ancillary state $|\chi\rangle$ does not depend on the input quantum states, the (forbidden) quantum cloner becomes a particular case of this restricted quantum adder. This follows from applying U to two equal state vectors $U|\Psi\rangle|\Psi\rangle = |\Psi\rangle|\chi\rangle$, since the inverse generates a quantum cloning operation. Therefore, although the general case of the quantum adder is not equivalent to a quantum cloner, it is still forbidden.

We adress now a different question, whether a quantum adder may exist for a given orthonormal basis. Let us consider the action of the unitary operator U onto a set of orthonormal vectors: $U|0\rangle\,|0\rangle = |0\rangle\,|B_0\rangle$, $U|0\rangle\,|i\rangle = \frac{1}{\sqrt{2}}(|0\rangle+|i\rangle)\,|B_i\rangle$ and $U|i\rangle\,|0\rangle = \frac{1}{\sqrt{2}}(|0\rangle+|i\rangle)\,|\tilde{B}_i\rangle$, with $i = 1, \ldots, d-1$. Hence, as U is a unitary matrix, it imposes some orthogonality conditions on the final vectors, $\langle B_0|B_i\rangle = \langle B_0|\tilde{B}_j\rangle = \langle B_i|\tilde{B}_j\rangle = 0$ and $\langle B_i|B_j\rangle = \langle \tilde{B}_i|\tilde{B}_j\rangle = \delta_{i,j}$, with $i, j = 1, \ldots, d-1$. The second subspace has dimension d, but these constraints require the existence of at least $2d-1$ orthonormal vectors, which is impossible. This argumentation proves that even in the case in which the phase is fixed, the quantum adder cannot be obtained without the use of an ancillary system.

Beyond the sum of quantum states in Eq. (8.1), we may also consider the statistical addition of density matrices. Here, the input states are the tensor product of any pair of density matrices $\sigma = \rho_1 \otimes \rho_2 \in \mathcal{B}(\mathbb{C}^{2d} \otimes \mathbb{C}^{2d})$, while the output state is the statistical sum $\rho = \frac{1}{2}(\rho_1 + \rho_2)$. The Kraus operators of the quantum channel realizing this adder are given by $E_i = \frac{1}{\sqrt{2}}(\mathbb{1}_d \otimes \langle i|)$

and $F_j = \frac{1}{\sqrt{2}}(\langle j| \otimes \mathbb{1}_d)$, with $1 \leq i, j \leq d$. These operators straightforwardly perform the sum, i.e., $\mathcal{E}(\sigma) = \sum_{k=1}^{d} E_k \sigma E_k^\dagger + \sum_{k=1}^{d} F_k \sigma F_k^\dagger = \frac{1}{2}(\rho_1 + \rho_2)$. Moreover, properly modified Kraus operators allow us to extend the previous result to any convex combination of input states. Therefore, the addition of density operators is always possible.

Let us compare the adders for state vectors and density operators. By writing the input states in Eq. (8.1) as density matrices, $\rho = |\Psi_1\rangle\langle\Psi_1| \otimes |\Psi_2\rangle\langle\Psi_2|$, both adders yield

$$\begin{aligned} U\rho U^\dagger &\propto |\Psi_1\rangle\langle\Psi_1| + |\Psi_1\rangle\langle\Psi_2| + |\Psi_2\rangle\langle\Psi_1| + |\Psi_2\rangle\langle\Psi_2|, \\ \mathcal{E}(\rho) &= \frac{1}{2}(|\Psi_1\rangle\langle\Psi_1| + |\Psi_2\rangle\langle\Psi_2|). \end{aligned} \tag{8.2}$$

By comparing the adders in Eq. (8.2), we can infer that the one in Eq. (8.1) would require the knowledge of the sum coherences, which were supposed unknown.

The self-consistent definition of the adder.

When proposing an approximate quantum adder we first have to make it self-consistent with respect to the global phase variation, which does not affect the experimental realization, but modifies the definition of the ideal output, and therefore the fidelity function. The absence of global phase invariance lies at the heart of the no-go and has to be avoided to make the quantum adder realizable. There are two ways to fix this behaviour of the adding machine. The first option is to relax the definition of the adder by inserting an intermediate phase factor $e^{i\phi}$. Thus, instead of matching the output state of the adder with $\psi_1 + \psi_2$, we match it with $\psi_1 + e^{i\phi}\psi_2$ for a certain ϕ, which is the result shown in Fig 8.2 for the basis adder. The second option is to restrict the domain of the quantum adder from the whole Hilbert space to a self-consistent region and to fix the value of the relative phase such that there is no phase ambiguity. The first approach would disable us to know exactly the ideal state of reference after summation and, for certain inputs, we wouldn't be able to distinguish the outcome states $|0\rangle$ and $|1\rangle$. We thus prefer the latter approach to evade the global phase problem without changing the most natural definition of a quantum state adder, by restricting our two input states to take the form

$$|\psi_i\rangle_{in} = \begin{pmatrix} \cos\theta_i \\ \sin\theta_i \end{pmatrix}, \tag{8.3}$$

where θ_i goes from 0 to $\pi/2$. The ideal state of reference after addition, with N as the normalization factor, is

$$|\Psi_{id}\rangle = |\psi_1\rangle_{in} + |\psi_2\rangle_{in} = \frac{1}{N}\begin{pmatrix} \cos\theta_1 + \cos\theta_2 \\ \sin\theta_1 + \sin\theta_2 \end{pmatrix}. \tag{8.4}$$

Notice that by choosing this parametrization we are effectively selecting the value of both the external and internal phases $\phi = 0$.

8.3 Approximate Quantum Adders

8.3.1 Basis Adder

We propose now the use of an ancillary system $|A\rangle$, which will assure the physicality and experimental feasibility of an approximate quantum adder for arbitrary unknown quantum states, see Fig. 8.2. This particular adder, U_b, computes the exact sum of the basis elements in qubit systems. Moreover, U_b is extended by linearity to the whole Hilbert space, and implements an approximate sum when the input states are superpositions of the basis elements. The adder is given by the following expression in which $|B_i\rangle$ are orthonormal and $|+\rangle = \frac{1}{\sqrt{2}}(|0\rangle + |1\rangle)$,

$$\begin{aligned} U_b|0\rangle|0\rangle|A\rangle &= |0\rangle|B_1\rangle, \qquad U_b|0\rangle|1\rangle|A\rangle = |+\rangle|B_2\rangle, \\ U_b|1\rangle|0\rangle|A\rangle &= |+\rangle|B_3\rangle, \qquad U_b|1\rangle|1\rangle|A\rangle = |1\rangle|B_1\rangle. \end{aligned} \tag{8.5}$$

To uniquely define our adder, we need to complete the action of U on the computational bases when the ancillary qubit is in state $|1\rangle$. From all the possible selections of the basis adder, we choose U in the following manner

$$\begin{aligned} &U\,|000\rangle = |000\rangle\,, \;\; U\,|010\rangle = |01{+}\rangle\,, \;\; U\,|100\rangle = |10{+}\rangle\,, \;\; U\,|110\rangle = |001\rangle\,, \\ &U\,|001\rangle = |110\rangle\,, \;\; U\,|011\rangle = |01{-}\rangle\,, \;\; U\,|101\rangle = |10{-}\rangle\,, \;\; U\,|111\rangle = |111\rangle\,. \end{aligned} \tag{8.6}$$

so that it can be decomposed as

$$U = P^{(2,7)}\; U^{(1,2)}_{\mathrm{CNOT}}\; U^{(2,3)}_{\mathrm{CHad}}\; U^{(1,2)}_{\mathrm{CNOT}}. \tag{8.7}$$

with $P^{(2,7)} = U^{(\bar{1},2)}_{\mathrm{CNOT}}\; U^{(\bar{1},3)}_{\mathrm{CNOT}}\; U^{2\bar{3},1}_{\mathrm{Toff}}\; U^{(\bar{1},3)}_{\mathrm{CNOT}}\; U^{(\bar{1},2)}_{\mathrm{CNOT}}$. Here, $U^{(i,j)}_{\mathrm{CNOT}}$ stands for Controlled-NOT (CNOT) gate with the ith qubit to be the control and the

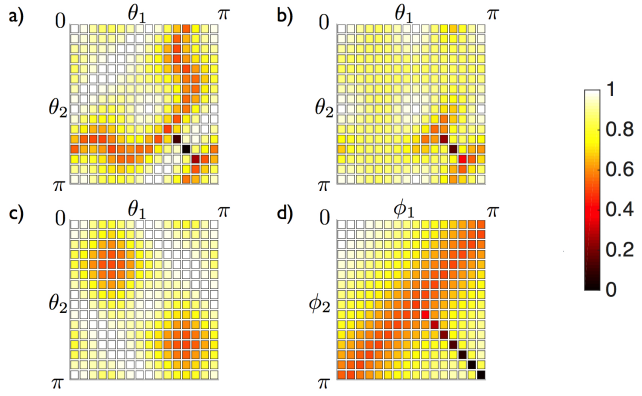

Figure 8.2: **Basis Adder.** Fidelity of the proposed approximate quantum adder as a function of the parameters of the input states $|\Psi_j\rangle = \cos\theta_j|0\rangle + \sin\theta_j e^{i\phi_j}|1\rangle$, where $j = 1, 2$. Here, a) $\phi_1 = \phi_2 = 0$, b) $\phi_1 = \phi_2 = \pi/4$, c) $\phi_1 = \phi_2 = \pi/2$, and d) $\theta_1 = \theta_2 = \pi/4$. Note that the diagonal line of each plot corresponds to the approximate quantum cloner that is related to our restricted quantum adder. In this case, the fidelities are the lowest.

jth qubit to be the target, $U_{\text{Toff}}^{ij,k}$ denotes the Toffoli gate, with qubits i and j controlling the kth one, U_{CHad} is the Controlled-Hadamard gate, and the overbar symbol on the control qubit means the role of 0 and 1 levels is exchanged in this qubit. The whole protocol of the basis adder U can be depicted with the quantum circuit diagram (QCD) of Fig. 8.3.

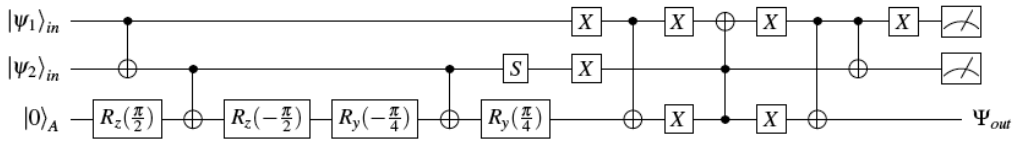

Figure 8.3: **QCD of the basis adder.** Here, X, S and $R_\alpha(\theta)$ correspond respectively to the Pauli X gate, the phase gate, and rotations of θ in the α Pauli matrix. Furthermore, the Toffoli gate can be decomposed into Hadamard, phase, CNOT, and $\pi/8$ gates [10].

By further observing QCD, in Fig. 8.3, we could eliminate the last CNOT

and X gates lying at the end without changing the output state, hence preserving the performance of this adder and reducing the experimental error. So far, we have achieved decomposing our basis adder U into 11 CNOTs and 23 single qubit rotations (one Hadamard gate counts as two rotations: a $\pi/2$ rotation along the y-axis followed by a π rotation along the x-axis) which in total add up to 34 gates.

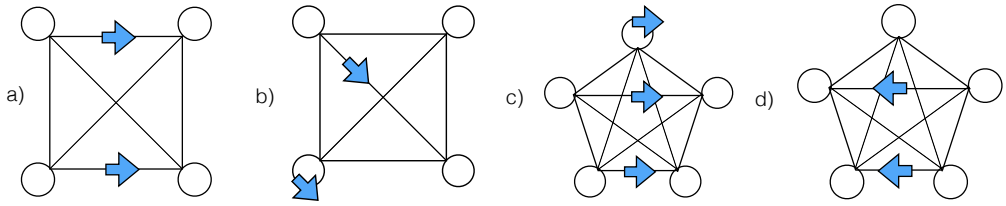

Figure 8.4: **Generalization of the basis adder.** (a) For even dimension d, tuples of B_{ij} states are obtained by grouping the vector connecting vertices i and $i+1$ with all the parallel vectors in the same direction. (b) The remaining d tuples are obtained by grouping the monogon of each vertex with all the vectors perpendicular to the line that connects the vertex with its opposite one, in a given direction. (c) For odd dimension d, tuples of B_{ij} states are obtained by grouping the vector connecting vertices i and $i+1$ with the monogon of the opposite vertex and all the diagonals parallel to the vector in the same direction. (d) The remaining d tuples are obtained with the same procedure for the opposite direction but excluding the monogons of the vertices, because they have been already grouped.

The basis adder can be generalized to act on qudits of dimension d. The most simple expression consists in defining the adder U, superposing the elements of the basis with a residual subspace exclusive of those particular elements,

$$U\left|i\right\rangle\left|j\right\rangle\left|A\right\rangle = \left|i+j\right\rangle\left|B_{ij}\right\rangle. \tag{8.8}$$

Here, $|i+j\rangle$ represents $\frac{1}{\sqrt{(2+2\delta_{ij})}}\left(|i\rangle+|j\rangle\right)$, and the ancillary state $|A\rangle$ has the same dimension as the input states, which enables that $\langle B_{\alpha\beta}|B_{ij}\rangle = \delta_{\alpha i}\delta_{\beta j}$ is satisfied $\forall\ i,j = 0,...,d-1$. In order to reduce the resources and enhance the fidelity we provide an alternative definition of the constituents of U in which the number of residual states B_{ij} is only $2d$ instead of d^2, which allows to replace the d dimensional ancillary state $|A\rangle$ with a qubit. This idea is supported on the fact that not all the B_{ij} need to be orthonormal for the

unitarity conditions to be satisfied. The B_{ij} can be combined in tuples of states that are represented with a single one, therefore reducing the dimension of the residual subspace. After analyzing this method for the low dimensional cases $d \leq 6$, we provide a discussion about its veracity for any d.

The procedure is to count the number of tuples of B_{ij} that do not need to be orthonormal, and contain the whole set of the d^2 B_{ij} states. This d^2 would represent the total number of B_{ij} if all of them were orthonormal. The unitarity condition implies that a set of orthonormal states is mapped into a set of orthonormal states, therefore $|B_{\alpha\beta}\rangle$ and $|B_{ij}\rangle$ only need to be orthonormal when any of the α, β coincides with any of the i, j. The reason is that, $\langle \alpha + \beta | i + j \rangle = \frac{1}{2} \left(\langle \alpha | i \rangle + \langle \alpha | j \rangle + \langle \beta | i \rangle + \langle \beta | j \rangle \right)$.

Our argument is that the problem of finding the minimum number of tuples can be encoded in the structure of regular convex polygons of d vertices. Each vector in a given direction between vertices i and j, encodes a B_{ij} element, while the opposite vector encodes the B_{ji} for $i \neq j$. Additionally, monogons in each vertex encode B_{ij} for $i = j$. Notice that the sum of the vertex monogons d with twice the diagonals, $d(d-3)$, and twice the sides, $2d$, equals d^2, the total number of B_{ij} if all were orthonormal. In the graphical analogy, the rule for obtaining tuples of B_{ij} states that do not need to be orthonormal is to group the sides, diagonals or monogons that do not share any vertex. More precisely, we provide a method that guarantees that the number of tuples is $2d$. For even d, each of the d tuples is obtained when grouping the vector $i, i+1$ with all the parallel diagonals and the vector in the opposite side and equal direction. The remaining d tuples are obtained when grouping the monogons in each vertex i with the diagonals that are perpendicular to the diagonal that connects the vertex i with its opposite vertex. For odd d, the d tuples are obtained when grouping the vector $i, i+1$ with all the parallel diagonals and the monogon at the opposite vertex. The remaining d tuples are obtained when grouping the same vector and diagonals in the opposite direction. See Fig. 8.4 for a scheme of the analogy between B_{ij} states and the regular convex polygons.

Therefore, a set of $2d$ $|B_{ij}\rangle$ states is enough to satisfy the unitarity conditions, implying that only an ancillary with dimension 2 is required. See, as an example, all the tuples for $d = 4$,

$$\begin{aligned} &\{B_{01}, B_{32}\}, \{B_{12}, B_{03}\}, \{B_{23}, B_{10}\}, \{B_{30}, B_{21}\}, \\ &\{B_{00}, B_{13}\}, \{B_{11}, B_{20}\}, \{B_{22}, B_{31}\}, \{B_{33}, B_{02}\}. \end{aligned} \tag{8.9}$$

8.3.2 Approximate Adders with Genetic Algorithms

With the goal of improving the basis adder, we have developed a program using genetic algorithms to find the optimal protocols for the adding operation. The algorithm, which is a variant of a previous program, see Chapter 6, works due to the formalism derived to translate each quantum circuit diagram to a sequence of instructions, and the fidelity, to its analogous fitness function.

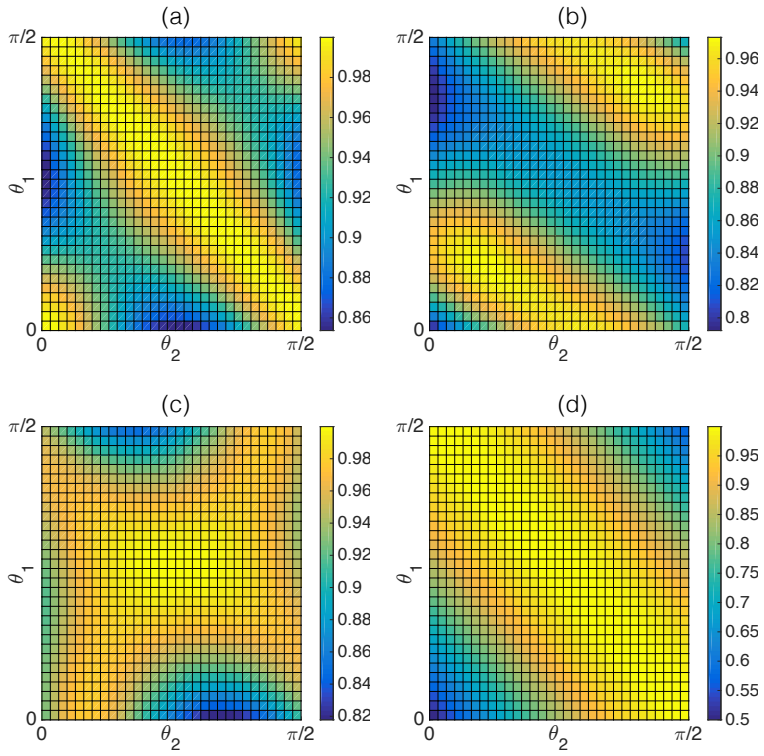

Figure 8.5: **Fidelities of the most promising quantum adders.** (a) The basis adder, with an average value of 94.9%, and a minimum value of 85.4%. (b) The complexity-reduced adder with an average fidelity of 90.0%, and minimum fidelity of 79.2%. (c) The trivial adder given by the $|+\rangle$ state, with an average theoretical fidelity of 90.2% and a minimum fidelity of 50%. (d) The 31-gate approximate adder with an average theoretical fidelity of 95.4%, and minimum fidelity of 81.2%.

Each cycle in the algorithm starts with four $p \times 3$ matrices, representing four sequences of gates from a finite set of gates, where p stands for the maximum number of gates allowed in the protocol which can be arbitrarily chosen. Each row in the matrices specifies a quantum gate from the set S_g,

$$\begin{aligned} S_g &= \{R_x^{(i)}(\theta),\, R_y^{(i)}(\theta),\, R_z^{(i)}(\theta),\, U_{\text{CNOT}}^{(i,j)}\}, \\ i,j &= 1,2,3;\ \theta = \pi, \pi/2, \pi/4, -\pi/4, -\pi/2, -\pi. \end{aligned} \tag{8.10}$$

with 61 possibilities ($U_{\text{CNOT}}^{(i,i)} = \mathbb{1}$). The initial population can be either randomly or purposely chosen, depending on the convenience of introducing a previous solution. After the initialization, the genetic algorithm hierarchically recombines the rows between different individuals, generating several new-born sequences with the same number of rows. After a stage of random mutations, all newly generated and the original input sequences will be sorted according to their fidelity. Finally, the highest four will be selected and kickstart the forthcoming cycle as the initial inputs. One can specify the total number of generations and maximum number of gates in the fidelity or circuit optimization. The more rows we allow for our protocol, the better it can approximate a potential optimal adder U since the versatility for realizing an arbitrary unitary matrix gets improved. However, it will be harder for the protocol to be carried out in a laboratory due to the increasing complexity. Hence, we have to make a compromise and set a limit of p according to physical conditions allowed in each particular lab.

Fidelity

The fidelity of the adder $\tilde{U}$ is defined as $F = \text{Tr}(|\Psi_{id}\rangle \langle\Psi_{id}|\ \rho_{out})$, for $\rho_{out} = \text{Tr}_{12}(\tilde{U}\,|\psi_1\rangle \langle\psi_1| \otimes |\psi_2\rangle \langle\psi_2| \otimes |0\rangle \langle 0|\, \tilde{U}^\dagger)$, where the partial trace is taken over the first two qubits. We have plotted the fidelity of the basis adder derived above in Fig. 8.5.a. Regarding the experimental fidelity of the protocol, our calculations are based on the recently reported gate errors for a superconducting circuit architecture [84], which are about 1% for a two-qubit Controlled-Phase gate and 0.1% for an arbitrary single-qubit gate. Recalling that in this particular platform each Controlled-NOT gate can be realized by 1 Controlled-Phase and 2 Hadamard gates, if the average theoretical fidelity is F_a, then an estimation of the experimental fidelity of the adder is

$$F_{exp} = F_a \times (0.999)^{N_s + 2N_{\text{CNOT}}} \times (0.99)^{N_{\text{CNOT}}}. \tag{8.11}$$

Here, N_s and N_{CNOT} stand for the number of single-qubit gates and the number of CNOT gates, respectively. After we take Eq. (8.11) into account, the remaining experimental fidelity is about 80%, which is still high.

Adders found by the genetic algorithms.

By setting the maximum number of gates to 20, we have found a complexity-reduced adder consisting of only two CNOTs having an average theoretical fidelity of 90% and a minimum of 79.2%. See Fig. 8.5.b and Fig. 8.6. Although its theoretical fidelity is lower than the one of the basis adder (94.9%), its implementation fidelity is actually the highest one, about 87%, if implemented in superconducting circuit platforms [84]. An interesting point to highlight here is that this adder has nearly the same average fidelity as the one given by a plus state, $|+\rangle$, in the output of the adder, see Fig. 8.5.c The difference is that the $|+\rangle$, which is trivial because it does not depend on the inputs, has a lower minimal fidelity of 50% and an average theoretical fidelity of 90.2%. Therefore, this trivial adder establishes the lower limit of the average fidelity for the adder to be considered interesting in the region we are confined into.

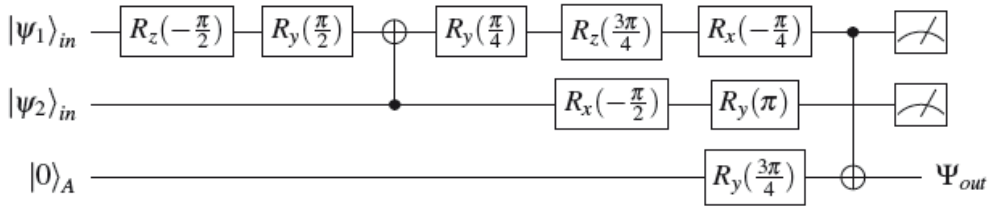

Figure 8.6: **Quantum circuit for the complexity reduced adder.**

If we allow for 40 gates, the GA achieves an approximate adder with an average theoretical fidelity above 95%, see Fig. 8.5.d and Fig. 8.7. This adder contains overall 31 gates, 13 of which are two-qubit CNOT gates. The expected experimental fidelity of this 31-gate adder is roughly the same as the basis adder which is about 80%.

It should be noticed that this adder and the adder we found previously with 10 gates shown in Fig. 8.3 are not commutative adders, i.e., the adding machine $\mathcal{M}$ defined by them does not satisfy

$$\mathcal{M}(\psi_1, \psi_2) = \mathcal{M}(\psi_2, \psi_1) \tag{8.12}$$

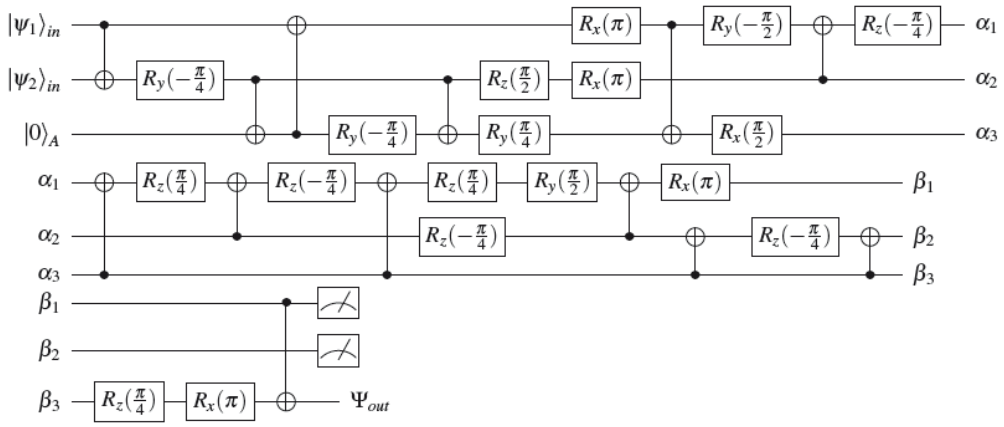

Figure 8.7: **Quantum circuit for the high fidelity adder.**

for arbitrary input states ψ_1 and ψ_2. The main reason is that the GA does not select the gate sequence according to the commutativity of the resulting unitary, but according to the average fidelity of the adder. Another result to highlight is the absence of a high-fidelity and universal quantum adder. The only result obtained so far in this respect is a fixed quantum state, with an overall fidelity of 50% and independent of the inputs, which is perpendicular to the region in which the adder is defined.

8.4 Conclusions

We have defined the quantum adder operation and proved a no-go about its existence in its most general form. This prohibition is of fundamental character in quantum physics, deeply related but different to the no-cloning theorem. Furthermore, we have shown that approximate versions of the quantum adder allow for an imperfect reproduction of the idea behind the adding mechanism. Lastly, we have studied how to simplify the implementation of the quantum adder by optimizing the gate sequence with the use of genetic algorithms. In conclusion, the debate around the quantum adder sheds light on a basic limitation of quantum protocols, while provides alternatives for avoiding the no-go.

Chapter 9

Outlook

> If you have never wept bitter tears because a wonderful story has come to an end and you must take your leave of the characters with whom you have shared so many adventures, whom you have loved and admired, for whom you have hoped and feared, and without whose company life seems empty and meaningless. If such things have not been part of your own experience, you probably won't understand what Bastian did next.
>
> *Michael Ende*

In this thesis, we have explored the possibility of bringing the complexity of biological systems down to the world of controllable quantum experiments. While we can argue that protocols described here are in the appropriate direction according to our definition of Quantum Biomimetics, in this chapter, we will focus in the goals that have not been accomplished. These motivate the future steps, in the direction of increasing the number of biological features or improving the way they emerge.

In particular, the issue of emergence may be considered as the main criticism to the work presented in the first part about Quantum Artificial Life.

The qubit-encoded individuals behave as puppets in the natural selection scenario we have designed, in the sense that they require an external hand for implementing each step in their evolution. Even though we assume that the interaction with the system is mandatory in any quantum simulation experiment, in the specific case of Artificial Life, it is desirable that the action is minimal for being able to claim that life inspired features really emerge in the system. Therefore, the continuation of this research line should be oriented towards providing autonomy to the individuals by developing a quantum algorithm where the life processes are the effect of a subtle combination of a variety of dynamics, without a previously arranged plot or intermediate measurements.

This idea produces the connection between Quantum Artificial Life and the works of the second part about Mnemonic Quantum Systems. Our intuition suggests that the inclusion of memory-like dynamics in the evolution can have the effect of dressing the system with more autonomous character.

In this sense, equations with memory effects can be achieved when limiting our effective model to a given subsystem. Therefore, these could be implemented when simulating the complete unitary dynamics over the whole system by incorporating the missing subspaces. But the exponential growth of the Hilbert space dimension requires an immense cost in resources. That is the reason why we have preferred to work with phenomenological equations, which can also be exploited as a source of memory and offer dynamical regimes uncovered by the system-environment approach.

An interesting research line to follow in future works is the design of quantum algorithms that are based on mnemonic equations. This would motivate to study a clear characterization of different memory dynamics together with the possibilities that each potential type offers in the development of quantum protocols. This achievement could help at isolating the properties of each type and, therefore, accelerate the improvement in efficiency for implementing each mnemonic family.

Regarding the third part of this thesis, Intelligent Quantum Systems, we would like to analyze each specific work separately, and mention possible directions for extending or improving the obtained results.

The main criticism to the protocol of genetic algorithms in Chapter 6 is that the optimization has to be done for each time in the evolution. The algorithm may be improved with an alternative definition of the fitness function consisting on the maximization of a normalized time integral of the fidelity. The goal is to reward the digital protocols that simulate the desired dynamics

in a given interval and not in a single point.

Regarding the feedback induced learning in Chapter 7, it would be convenient to study the analytic solutions of the time delayed equation for obtaining clear bounds regarding the scalability and complexity classes of the problems to solve. Additionally, to find tasks that can be encoded in multitask controlled unitary operations would be desirable for enhancing the versatility of the algorithm.

Chapter 8 about quantum adders lacks of any detailed example of applications in which the quantum adder is necessary. Two suggestions for future routes in this direction are the development of quantum neural networks and the design of cryptographic protocols which could make the approximate versions of the quantum adder useful.

Finally, as a general comment, we should always keep in mind that the only possible adaptation of the theoretical ideas to experimental quantum platforms is what makes the protocols valuable. Therefore, one of the most important follow ups of the work in this thesis is its consolidation via the experimental implementation of our quantum protocols.

In conclusion, we have created a set of tools for simulating bio-inspired processes that bring new possibilities to the framework of quantum simulation and quantum computation. The results presented here under the label of Quantum Biomimetics can be the light guiding future designs and implementations in the recreation of biological processes in quantum technologies.

Part IV

Appendices

Appendix A

Theorems

• Here we give the proof of theorem 1 in the paper.

Proof.

$$\begin{aligned}\langle \theta \otimes \mathbb{1} \rangle &= \mathrm{Tr}[U(\rho \otimes \rho_e)U^\dagger(\theta \otimes \mathbb{1})] \\ &= \mathrm{Tr}[\sum_{i,j=1}^{n} s_i \rho s_j^\dagger \theta \otimes x_i \rho_e x_j^\dagger].\end{aligned}$$

When looking at the second subspace, $x_i \rho_e x_j^\dagger$, only the terms with $i = j$ are left in the diagonal, therefore only those are relevant for the trace. We consider $i = j$ in the first subspace, $s_i \rho s_i^\dagger \theta$. The remaining is the product between the diagonal terms of the density matrix ρ and the observable θ, that is precisely.

$$\mathrm{Tr}[\rho\theta] = \langle \theta \rangle$$

This shows that the mean value of θ is effectively cloned in the first individual by means of U. The proof for the second individual is obtained in a similar way. □

• Now we prove theorem 2 in the paper.

Proof.

$$\begin{aligned}\langle \tau \otimes \tau \rangle &= \mathrm{Tr}[U(\rho \otimes \rho_e)U^\dagger(\tau \otimes \tau)] \\ &= \mathrm{Tr}[\sum_{i,j=1}^{n} s_i \rho s_j^\dagger \tau \otimes x_i \rho_e x_j^\dagger \tau].\end{aligned} \tag{A.1}$$

The second subspace, $x_i \rho x_j^\dagger \tau$, will only contribute to the trace when it is diagonal. Since τ is antidiagonal the only effective combination of i, j is $(i = 1, j = n)$, $(i = 2, j = n - 1)$,... When applying this restriction to the first subspace, $s_i \rho s_j^\dagger \tau$, the global expresion turns out to be $\mathrm{Tr}[\rho\tau]$, only if the matrix elements of τ are 0 or 1. We have thus shown how τ is promoted into the global state of the system.

□

Properties of the cloning operation

• We show here that the τ operator is also transmitted when cloning in any basis. When the unitary operation U is rotated with the matrix R it propagates the information of the rotated matrix τ'.

$$\begin{aligned}
&\mathrm{Tr}[\rho\tau'] = \mathrm{Tr}[U'(\rho \otimes \rho_e)U'^\dagger(\tau \otimes \tau)] = \\
&\mathrm{Tr}[(R^\dagger \otimes R^\dagger)U(R \otimes \mathbb{1})(\rho \otimes \rho_e)(R^\dagger \otimes \mathbb{1})U^\dagger \\
&(R \otimes R)(R^\dagger \tau R \otimes R^\dagger \tau R)] = \\
&\mathrm{Tr}[U(R \otimes \mathbb{1})(\rho \otimes \rho_e)(R^\dagger \otimes \mathbb{1})U^\dagger(R \otimes R)(R^\dagger \tau \otimes R^\dagger \tau)] = \\
&\mathrm{Tr}[UR\rho R^\dagger U^\dagger(\tau \otimes \tau)] = \mathrm{Tr}[U\tilde{\rho}U^\dagger(\tau \otimes \tau)] = \mathrm{Tr}[\tilde{\rho}\tau].
\end{aligned}$$

$$\mathrm{Tr}[\rho\tau'] = \mathrm{Tr}[\rho R^\dagger \tau R] = \mathrm{Tr}[R\rho R^\dagger \tau] = \mathrm{Tr}[\tilde{\rho}\tau].$$

Appendix B

Proposition 1

In this section, an upper bound for the truncation error of the algorithm is provided. In order to quantify the error, we use the trace norm of a matrix, defined as the sum of the singular values of the matrix: $\|\sigma\|_1 \equiv \sum_i \sigma_i$. The following recursion relation holds,

$$\begin{aligned} \|\rho(t) - \tilde{\rho}_n(t)\|_1 &\leq \int_0^t ds\, h(t,s) \|\mathcal{E} - \mathcal{I}\| \|\rho(t) - \tilde{\rho}_{n-1}(t)\|_1 \\ &\leq yc \int_0^t ds\, \|\rho(s) - \tilde{\rho}_{n-1}(s)\|_1, \end{aligned} \tag{B.1}$$

where $\rho(t)$ is the ideal solution at time t, $\tilde{\rho}_n(t)$ is nth order truncation at time t, $h(t,s) \leq c$, and $y \equiv \|\mathcal{E} - \mathcal{I}\|$, in which the superoperator norm is induced by the trace norm, i.e. $\|\mathcal{A}\| \equiv \sup_\sigma \frac{\|\mathcal{A}\sigma\|_1}{\|\sigma\|_1}$. The truncation error can be thus evaluated by induction, by considering the 0th order truncation error,

$$\|\rho(t) - \tilde{\rho}_0(t)\|_1 \leq y \int_0^t ds\, h(t,s) \|\rho(s)\|_1. \tag{B.2}$$

A bound on $\|\rho(s)\|_1$ can be found by using a Grönwall's inequality.

Theorem 3 (Grönwall's inequality [196])**.** *Let u be a continuous function defined on $J = [\alpha, \beta]$ and let the function $g(t,s)$ be continuous and nonnegative on the triangle $\Delta : \alpha \leq s \leq t \leq \beta$ and nondecreasing in t for each $s \in J$. Let $n(t)$ be a positive continuous and nondecreasing function for $t \in J$. If*

$$u(t) \leq n(t) + \int_\alpha^t ds\, g(t,s) u(s), \qquad t \in J, \tag{B.3}$$

then

$$u(t) \leq n(t) e^{\int_\alpha^t ds\, g(t,s)}, \qquad t \in J. \tag{B.4}$$

One can prove from the Volterra equation that $\|\rho(t)\|_1 \leq \|\rho(0)\|_1 + y\int_0^t ds\, h(t,s)\|\rho(s)\|_1$. Theorem 3 implies that

$$\|\rho(t)\|_1 \leq e^{y\int_0^t ds\, h(t,s)}, \tag{B.5}$$

where we have set $\|\rho(0)\|_1 = 1$. Here, we have assumed that $H(t,s) \geq 0$, to satisfy the hypothesis on $h(t,s) = \int_s^t d\tau\, H(\tau, s)$, in order to apply Theorem 3. By plugging Eq. (B.5) into Eq. (B.2), we find that

$$\|\rho(t) - \tilde{\rho}_0(t)\|_1 \leq y\int_0^t ds\, h(t,s) e^{y\int_0^s d\tau\, h(s,\tau)} \leq e^{cyt} - 1, \tag{B.6}$$

where in the second inequality, we have used that $h(s,\tau) \leq h(t,\tau)$ for $s \leq t$, allowing us to perform the integration. We can now prove by induction that

$$\|\rho(t) - \tilde{\rho}_M(t)\|_1 \leq \sum_{i=M+1}^{\infty} \frac{(cyt)^i}{i!}, \tag{B.7}$$

for any natural M. The case $M = 0$ is just the inequality found in Eq. (B.6). Let us assume that Eq. (B.7) holds for $M = n - 1$. Then,

$$\begin{aligned} \|\rho(t) - \tilde{\rho}_n(t)\|_1 &\leq yc\int_0^t ds\, \|\rho(s) - \tilde{\rho}_{n-1}(s)\|_1 \\ &\leq yc\int_0^t ds \sum_{i=n}^{\infty} \frac{(cys)^i}{i!} = \sum_{i=n+1}^{\infty} \frac{(cyt)^i}{i!}, \end{aligned} \tag{B.8}$$

which concludes the proof of Eq. (B.7).

In the following, we will prove that $\sum_{i=M+1}^{\infty} x^i/i! \leq \varepsilon$ holds, provided that $M \geq (e+1)x + \log(1/\varepsilon) - 1$. Indeed, we have that

$$\begin{aligned} \sum_{i=M+1}^{\infty} \frac{x^i}{i!} \leq e^x \frac{x^{M+1}}{(M+1)!} &\leq e^x \left(\frac{ex}{M+1}\right)^{M+1} = e^x \left(1 + \frac{ex - (M+1)}{M+1}\right)^{M+1} \\ &\leq e^x e^{ex-(M+1)} \leq \varepsilon. \end{aligned} \tag{B.9}$$

In the first inequality, we have used the Lagrange error formula for the Taylor expansion of the exponential series. In the second inequality, we have used the Stirling inequality $n! \geq \left(\frac{n}{e}\right)^n$. In the third inequality, we have used that $\left(1 + \frac{a}{b}\right)^b \leq e^a$. Finally, in the last inequality of Eq. (9), we have used the lower bound on M. By applying the last result to $x = cyt$, we finish the proof of Proposition 1.

Proposition 3

In Proposition 3, we estimate the error made when approximating the equation

$$\partial_t \rho(t) = \int_0^t ds\, K(t,s) \mathcal{L} \rho(s) \tag{B.10}$$

by the equation which corresponds to the semi-Markovian process,

$$\partial_t \rho(t) = \int_0^t ds\, H(t,s) \left[\mathcal{E}_\lambda - \mathcal{I}\right] \rho(s), \tag{B.11}$$

where $H(t,s) = K(t,s)/\lambda$ and $\mathcal{E}_\lambda = e^{\lambda \mathcal{L}}$, with the same initial condition for both equations. Let us denote by $\rho_1(t)$ and $\rho_2(t)$ the solutions to Eqs. (B.10) and (B.11), respectively. Considering the corresponding Volterra equations, we can upper bound the distance between $\rho_1(t)$ and $\rho_2(t)$,

$$\begin{aligned}
\|\rho_1(t) - \rho_2(t)\|_1 &= \left\| \int_0^t ds\, k(t,s) \left(\mathcal{L}\rho_1(s) - \frac{[e^{\lambda\mathcal{L}} - \mathcal{I}]}{\lambda} \rho_2(s) \right) \right\|_1 \\
&= \left\| \int_0^t ds\, k(t,s) \left(\mathcal{L}\left(\rho_1(s) - \rho_2(s)\right) - \frac{1}{\lambda} \sum_{i=2}^{\infty} \frac{(\lambda\mathcal{L})^i}{i!} \rho_2 \right) \right\|_1 \\
&\leq \int_0^t ds\, k(t,s) \|\mathcal{L}\| \|\rho_1(s) - \rho_2(s)\|_1 \\
&+ \frac{\lambda^2 \|\mathcal{L}\|^2 e^{\lambda\|\mathcal{L}\|}}{2} \int_0^t ds\, h(t,s) \|\rho_2(s)\|_1,
\end{aligned} \tag{B.12}$$

where we have used the definitions $h(t,s) \equiv \int_s^t d\tau\, H(\tau,s)$ and $k(t,s) \equiv \int_s^t d\tau\, K(\tau,s)$. In Eq. (B.12), we have used the triangle inequality and, then, the Lagrange bound for the Taylor series truncation, i.e. $\sum_{i=2}^{\infty} \frac{\lambda^i \|\mathcal{L}\|^i}{i!} \leq \frac{\lambda^2 \|\mathcal{L}\|^2}{2} e^{\lambda\|\mathcal{L}\|}$. As in Proposition 1, we can bound $\|\rho_2(s)\|_1$ by using the Grönwall's inequality from Theorem 3: $\|\rho_2(s)\|_1 \leq e^{\int_0^s d\tau\, h(s,\tau) \|\mathcal{E}_\lambda - \mathcal{I}\|}$, with $\|\rho(0)\|_1 = 1$. Now, we can bound the second term in Eq. (B.12), obtaining

$$\begin{aligned}
&\|\rho_1(t) - \rho_2(t)\| \leq \\
&\int_0^t ds\, k(t,s) \|\mathcal{L}\| \|\rho_1(s) - \rho_2(s)\|_1 + \frac{\lambda^2 \|\mathcal{L}\|^2 e^{\lambda\|\mathcal{L}\|}}{2\,\|\mathcal{E}_\lambda - \mathcal{I}\|} \left(e^{\int_0^t ds\, h(t,s) \|\mathcal{E}_\lambda - \mathcal{I}\|} - 1 \right).
\end{aligned} \tag{B.13}$$

We have used that $h(s,\tau) \leq h(t,\tau)$, for $s \leq t$, and performed the integration. The second term in Eq. (B.13) is positive and nondecreasing in time, so we can apply the Grönwall's inequality from Theorem 3,

$$\begin{aligned}\|\rho_1(t) - \rho_2(t)\|_1 &\leq \frac{\lambda^2 \|\mathcal{L}\|^2 e^{\lambda\|\mathcal{L}\|}}{2\,\|\mathcal{E}_\lambda - \mathcal{I}\|} \left(e^{\int_0^t ds\, h(t,s)\|\mathcal{E}_\lambda - \mathcal{I}\|} - 1\right) e^{\int_0^t ds\, k(t,s)\|\mathcal{L}\|} \\ &\leq \frac{\lambda \|\mathcal{L}\|^2 e^{\lambda\|\mathcal{L}\|}}{2\,\|\mathcal{E}_\lambda - \mathcal{I}\|/\lambda} \left(e^{ct\|\mathcal{E}_\lambda - \mathcal{I}\|/\lambda} - 1\right) e^{ct\|\mathcal{L}\|}, \end{aligned} \tag{B.14}$$

where we have set $h(t,s) = k(t,s)/\lambda$ and we have assumed $k(t,s) \leq c$.

Finally, let us consider two parameter regimes. For $c\|\mathcal{L}\|t \leq 1/e$, the expression in Eq. (B.14) is bounded by ε, provided that $\lambda \leq \log\left(\frac{1}{c\|\mathcal{L}\|t}\right) \frac{\varepsilon}{\|\mathcal{L}\|}$,

$$\begin{aligned}\frac{\lambda\|\mathcal{L}\|^2 e^{\lambda\|\mathcal{L}\|}}{2} \frac{e^{ct\|\mathcal{E}_\lambda - \mathcal{I}\|/\lambda} - 1}{\|\mathcal{E}_\lambda - \mathcal{I}\|/\lambda} e^{ct\|\mathcal{L}\|} &\leq \frac{e}{2} \left(\lambda\,\|\mathcal{L}\|\right) \left(c\,\|\mathcal{L}\|\,t\right) e^{\lambda\|\mathcal{L}\|} \\ &\leq \frac{e}{2} \log\left(\frac{1}{c\,\|\mathcal{L}\|\,t}\right) \left(c\,\|\mathcal{L}\|\,t\right)^{1-\varepsilon} \varepsilon \leq \varepsilon, \end{aligned} \tag{B.15}$$

where we have used in the first inequality that

$$z \equiv ct\|\mathcal{E}_\lambda - \mathcal{I}\|/\lambda \leq ct\left(e^{\lambda\|\mathcal{L}\|} - 1\right)/\lambda \leq ct\,\|\mathcal{L}\|\,e^{\lambda\|\mathcal{L}\|} \leq \left(ct\,\|\mathcal{L}\|\right)^{1-\varepsilon} < \; e^{-1/2}, \tag{B.16}$$

in order to apply the inequality $(e^z - 1)/z < e^{1/2}e^{e^{-1/2}} - 1 < e^{1/2}$ $(0 \leq z < e^{-1/2})$, and the last inequality holds for $\varepsilon < 1/2$. For $c\,\|\mathcal{L}\|\,t > 1/e$, the expression in Eq. (B.14) is bounded by ε, provided that $\lambda \leq \frac{e^{-(1+e^\varepsilon)c\|\mathcal{L}\|t}}{c\|\mathcal{L}\|^2 t}\varepsilon$. In fact, for this parameter choice, we have that $\lambda\,\|\mathcal{L}\| < \varepsilon$, which implies $\|\mathcal{E}_\lambda - \mathcal{I}\|/\lambda \leq \left(e^{\lambda\|\mathcal{L}\|} - 1\right)/\lambda \leq e^\varepsilon\,\|\mathcal{L}\|$. Hence, the relation

$$\begin{aligned}\frac{\lambda\|\mathcal{L}\|^2 e^{\lambda\|\mathcal{L}\|}}{2} \frac{e^{ct\|\mathcal{E}_\lambda - \mathcal{I}\|/\lambda} - 1}{\|\mathcal{E}_\lambda - \mathcal{I}\|/\lambda} e^{ct\|\mathcal{L}\|} &\leq \frac{\lambda\left(c\,\|\mathcal{L}\|^2\,t\right) e^{\lambda\|\mathcal{L}\|}}{2} e^{ct(\|\mathcal{E}_\lambda - \mathcal{I}\|/\lambda + \|\mathcal{L}\|)} \\ &\leq \frac{e^\varepsilon}{2}\varepsilon \leq \varepsilon \end{aligned} \tag{B.17}$$

holds. Here, we have used in the first inequality that $(e^z - 1)/z < e^z$, applying it to $z \equiv ct\|\mathcal{E}_\lambda - \mathcal{I}\|/\lambda$, and the last inequality holds for $\varepsilon < 1/2$.

Observable decomposition in sum of unitary matrices

Any observable O can be decomposed as a sum of two unitary matrices U_a and U_b, as $O = U_a + \gamma U_b$, with $\gamma > 0$ and $\|O\| \leq 1 + \gamma$ [91]. The first step is the diagonalization of O, $O = VDV^\dagger$, and obtain the equations for a_i and b_i, the eigenvalues of U_a and U_b, as a function of γ and d_i, the eigenvalues of O, as follows,

$$d_i = a_i + \gamma b_i, \qquad |a_i| = 1, \qquad |b_i| = 1. \tag{B.18}$$

The eigenvalues are decomposed into real and imaginary parts,

$$\begin{aligned}
\mathrm{Re}(a_i) &= \frac{d_i^2 - \gamma^2 + 1}{2d_i}, \qquad \mathrm{Im}(a_i) = \frac{\sqrt{-d_i^4 + 2d_i^2(\gamma^2+1) - (\gamma^2-1)^2}}{2d_i}, \\
\mathrm{Re}(b_i) &= \frac{d_i^2 + \gamma^2 - 1}{2d_i\gamma}, \qquad \mathrm{Im}(b_i) = \frac{\sqrt{-d_i^4 + 2d_i^2(\gamma^2+1) - (\gamma^2-1)^2}}{2d_i\gamma},
\end{aligned}$$

and the unitary matrices obtained,

$$\left(U_{a(b)}\right)_{ij} = V_{in}^\dagger a_n(b_n) V_{nj}. \tag{B.19}$$

There is a restriction imposed by the fact that the imaginary parts of a and b have to be real numbers, which translates into the condition

$$|-1 + d_i| \leq \gamma \leq 1 + d_i. \tag{B.20}$$

Appendix C

Description of the Genetic Algorithm

In this section, we describe the Genetic Algorithm [154, 46] used to obtain the decomposition of the local Trotter blocks [3, 9]. The sequence of quantum gates is codified in a matrix representing in the protocol the genetic code of an individual. This matrix contains as many columns (genes) as allowed resources, and sufficient rows to determine the type of gate and the qubits on which it acts. The next step is to engineer a fitness or evaluation function which maps every individual into a real number. This allows to classify the individuals with respect to an adequate criterion for the optimization purposes. In our case, the fitness function corresponds to the fidelity with respect to the ideal block dynamics. Finally, each cycle of the algorithm consists of three stages: breeding, mutation, and natural selection.

In the breeding stage, a new generation of individuals is obtained by combining the genetic code of the predecessors, which provides the genetic code of the offspring. We have used a hierarchical combination method, which allows the number of broods of each individual to depend on its fidelity. In particular, for an initial population of 4 individuals sorted by fidelity, our algorithm creates an offspring of 9, 6 of which acquire genetic material of the first precursor, 5 of the second, 4 of the third, and 3 of the fourth. Notice that each newborn individual is produced with the genetic information of two predecessors, as it can be seen from the fact that adding the numbers of each progeny equals two times the number of newborn individuals. Notice that this is not the most general situation, since we could have considered individuals as a combination of more predecessors. Additionally, the amount of genes each precursor provides, in this case the number of matrix columns, also depends on the hierarchy induced by fidelity.

In the mutation stage, every individual is allowed to mutate by randomly modifying any sequence of genetic material, with equal probability for all individuals. This probability settles the threshold to overcome for a random number for a mutation event to occur, case in which another set of random numbers provides the new genes to insert in the genetic material.

In the last stage of the cycle, old and new generations of individuals are combined in the same population group. Afterwards, they are sorted depending on their fidelity, and those which show the highest fidelity are selected as the initial population of the forthcoming cycle.

We have observed that it is convenient to combine numerical trials with high and low mutation rates to enhance the breeding or the mutation stages depending on the intermediate results.

Number of Architectures

We derive here the formula $P = (q^2 - q)^n n!$ for the number of architectures in terms of the number of ancillary qubits q and the number of imperfect gates n. We impose the condition of applying each two-qubit gate once and only once, and that the gates are asymmetric, so applying it to qubits (i, j) is different to apply it to qubits (j, i). Therefore, one of the q qubits is selected as the control, and one of the remaining $q - 1$ as the target. This process is repeated for each of the n gates, so we obtain $(q(q-1))^n$ possibilities. Finally, the n gates may be applied in any possible order, so there are $n!$ re-orderings. Therefore, by combining both results, the number of total architectures turns into $n!\,(q^2 - q)^n$.

Errors in architectures building the CNOT gate

We compare the mean error of the integrated CNOT gate obtained with GA over many realizations of imperfect gates with the average of the highest fidelity imperfect CNOT gate involved in the architecture. For this purpose, we take a sampling of 1000 different experiments, and we average the error of the best gate. We estimate the error of the integrated CNOT and obtain the percentage of improvement in the error. These results are summarized in Table C.1. As it is shown, the probability to have a high-fidelity gate is increased when the number of gates is aucmented. Accordingly, there are

more possible architectures that minimize the error in the integrated CNOT. For the case of $q = 5$ and $n = 7$, we obtain similar errors to the ones for $q = 4$. This could well be because the number of ancillary qubits is of the same order of the involved gates, and then no measurable improvement is expected since there is no cancellation of gate errors. Nevertheless, the optimal relation between number qubits and involved gates is still an open question.

Number of qubtis and gates (q, n)	$(4, 3)$	$(4, 5)$	$(4, 7)$	$(5, 7)$
Error of best gate	0.1271	0.1205	0.1150	0.1150
Error of architecture	0.1771	0.0988	0.0807	0.0810
Approximate improvement	-39%	18%	30%	30%

Table C.1: **Overall CNOTs errors.** Average errors of integrated CNOTs and highest fidelity CNOTs for the protocols involving q qubits and n gates.

Bibliography

[1] R. P. Feynman, Simulating physics with computers, *Int. J. Theor. Phys.* **21**, 467 (1982).

[2] D. Deutsch, Quantum theory, the Church-Turing principle and the Universal Quantum Computer, *Proc. Roy. Soc. London A* **400**, 97 (1985).

[3] S. Lloyd, Universal quantum simulators, *Science* **273,** 1073 (1996).

[4] Y. Salathé, M. Mondal, M. Oppliger, J. Heinsoo, P. Kurpiers, A. Potočnik, A. Mezzacapo, U. Las Heras, L. Lamata, E. Solano, S. Filipp, and A. Wallraff, Digital Quantum Simulation of Spin Models with Circuit Quantum Electrodynamics, *Phys. Rev. X* **5**, 021027 (2015).

[5] R. Barends, L. Lamata, J. Kelly, L. García-Álvarez, A. G. Fowler, A. Megrant, E. Jeffrey, T. C. White, D. Sank, J. Y. Mutus, B. Campbell, Yu Chen, Z. Chen, B. Chiaro, A. Dunsworth, I.-C. Hoi, C. Neill, P. J. J. O'Malley, C. Quintana, P. Roushan, A. Vainsencher, J. Wenner, E. Solano, and J. M. Martinis, Digital quantum simulation of fermionic models with a superconducting circuit, *Nat. Commun.* **6**, 7654 (2015).

[6] R. Barends, A. Shabani, L. Lamata, J. Kelly, A. Mezzacapo, U. Las Heras, R. Babbush, A. G. Fowler, B. Campbell, Yu Chen, Z. Chen, B. Chiaro, A. Dunsworth, E. Jeffrey, E. Lucero, A. Megrant, J. Y. Mutus, M. Neeley, C. Neill, P. J. J. O'Malley, C. Quintana, P. Roushan, D. Sank, A. Vainsencher, J. Wenner, T. C. White, E. Solano, H. Neven, and J. M. Martinis, Digitized adiabatic quantum computing with a superconducting circuit, *Nature* **534**, 222 (2016).

[7] T. E. Lee, U. Alvarez-Rodriguez, X.-H. Cheng, L. Lamata, and E. Solano, *Phys. Rev. A* **92**, 032129 (2015).

[8] X. Zhang, Y. Shen, J. Zhang, J. Casanova, L. Lamata, E. Solano, M.-H. Yung, J.-N. Zhang, and K. Kim, Time reversal and charge conjugation in an embedding quantum simulator, *Nat. Commun.* **6**, 7917 (2015).

[9] M. Suzuki, Fractal decomposition of exponential operators with applications to many-body theories and Monte Carlo simulations, *Phys. Lett. A*, **146**, 319 (1990).

[10] M. A. Nielsen and I. L. Chuang, Quantum Computation and Quantum Information, (Cambridge University Press 2000)

[11] H.-P. Breuer and F. Petruccione, *The Theory of Open Quantum Systems* (Oxford University Press, New York, 2002).

[12] D. Bacon, A. M. Childs, I. L. Chuang, J. Kempe, D. W. Leung, and X. Zhou, Universal simulation of Markovian quantum dynamics, *Phys. Rev. A.* **64**, 062302 (2001).

[13] M. Kliesch, T. Barthel, C. Gogolin, M. Kastoryano, and J. Eisert, Dissipative Quantum Church-Turing Theorem, *Phys. Rev. Lett* **107**, 120501 (2011).

[14] R. Sweke, I. Sinayskiy, D. Bernard, and F. Petruccione, Universal simulation of Markovian open quantum systems, *Phys. Rev. A* **91**, 062308 (2015).

[15] R. Di Candia, J. S. Pedernales, A. del Campo, E. Solano, and J. Casanova, Quantum Simulation of Dissipative Processes without Reservoir Engineering, *Sci. Rep.* **5**, 9981 (2015).

[16] M. H. Devoret and R. J. Schoelkopf, Superconducting Circuits for Quantum Information: An Outlook. *Science* **339**, 1169 (2013).

[17] A. A. Houck, H. E. Türeci, and J. Koch, On-chip quantum simulation with superconducting circuits, *Nat. Phys.* **8**, 292 (2012).

[18] D. Leibfried, R. Blatt, C. Monroe, and D. Wineland, Quantum dynamics of single trapped ions. *Rev. Mod. Phys.* **75**, 281 (2003).

[19] H. Häffner, C. F. Roos, and R. Blatt, Quantum computing with trapped ions *Physics Reports* **469**, 155 (2008).

[20] R. Blatt and C. F. Roos, Quantum simulations with trapped ions *Nat. Phys.* **8**, 277 (2012).

[21] E. Knill, R. Laflamme, and G. J. Milburn, A scheme for efficient quantum computation with linear optics. *Nature* **409**, 46 (2001).

[22] P. Kok, W. J. Munro, K. Nemoto, T. C. Ralph, J. P. Dowling, and G. J. Milburn, Linear optical quantum computing with photonic qubits. *Rev. Mod. Phys.* **79**, 135 (2007).

[23] A. Aspuru-Guzik and P. Walther, Photonic quantum simulators. *Nat. Phys.* **8**, 285 (2012).

[24] T. Meany, M. Gräfe, R. Heilmann, A. Perez-Leija, S. Gross, M. J. Steel, M. J. Withford, and A. Szameit, Laser written circuits for quantum photonics, Laser Photon. Rev. **9**, 363 (2015).

[25] P. W. Shor, Polynomial time algorithms for prime factorization and discrete logarithms on a quantum computer. *SIAM J. Sci. Statist. Comput.* **26**, 1484 (1997).

[26] L. K. Grover, A fast quantum mechanical algorithm for database search. *Phys. Proceedings, 28th Annual ACM Symposium on the Theory of Computing* (STOC), 212 (1996).

[27] L. M. K. Vandersypen, M. Steffen, G. Breyta, C. S. Yannoni, M. H. Sherwood, and I. L. Chuang, Experimental realization of Shor's quantum factoring algorithm using nuclear magnetic resonance, *Nature* **414**, 883 (2001).

[28] T. Monz, D. Nigg, E. A. Martinez, M. F. Brandl, P. Schindler, R. Rines, S. X. Wang, I. L. Chuang, and R. Blatt, Realization of a scalable Shor algorithm *Science* **351**, 1068 (2016).

[29] J. A. Jones, M. Mosca, and R. H. Hansen, Implementation of a quantum search algorithm on a quantum computer, *Nature* **393**, 344 (1998).

[30] I. L. Chuang, N. Gershenfeld, and M. Kubinec, Experimental Implementation of Fast Quantum Searching, *Phys. Rev. Lett.* **80**, 3408 (1998).

[31] P. Walther, K. J. Resch, T. Rudolph, E. Schenck, H. Weinfurter, V. Vedral, M. Aspelmeyer, and A. Zeilinger, Experimental one-way quantum computing, *Nature* **434** 169 (2005).

[32] R. Di Candia, B. Mejia, H. Castillo, J. S. Pedernales, J. Casanova, and E. Solano, Embedding Quantum Simulators for Quantum Computation of Entanglement, Phys. Rev. Lett. **111**, 240502 (2013).

[33] L. García-Álvarez, U. Las Heras, A. Mezzacapo, M. Sanz, E. Solano, and L. Lamata, Quantum chemistry and charge transport in biomolecules with superconducting circuits, Sci. Rep. **6**, 27836 (2016).

[34] I. Arrazola, J. S. Pedernales, L. Lamata, and E. Solano, Digital-Analog Quantum Simulation of Spin Models in Trapped Ions, Sci. Rep. **6**, 30534 (2016).

[35] A.B. Finnila, M.A. Gomez, C. Sebenik, C. Stenson, and J.D. Doll, Quantum annealing: A new method for minimizing multidimensional functions, *Chem. Phys. Lett.* **219**, 343 (1994).

[36] T. Kadowaki and H. Nishimori, Quantum annealing in the transverse Ising model, *Phys. Rev. E* **58**, 5355 (1998).

[37] J. B. Spring, B. J. Metcalf, P. C. Humphreys, W. S. Kolthammer, X.-M. Jin, M. Barbieri, A. Datta, N. Thomas-Peter, N. K. Langford, D. Kundys, J. C. Gates, B. J. Smith, P. G. R. Smith, and I. A. Walmsley, Boson Sampling on a Photonic Chip, *Science* **339**, 798 (2013).

[38] M. A. Broome, A. Fedrizzi, S. Rahimi-Keshari, J. Dove, S. Aaronson, T. C. Ralph, and A. G. White, Photonic Boson Sampling in a Tunable Circuit, *Science*, **339** 794 (2013).

[39] M. Tillmann, B. Dakić, R. Heilmann, S. Nolte, A. Szameit, and P. Walther, Experimental boson sampling, *Nat. Photonics* **7**, 540 (2013).

[40] A. Crespi, R. Osellame, R. Ramponi, D. J. Brod, E. F. Galvão, N. Spagnolo, C. Vitelli, E. Maiorino, P. Mataloni, and F. Sciarrino, Integrated multimode interferometers with arbitrary designs for photonic boson sampling, *Nat. Photonics* **7**, 545 (2013).

[41] J. F. V. Vincent, O. A. Bogatyreva, N. R. Bogatyrev, A. Bowyer, and A. Pahl, Biomimetics: it's practice and theory *J. R. Soc. Interface* **3,** 471 (2006).

[42] B. Bhushan, Biomimetics: lessons from naturean overview, *Phil. Trans. R. Soc. A.* **367**, 1445 (2009).

[43] D. Floreano and C. Mattiussi, *Bio-Inspired Artificial Intelligence* (MIT Press, Cambridge, 2008)

[44] C. G. Langton, *Artificial Life: An Overview* (MIT Press, 1995)

[45] M. A. Bedau, Artificial life: organization, adaptation and complexity from the bottom up, *Trends Cogn. Sci.* **7,** 505 (2003).

[46] L. D. Chambers, *Practical Handbook of Genetic Algorithms* (CRC Press, Boca Raton,1998).

[47] S. Russell and P. Norvig, *Artificial Intelligence*, (Pearson, 2010)

[48] D. Abbot, P. C. W. Davies, A. K. Pati et al. *Quantum Aspects of Life*, (Imperial College Press, London, 2008).

[49] W. K. Wootters and W. H. Zurek, A single quantum cannot be cloned. *Nature* **299,** 802 (1982).

[50] V. Buzek and M. Hillery, Quantum copying: Beyond the no-cloning theorem. *Phys. Rev. A* **54,** 1844 (1996).

[51] V. Scarani, S. Iblisdir, N. Gisin, and A. Acín, Quantum Cloning *Rev. Mod. Phys.* **77,** 1225 (2005).

[52] Y. Delgado, L. Lamata, J. León, D. Salgado, and E. Solano, E. Sequential quantum cloning *Phys. Rev. Lett.* **98,** 150502 (2007).

[53] N. Gisin and S. Massar, Optimal quantum cloning machines *Phys. Rev. Lett.* **79,** 2153 (1997).

[54] L. Lamata, J. León, D. Pérez-García, D. Salgado, and E. Solano, Sequential implementation of global quantum operations *Phys. Rev. Lett.* **101,** 180506 (2008).

[55] H. Saberi, Ancilla-assisted sequential approximation of nonlocal unitary operations *Phys. Rev. A* **84,** 032323 (2011).

[56] A. Ferraro, A. Galbiati, and M. Paris, Cloning of observables *J. Phys. A* **39,** L219 (2006).

[57] G. Lindblad, A general no-cloning theorem *Lett. Math. Phys.* **47,** 189 (1999).

[58] T. Brougham, E. Andersson, and S. M. Barnett, Cloning and joint measurements of incompatible components of spin *Phys. Rev. A.* **73,** 062319 (2006).

[59] P. Gruber, D. Bruckner, C. Hellmich, H.-B. Schmiemayer, H. Stachelberger, and I. C. Gebeshuber *Biomimetics - Materials, Structures and Processes*, (Springer Verlag, Berlin Heidelberg 2011).

[60] A. R. Parker and H. E. Townley, Biomimetics of photonics nanostructures *Nature Nanotechnology* **2**, 347 (2007).

[61] M. Vilfan, A. Potočnik, B. Kavčič, N. Osterman, I. Poberaj, A. Vilfan, and D. Babič, Self-assembled artificial cilia *Proc. Natl. Acad. Sci.* **107**, 1844 (2010).

[62] Schrödinger, E. *What Is Life?* (Cambridge University Press, Cambridge, 1944).

[63] D. Gottesman, Fault-Tolerant Quantum Computation with Higher-Dimensional Systems, *Chaos Solitons Fractals* **10**, 1749 (1999).

[64] X. Wang, B. C. Sanders, and D. W. Berry, Entangling power and operator entanglement in qudit systems *Phys. Rev. A.* **67**, 042323 (2003).

[65] H. Barnum, C. M. Caves, C. A. Fuchs, R. Jozsa, B. Schumacher, Noncommuting mixed states cannot be broadcast *Phys. Rev. Lett.* **76,** 2818 (1996).

[66] S. Meznaric, S. R. Clark, and A. Datta, Quantifying the Nonclassicality of Operations *Phys. Rev. Lett.* **110,** 070502 (2013).

[67] M. Sanz, D. Pérez-García, M. M. Wolf, and J. I. Cirac, A quantum version of Wielandt's inequality *IEEE Trans. Inf. Theory.* **56**, 4668 (2010).

[68] W. H. Zurek, Quantum Darwinism *Nature Phys.* **5**, 181 (2009).

[69] A. Sørensen and K. Mølmer, Quantum computation with ions in thermal motion *Phys. Rev. Lett.* **82**, 1971 (1999).

[70] J. I. Cirac and P. Zoller, Quantum computation with cold trapped ions *Phys. Rev. Lett.* **74**, 4091 (1995).

[71] W. Aguilar, G. Santamaría-Bonfil, T. Froese, and C. Gershenson, The past, present, and future of artificial life *Front. Robot. AI* **1**, 8 (2014).

[72] J. C. López Alfonso, N. Jagiella, L. Nuñez, M. A. Herrero, and D. Drasdo, Estimating Dose Painting Effects in Radiotherapy: A Mathematical Model. *PLoS ONE* **9**, e89380 (2014).

[73] B. Chopard and M. Droz, Cellular automata modeling of physical systems (Cambridge University Press, Cambridge, UK, 1998).

[74] M. Gardner, The fantastic combinations of John Conway's new solitaire game "life". *Scientific American* **223**, 120 (1970).

[75] T. S. Ray, Ecology and Optimization of Digital Organisms, Santa Fe Institute, (1992). Available at: http://www.santafe.edu/media/workingpapers/92-08-042.pdf (Accessed: 2nd January 2016)

[76] P. Arrighi and J. Grattage, A Quantum Game of Life. Paper presented at Journées Automates Cellulaires, Turku, Finland (2010, December 15).

[77] D. Bleh, T. Calarco, and S. Montangero, Quantum Game of Life. *EPL* **97**, 20012 (2012).

[78] M. A. Martin-Delgado, On Quantum Effects in a Theory of Biological Evolution, *Sci. Rep.* **2**, 302 (2012).

[79] G. D. Paparo, V. Dunjko, A. Makmal, M. A. Martin-Delgado, and H. J. Briegel, Quantum speedup for active learning agents, *Phys. Rev. X* **4**, 031002 (2014).

[80] MIT Technology Review, Quantum Life Spreads Entanglement Across Generations, (2015). Available at: http://www.technologyreview.com/view/537676/quantum-life-spreads-entanglement-across-generations/ (Accessed: 19th May 2015)

[81] K. Mølmer and A. Sørensen, Multiparticle Entanglement of Hot Trapped Ions *Phys. Rev. Lett.* **82**, 1835 (1999).

[82] J. T. Barreiro, M. Müller, P. Schindler, D. Nigg, T. Monz, M. Chwalla, M. Hennrich, C. F. Roos, P. Zoller, and R. Blatt, An open-system quantum simulator with trapped ions *Nature* **470**, 486 (2011).

[83] T. Monz, K. Kim, W. Hänsel, M. Riebe, A. S. Villar, P. Schindler, M. Chwalla, M. Hennrich, and R. Blatt, Realization of the Quantum Toffoli Gate with Trapped Ions *Phys. Rev. Lett.* **102**, 040501 (2009).

[84] R. Barends, J. Kelly, A. Megrant, A. Veitia, D. Sank, E. Jeffrey, T. C. White, J. Mutus, A. G. Fowler, B. Campbell, Y. Chen, Z. Chen, B. Chiaro, A. Dunsworth, C. Neill, P. O'Malley, P. Roushan, A. Vainsencher, J. Wenner, A. N. Korotkov, A. N. Cleland, and J. M. Martinis, Superconducting quantum circuits at the surface code threshold for fault tolerance, Nature **508**, 500 (2014).

[85] J. Raftery, D. Sadri, S. Schmidt, H. E. Türeci, and A. A. Houck, Observation of a Dissipation-Induced Classical to Quantum Transition *Phys. Rev. X* **4**, 031043 (2014).

[86] A. Fedorov, L. Steffen, M. Baur, M. P. da Silva, and A. Wallraff, Implementation of a Toffoli gate with superconducting circuits *Nature* **481**, 170 (2012).

[87] B. P. Lanyon, M. Barbieri, M. P. Almeida, T. Jennewein, T. C. Ralph, K. J. Resch, G. J. Pryde, J. L. O'Brien, A. Gilchrist, and A. G. White, Simplifying quantum logic using higher-dimensional Hilbert spaces *Nat. Phys.* **5**, 134 (2008).

[88] T. C. Ralph, N. K. Langford, T. B. Bell, and A. G. White, Linear optical controlled-NOT gate in the coincidence basis, *Phys. Rev. A* **65**, 062324 (2002).

[89] S. Trotzky, Y.-A. Chen, A. Flesch, I. P. McCulloch, U. Schollwöck, J. Eisert, and I. Bloch, Probing the relaxation towards equilibrium in an isolated strongly correlated one-dimensional Bose gas. *Nat. Phys.* **8**, 325 (2012).

[90] J. C. Loredo, M. P. Almeida, R. Di Candia, J. S. Pedernales, J. Casanova, E. Solano, and A. G. White, Measuring Entanglement in a Photonic Embedding Quantum Simulator, *Phys. Rev. Lett.* **116**, 070503 (2016).

[91] A. Mezzacapo, M. Sanz, L. Lamata, I. L. Egusquiza, S. Succi, and E. Solano, Quantum Simulator for Transport Phenomena in Fluid Flows, *Sci. Rep.* **5**, 13153 (2015).

[92] H.-P. Breuer, E.-M. Laine, J. Piilo, and B. Vacchini, Colloquium: Non-Markovian dynamics in open quantum systems, *Rev. Mod. Phys.* **88**, 021002 (2016).

[93] A. Rivas, S. F. Huelga, and M. Plenio, Quantum non-Markovianity: characterization, quantification and detection, *Rep. Prog. Phys.* **77**, 094001 (2014).

[94] B. Vacchini, A. Smirne, E.-M. Laine, J. Piilo, and H.-P. Breuer, Markovian and non-Markovian dynamics in quantum and classical systems, *New J. Phys.* **13**, 093004 (2011).

[95] C. Addis, B. Bylicka, D. Chruściński, and S. Maniscalco, Comparative study of non-Markovianity measures in exactly solvable one and two qubit models, *Phys. Rev. A* **90**, 052103 (2014).

[96] I. de Vega and D. Alonso, Dynamics of non-Markovian open quantum systems, arXiv:1511.06994 (2015).

[97] F. A. Pollock, C. Rodríguez-Rosario, T. Frauenheim, M. Paternostro, and K. Modi, Complete framework for efficient characterisation of non-Markovian processes, arXiv:1512.00589 (2015).

[98] A. Chiuri, C. Greganti, L. Mazzola, M. Paternostro, and P. Mataloni, Linear Optics Simulation of Quantum Non-Markovian Dynamics, *Sci. Rep.* **2**, 968 (2012).

[99] B. Dive, F. Mintert, and D. Burgarth, Quantum simulations of dissipative dynamics: Time-dependence instead of size, *Phys. Rev. A* **92**, 032111 (2015).

[100] D. Chruściński and A. Kossakowski, Sufficient conditions for memory kernel master equation, *Phys. Rev. A* **94**, 020103(R) (2016).

[101] R. Sweke, M. Sanz, I. Sinayskiy, F. Petruccione, and E. Solano, Digital quantum simulation of many-body non-Markovian dynamics, *Phys. Rev. A* **94**, 022317 (2016).

[102] X. Meng, Y. Li, J.-W. Zhang, and H. Guo, Multiple-scale integro-differential perturbation method for generic non-Markovian environments, arXiv:1603.06261 (2016).

[103] F. Ciccarello, G. M. Palma, and V. Giovannetti, Collision-model-based approach to non-Markovian quantum dynamics, *Phys. Rev. A* **87**, 040103(R) (2013).

[104] S. Kretschmer, K. Luoma, and W. T. Strunz, Collision model for non-Markovian quantum dynamics, *Phys. Rev. A* **94**, 012106 (2016).

[105] R. Rosenbach, J. Cerrillo, S. F. Huelga, J. Cao, and M. B. Plenio, Efficient simulation of non-Markovian system-environment interaction, *New. J. Phys.* **18**, 023035 (2016).

[106] I. Semina and F. Petruccione, The simulation of the non-Markovian behaviour of a two-level system, *Phys. A* **450**, 395 (2016).

[107] J. Jin, V. Giovannetti, R. Fazio, F. Sciarrino, P. Mataloni, A. Crespi, and Roberto Osellame, All-optical non-Markovian stroboscopic quantum simulator, *Phys. Rev. A* **91** 012122 (2015).

[108] M. Li, A numerical simulation algorithm for Non-Markovian dynamics in open quantum systems, Proceeding of the 11th World Congress on Intelligent Control and Automation Shenyang, China, June 29 - July 4 2014

[109] C. Addis, G. Karpat, C. Macchiavello, and S. Maniscalco, Dynamical Memory Effects in Correlated Quantum Channels, arXiv:1607.00134 (2016).

[110] J. C. Adcock, E. Allen, M. Day, S. Frick, J. Hinchliff, M Johnson, S. Morley-Short, S. Pallister, A. B. Price, and S. Stanisic, Advances in quantum machine learning, arXiv:1512.02900 (2015).

[111] M. Schuld, I. Sinayskiy, and F. Petruccione, An introduction to quantum machine learning, *Contemp. Phys.* **56**, 172 (2015).

[112] P. Pfeiffer, I. L. Egusquiza, M. Di Ventra, M. Sanz, and E. Solano, Quantum Memristors, *Sci. Rep.* **6**, 29507 (2016).

[113] J. Salmilehto, F. Deppe, M. Di Ventra, M. Sanz, and E. Solano, Quantum Memristors with Superconducting Circuits, arXiv:1603.04487 (2016).

[114] D. B. Strukov, G. S. Snider, D. R. Stewart, and R. S. Williams, The missing memristor found, *Nature* **453**, 80 (2008).

[115] A. Lendlein and S. Kelch, Shape-Memory Polymers, *Angew. Chem. Int. Ed.* **41**, 2034 (2002).

[116] K. Gopalsamy, *Stability and Oscillations in Delay Differential Equations of Population Dynamics* (Springer, 1992).

[117] D. Wang, Algorithmic Quantum Channel Simulation, PhD Thesis, University of Calgary, (2015)

[118] H.-P. Breuer and B. Vacchini, Quantum Semi-Markov Processes, *Phys. Rev. Lett.* **101**, 140402 (2008).

[119] A.-A. Budini, Stochastic representation of a class of non-Markovian completely positive evolutions, *Phys. Rev. A.* **69**, 042107 (2004).

[120] J. S. Pedernales, R. Di Candia, I. L. Egusquiza, J. Casanova and E. Solano, Efficient Quantum Algorithm for Computing n-time Correlation Functions, *Phys. Rev. Lett.* **113**, 020505 (2014).

[121] A. Mari and J. Eisert, Positive Wigner Functions Render Classical Simulation of Quantum Computation Efficient, *Phys. Rev. Lett.* **109**, 230503 (2012).

[122] H. Pashayan, J. J. Wallman, and S. D. Bartlett, Estimating Outcome Probabilities of Quantum Circuits Using Quasiprobabilities, *Phys. Rev. Lett.* **115**, 070501 (2015).

[123] S. Mandrà, Z. Zhu, W. Wang, A. Perdomo-Ortiz, and H. G. Katzgraber, Strengths and Weaknesses of Weak-Strong Cluster Problems: A Detailed Overview of State-of-the-art Classical Heuristics vs Quantum Approaches, *Phys. Rev. A.* **94**, 022337 (2016).

[124] A. L. Grimsmo, Time-Delayed Quantum Feedback Control, *Phys. Rev. Lett.* **115**, 060402 (2015).

[125] J. Zhang, Y.-X. Liu, R.-B. Wu, K. Jacobs, and F. Nori, Quantum feedback: theory, experiments, and applications, arXiv:1407.8536 (2014).

[126] G. Zhang and M. R. James, Quantum Feedback Networks and Control: A Brief Survey, *Chin. Sci. Bull.* **57**, 2200 (2012).

[127] A. D. Myshkis, Mixed Functional Differential Equations, *J. Math. Sci.* **129**, 5 (2005).

[128] A. Rustichini, Functional Differential Equations of Mixed Type: The Linear Autonomous Case, *J. Dyn. Diff. Eq.* **1**, 2 (1989).

[129] J. Mallet-Paret, The Fredholm alternative for functional differential equations of mixed type, *J. Dyn. Diff. Eq.* **11**, 1 (1999).

[130] L. Berezansky, E. Braverman, and S. Pinelas, On nonoscillation of mixed advanced-delay differential equations with positive and negative coefficients, *Comput. Math. Appl.* **58**, 766 (2009).

[131] N. J. Ford, P. M. Lumb, P. M. Lima, and M. F. Teodoro, The numerical solution of forward-backward differential equations: Decomposition and related issues, *J. Comput. Appl. Math.* **234**, 2745 (2010).

[132] J. C. Lucero, Advanced-delay differential equation for aeroelastic oscillations in physiology, *Biophys. Rev. Lett.* **3**, 125 (2008).

[133] F. Collard, O. Licandro, and L. A. Puc, The short-run dynamics of optimal growth models with delays, *Ann. Econ. Stat.* **90**, 127 (2008).

[134] H. Chi, J. Bell, and B. Hassard, Numerical solution of a nonlinear advance-delay-differential equation from nerve conduction theory, *J. Math. Biol.* **24**, 583 (1986).

[135] L. S. Schulman, Some differential-difference equations containing both advance and retardation, *J. Math. Phys.* **15**, 295 (1974).

[136] J. A. Wheeler and R. P. Feynman, Interaction with the Absorber as the Mechanism of Radiation, *Rev. Mod. Phys.* **17**, 157 (1945).

[137] J. A. Wheeler and R. P. Feynman, Classical Electrodynamics in Terms of Direct Interparticle Action, *Rev. Mod. Phys.* **21**, 425 (1949).

[138] S. Whalen, Open Quantum Systems with Time-Delayed Interactions, PhD Thesis, University of Auckland, (2015).

[139] H. Pichler and P. Zoller, Photonic Circuits with Time Delays and Quantum Feedback, *Phys. Rev. Lett.* **116**, 093601 (2016).

[140] S. Mavadia, V. Frey, J. Sastrawan, S. Dona, and M. J. Biercuk, Prediction and real-time compensation of qubit decoherence via machine-learning, arXiv:1604.03991 (2016).

[141] S. Lloyd and J.-J. E. Slotine, Quantum feedback with weak measurements, *Phys. Rev. A.* **62**, 012307 (2000).

[142] G. G. Gillett, R. B. Dalton, B. P. Lanyon, M. P. Almeida, M. Barbieri, G. J. Pryde, J. L. O'Brien, K. J. Resch, S. D. Bartlett, and A. G. White, Experimental Feedback Control of Quantum Systems Using Weak Measurements, *Phys. Rev. Lett.* **104**, 080503 (2010).

[143] D. Ristè and L. DiCarlo, Digital Feedback in Superconducting Quantum Circuits, arXiv: 1508.01385 (2015).

[144] T. Eichelkraut, C. Vetter, A. Perez-Leija, H. Moya-Cessa, D. N. Christodoulides, and A. Szameit, Coherent random walks in free space, *Optica* **4**, 268 (2014).

[145] A. Szameit and S. Nolte, Discrete optics in femtosecond-laser-written photonic structures, *J. Phys. B: At., Mol. Opt. Phys.* **43**, 163001 (2010).

[146] W. K. Lai, V. Bužek, and P. L. Knight, Nonclassical fields in a linear directional coupler, *Phys. Rev. A.* **43**, 6323 (1991).

[147] D. Deutsch, Quantum mechanics near closed timelike lines, *Phys. Rev. D.* **44**, 3197 (1991).

[148] S. Lloyd, L. Maccone, R. Garcia-Patron, V. Giovannetti, Y. Shikano, S. Pirandola, L. A. Rozema, A. Darabi, Y. Soudagar, L. K. Shalm, and A. M. Steinberg, Closed Timelike Curves via Postselection: Theory and Experimental Test of Consistency, *Phys. Rev. Lett.* **106**, 040403 (2011).

[149] M. Ringbauer, M. A. Broome, C. R. Myers, A. G. White, and T. C. Ralph, Experimental simulation of closed timelike curves, *Nat. Commun.* **5**, 4145 (2014).

[150] G. Lenz, I. Talanina, and C. Martijn de Sterke, Bloch Oscillations in an Array of Curved Optical Waveguides, *Phys. Rev. Lett.* **83**, 963 (1999).

[151] U. Peschel, T. Pertsch, and F. Lederer, Optical Bloch oscillations in waveguide arrays, *Opt. Lett.* **23**, 1701 (1998).

[152] M. Lebugle, M. Gräfe, R. Heilmann, A. Perez-Leija, S. Nolte, and A. Szameit, Experimental observation of N00N state Bloch oscillations, *Nat. Commun.* **6**, 8273 (2015).

[153] J. G. Muga, J. P. Palao, B. Navarro, and I. L. Egusquiza, Complex absorbing potentials, *Phys. Rep.* **395**, 357 (2004).

[154] E. Alpaydin, *Introduction to Machine Learning* (MIT, Cambridge, 2014).

[155] B. Gross, *A solar energy system that tracks the sun*, TED Talk 2003 (unpublished).

[156] G. S. Hornby, A. Globus, D. S. Linden, and J. D. Lohn, *Automated antenna design with evolutionary algorithms*, (American Institute of Aeronautics and Astronautics, Inc., Reston, 2006)

[157] T. Geijtenbeek, M. van de Panne, and F. van der Stappen, Flexible Muscle-Based Locomotion for Bipedal Creatures, *ACM Trans. Graph.* **32**, 6 (2013).

[158] R. S. Zebulum, M. A. C. Pacheco, and M. M. B. R. Vellasco, *Evolutionary Electronics, Automatic Design of Electronic Circuits and Systems by Genetic Algorithms*, (CRC Press, Boca Raton, FL,2002).

[159] W. M. Aly, Analog electric circuits synthesis using a genetic algorithms approach, *Int. J. Comput. Appl.* **121**, 28 (2015).

[160] P. W. Shor, Scheme for reducing decoherence in quantum computer memory, *Phys. Rev. A.* **52**, R2493 (1995).

[161] A. M. Steane, Error Correcting Codes in Quantum Theory, *Phys. Rev. Lett.* **77**, 793 (1996).

[162] S. L. Braunstein, Quantum error correction for communication with linear optics, *Nature* **394**, 47 (1998).

[163] J. Chiaverini, D. Leibfried, T. Schaetz, M. D. Barrett, R. B. Blakestad, J. Britton, W. M. Itano, J. D. Jost, E. Knill, C. Langer, R. Ozeri, and D. J. Wineland, Realization of quantum error correction, *Nature* **432**, 602 (2004).

[164] D. Ristè, S. Poletto, M.-Z. Huang, A. Bruno, V. Vesterinen, O.-P. Saira, and L. DiCarlo, Detecting bit-flip errors in a logical qubit using stabilizer measurements, *Nat. Comm.* **6**, 6983 (2015).

[165] D. W. Berry, G. Ahokas, R. Cleve, and B. C. Sanders, Efficient Quantum Algorithms for Simulating Sparse Hamiltonians, *Commun. Math. Phys.* **270**, 359 (2007).

[166] N. Wiebe, D. W. Berry, P. Høyer, and B. C. Sanders, Simulating quantum dynamics on a quantum computer, *J. Phys. A* **44**, 445308 (2011).

[167] U. Las Heras, A. Mezzacapo, L. Lamata, S. Filipp, A. Wallraff, and E. Solano, Digital Quantum Simulation of Spin Systems in Superconducting Circuits, *Phys. Rev. Lett.* **112**, 200501 (2014).

[168] G. C. Knee and W. J. Munro, Optimal Trotterization in universal quantum simulators under faulty control, *Phys. Rev. A* **91**, 052327 (2015).

[169] U. Las Heras, L. García-Álvarez, A. Mezzacapo, E. Solano, and L. Lamata, Quantum Simulation of Spin Chains Coupled to Bosonic Modes with Superconducting Circuits, in *Mathematics for Industry 11*, edited by R. S. Anderssen *et al.* (Springer Japan, 2015).

[170] V. Nebendahl, H. Häffner, and C. F. Roos, Optimal control of entangling operations for trapped-ion quantum computing, *Phys. Rev. A* **79**, 012312 (2009).

[171] T. Choi, S. Debnath, T. A. Manning, C. Figgatt, Z.-X. Gong, L.-M. Duan, and C. Monroe, Optimal Quantum Control of Multimode Couplings between Trapped Ion Qubits for Scalable Entanglement, Phys. Rev. Lett. **112**, 190502 (2014).

[172] S. Machnes, U. Sander, S. J. Glaser, P. de Fouquières, A. Gruslys, S. Schirmer, and T. Schulte-Herbrüggen, Comparing, optimizing, and benchmarking quantum-control algorithms in a unifying programming framework, *Phys. Rev. A* **84**, 022305 (2011).

[173] A. Turing, On computable numbers, with an application to the Entscheidungsproblem, *Proc. London Math. Soc.* **42,** 230 (1936).

[174] M. Sipser, *Introduction to the Theory of Computation* (Cengage Learning, 2012).

[175] P. Wittek, *Quantum Machine Learning* (Academic Press, San Diego, 2014).

[176] P. Rebentrost, M. Mohseni, and S. Lloyd, Quantum Support Vector Machine for Big Data Classification, *Phys. Rev. Lett.* **113**, 130503 (2014).

[177] V. Dunjko, J. M. Taylor, and H. J. Briegel, Quantum-Enhanced Machine Learning, *Phys. Rev. Lett.* **117**, 130501 (2016).

[178] A. A. Ezhov and D. Ventura, Quantum Neural Networks, in Future directions for intelligent systems and information sciences. (Physica-Verlag HD, 2000)

[179] S. Gupta and R.K.P. Zia, Quantum Neural Networks, J. Comput. System Sci. **63**, 355 (2001).

[180] M.V.Altaisky, Quantum neural network, arXiv:0107012 (2001).

[181] M. Schuld, I. Sinayskiy, and F. Petruccione, The quest for a Quantum Neural Network, Quantum Inf. Process. **13**, 2567 (2014).

[182] N. Wiebe, A. Kapoor, and K. M. Svore, Quantum Perceptron Models, arXiv:1602.04799 (2016).

[183] B. Schölkopf, A. J. Smola. *Learning with Kernels: Support Vector Machines, Regularization, Optimization and Beyond* (MIT Press, Cambridge, 2002).

[184] G. Gutoski and N. Johnston, Process tomography for unitary quantum channels, *J. Math. Phys.* **55**, 032201 (2014).

[185] C. H. Baldwin, A. Kalev, and I. H. Deutsch, Quantum process tomography of unitary and near-unitary maps, *Phys. Rev. A* **90**, 012110 (2014).

[186] M. Holzäpfel, T. Baumgratz, M. Cramer, and M. B. Plenio, Scalable reconstruction of unitary processes and Hamiltonians, *Phys. Rev. A* **91**, 042129 (2015).

[187] D. V. Bugg, *Electronics: Circuits, Amplifiers and Gates* (CRC Press, 2006).

[188] V. Vedral, A. Barenco, and A. Ekert, Quantum networks for elementary arithmetic operations, *Phys. Rev. A* **54**, 147 (1996).

[189] M. A. Nielsen and I. L. Chuang, Programmable Quantum Gate Arrays, *Phys. Rev. Lett.* **79**, 321 (1997).

[190] A. K. Pati, General impossible operations in quantum information, *Phys. Rev. A* **66**, 062319 (2002).

[191] K. S. Kumar and G. S. Paraoanu, A quantum no-reflection theorem and the speeding up of Grover's search algorithm, *EPL* **93**, 20005 (2011).

[192] M. Oszmaniec, A. Grudka, M. Horodecki, and A. Wójcik, Creating a Superposition of Unknown Quantum States, *Phys. Rev. Lett.* **116**, 110403 (2016).

[193] X.-M. Hu, M.-J. Hu, J.-S. Chen, B.-H. Liu, Y.-F. Huang, C.-F. Li, G.-C. Guo, and Y.-S. Zhang, Experimental creation of superposition of unknown photonic quantum states, *Phys. Rev. A* **94**, 033844 (2016).

[194] K. Li, G. Long, H. Katiyar, T. Xin, G. Feng, D. Lu, and R. Laflamme, Experimentally superposing two pure states with partial prior knowledge, arXiv:1608.04349 (2016).

[195] S. Sami and I. Chakrabarty, A note on superposition of two unknown states using Deutsch CTC model, arXiv:1605.06005 (2016).

[196] W. F. Ames and B. G. Pachpatte, *Inequalities for Differential and Integral Equations* (Academic Press Limited, London, 1998).